Energy

FOSSIL

DOE/PC/30234-T3
(DE84009555)

MICROBUBBLE FLOTATION OF FINE COAL

Final Report

By
R. H. Yoon

March 1984
Date Published

Work Performed Under Contract No. FG22-80PC30234

Virginia Polytechnic Institute and State University
Blacksburg, Virginia

Technical Information Center
Office of Scientific and Technical Information
United States Department of Energy

DISCLAIMER

DISCLAIMER

This report has been reproduced directly from the best available copy.

Available from the National Technical Information Service, U. S. Department of Commerce, Springfield, Virginia 22161.

Price: Printed Copy A09
Microfiche A01

Codes are used for pricing all publications. The code is determined by the number of pages in the publication. Information pertaining to the pricing codes can be found in the current issues of the following publications, which are generally available in most libraries: *Energy Research Abstracts (ERA); Government Reports Announcements* and Index (*GRA* and I); *Scientific and Technical Abstract Reports (STAR);* and publication NTIS-PR-360 available from NTIS at the above address.

DOE/PC/30234-T3
(DE84009555)
Distribution Category UC-90b

Final Report

MICROBUBBLE FLOTATION OF FINE COAL

by

R. H. Yoon

Department of Mining and Minerals Engineering
Virginia Polytechnic Institute and State University
Blacksburg, Virginia 24061

Grant Number
DE-FG22-80PC30234

Program Officer:

Kenneth J. Miller
Pittsburgh Energy Technology Center
U.S. Department of Energy
P. O. Box 10940
Pittsburgh, Pennsylvania 15236

Date Published - March 1984

TABLE OF CONTENTS

ACKNOWLEDGMENT

The author wishes to express sincere gratitude to Mr. Kenneth J. Miller of the Pittsburgh Energy Technology Center (PETC), U. S. Department of Energy, for his helpful suggestions and guidance throughout the course of this project. He also wishes to thank the coal companies that provided the samples for this investigation, Professor Felix Sebba of Virginia Polytechnic Institute and State University for his input at the beginning of the project, and Dr. W. W. Wen and Mr. Albert W. Deurbrouck of PETC for their interest and encouragement.

Acknowledgments are also due to Mr. R. Darrell Trigg, who produced the bulk of the flotation data presented in this report, to Mr. Gregory S. Halsey, who carried out the kinetics experiments, to Mr. Gerald Luttrell, who helped with the drawings and calculations regarding hydrodynamics, and to Mr. Terry Douglas, who did the streaming current and electrophoretic measurements. Special thanks are also given to Beth Dillinger for editing and typing the manuscript.

LIST OF FIGURES

LIST OF TABLES

MICROBUBBLE FLOTATION OF FINE COAL

Abstract

Fine coal flotation has been a longstanding problem in industry. Coal particles below approximately 38 microns in diameter are difficult to float, and the process consumes large amounts of reagents. Hydrodynamic analyses have shown, however, that the use of air bubbles smaller than those that are generated in conventional flotation machines (0.2-3 mm diameter) can improve the flotation rate and, hence, the coal recovery. Theoretically, a tenfold reduction in average bubble size should result in a thousandfold increase in the flotation rate constant at a given gas flow rate. Therefore, work has been done to use microbubbles less than 100 microns in diameter for the flotation of fine coal particles.

Seven different U.S. coal samples have been tested in the present work. The feed size varies from -100 mesh to -500 mesh. Flotation kinetics tests have been conducted on some of these coal samples as a function of bubble size at a constant gas flow rate. The results show a drastic improvement in flotation rate with the use of microbubbles, which may account for the improved recoveries obtained with the microbubble flotation technique. In addition, test results obtained with ultrafine coal samples (-20 microns) indicate that the microbubble flotation process is more selective than conventional flotation. This improved selectivity has been explained tentatively by the increased bubble loading and the reduced turbulence around the microbubbles. Various techniques have been employed to further enhance the selectivity of the process by minimizing the ash entrapment problem.

To better understand the mechanisms of microbubble flotation, basic information regarding surface tension, contact angle, viscosity, streaming currents of microbubbles, electrophoretic mobilities of coal and mineral matter, and stability of microbubble suspensions has been obtained.

I. INTRODUCTION

1.1 General

Froth flotation was first discovered and patented in 1906 as a "remarkable phenomenon" that could be utilized to recover fine mineral particles from slimes (Hines, 1962). Today this process is widely used for beneficiating a wide variety of ores, coal, oil shale, tar sand, industrial wastes, algae and other biological substances. The beneficiation by froth flotation is accomplished as air bubbles laden with hydrophobic particles rise to the surface of a pulp, leaving behind particles that are hydrophilic. Various chemical reagents are used to enhance or alter the surface characteristics of particles in the pulp, rendering them either hydrophobic or hydrophilic.

The complexity of this physico-chemico-mechanical process was noted by I. W. Wark (1938): "So many variables influence flotation that it will be long before every one of them can be investigated and its influence on the process determined." Some of these variables include pH, pulp density, temperature, types and concentrations of reagents, air flow rate, bubble size and particle size.

The recovery of fine particles is one of the more important problems facing mineral processing engineers today. Fines are produced during the processing of low-

grade ores which are often fine-grained and complex, requiring fine grinding to achieve liberation. In the coal industry, fines are generated as a result of the increased mechanization in mining techniques. Flotation recovery usually drops, however, in the fine particle size range. Recent reports show, for example, that one-third of the phosphate mined in Florida, one-half of the tin mined in Bolivia, and one-fifth of the world's tungsten are lost as fines (Somasundaran, 1979). Until recently, coal fines were also frequently discarded (Aplan, 1976), producing black water problems and a loss in profits to coal companies.

World coal production is likely to increase at least 2.5-3.0 times in the coming two decades (Konar, 1982). Although coal reserves are large in comparison with other fossil fuels and coal is expected to play an important role as a future energy source, the present world recession and surplus of oil on the international market has dampened early expectations that coal would be converted into oil and gas on a large scale before the end of this century and replace diminishing natural supplies. It is now expected that coal's major role in the near and medium term will be in the industrial and utility markets, both to replace oil and to meet increased demand (Dainton, 1980). The most exciting development in coal research today is the production of super-clean coal and its use as feedstock for

coal-water or coal-oil mixtures, which are excellent substitutes for oil in the utility industry.

In the U.S., only 15-20% of the mined coal (approximately 800 million tons) consumed yearly is cleaned (Baur, 1981), with approximately 5% of this cleaned by froth flotation (Konar, 1982). However, virtually all new coal preparation plants now incorporate flotation into their basic flowsheet. For example, Marietta Coal Company discarded 3.5-7.0% of its production in the past. Approximately 70% of this is now being recovered by tripling the plant flotation capacity and establishing a fine coal circuit. At a 600 tph throughput capacity, the additional recovery amounts to 16-32 tph (Falas, 1982).

Developing circumstances demand that coal cleaning be more efficient and economical. Some of these include higher coal prices and transportation cost, diminishing coal quality, utilities' desire to increase generating capacity, and increasingly stringent air-quality standards. Some coal seams will require fine grinding for sufficient liberation of ash particles to meet these standards. However, Zimmerman (1979) shows that difficulties develop in terms of flotation rate when trying to recover fine coal below 140 mesh (0.1 mm). Some of these difficulties are attributed to the low probability of collision between fine coal particles and the relatively large air bubbles produced in

conventional flotation cells. Investigations have suggested, however, that the use of smaller air bubbles can improve the recovery of fines (Reay and Ratcliff, 1975; Collins and Jameson, 1976).

The main objective of the present work is to generate small air bubbles in the range of 50-100 microns in diameter and to use them for cleaning fine coal. The basic strategy is to finely pulverize a coal to micron sizes for the liberation of mineral matter and then subject it to froth flotation using these microbubbles. In some experiments, attempts have been made to produce super-clean coal containing less than 2% ash by this process.

Improvements in the recovery of fine coal will not only allow coal companies to increase their profits, but will also help eliminate the black water problem. At present, coal-water and coal-oil mixtures are being prepared using coals containing 4 to 8% ash, but the use of super-clean coal will make them more attractive oil substitutes. Furthermore, the general knowledge gained from this research in the area of fine particle flotation will help solve problems in the mineral processing industry in general.

The flotation work involved in the present investigation is divided roughly into two parts. The first part deals with the microbubble flotation of fine coal in the -100, -200 and -400 mesh size range, and the second part deals

with the microbubble flotation of ultrafine coal (-10 micron) prepared by attrition milling. Much of the results obtained in the first part have already been reported (Yoon and Miller, 1982; Sebba and Yoon, 1982; Halsey, Yoon and Sebba, 1982; Yoon, 1982). In this final report, only those that have not been published are given.

1.2 Literature Review

The bubble-particle interaction can be represented by the collision efficiency, E_c, defined as the fraction of particles in the path of a rising bubble that actually collide with the bubble, and the adhesion efficiency, E_a, defined as the fraction of particles colliding with the bubble that actually stick to it. These two parameters can be combined to give the collection efficiency, E,

$$E = E_c \times E_a, \qquad [1]$$

which is the fraction of particles in the path of a bubble that is actually carried to the froth by the bubble. The

decrease in flotation recovery in the fine size range is primarily due to a reduced collision probability, E_c (Fuerstenau, 1980).

If the chemical environment of the system is right (e.g., if the particle is sufficiently hydrophobic), E_a can be unity (Anfruns and Kitchener, 1976; Reay and Ratcliff, 1973). Being hydrophobic may not be enough, however, because if a particle is too small, it will not have enough momentum to thin and rupture the aqueous film and no flotation will be possible (Klassen and Mokrousov, 1963; Collins and Read, 1971). Because of their small mass, fines are often recovered as a result of being entrained in liquid that is carried over into the froth or being entrapped between mineral-laden bubbles rising to the froth. Other factors affecting the adhesion efficiency may include induction time, defined as the minimum contact time required for bubble-particle adhesion, the surface charge of particles and bubbles, dynamic surface tension and contact angle. Some of these parameters are related to the particle size. For example, Klassen and Mokrousov (1963) and Jowett (1980) showed that the induction time increases rapidly with increasing particle size, which explains the poor flotation of very large particles.

The collision efficiency, E_c, is affected by the size and mass of the particles. Whether or not a particle

collides with a bubble depends on the balance of viscous, inertial, and gravitional forces acting on it and the form of the streamlines around the rising bubble (Flint and Howarth, 1971). Since gravitional and inertial forces have little effect on ultrafine particles, the shape of the streamlines around the rising bubble in relation to the particle size should control the probability of a bubble-particle collision. Derjaguin and Dukhin (1960) deduced that for a particular bubble size, there is a critical size of particle below which no collisions can occur. Hydrodynamic analyses done by many investigators (Sutherland, 1948; Flint and Howarth, 1971; Reay and Ratcliff, 1973; Anfruns and Kitchener, 1976) have shown unequivocally that E_c and the flotation rate decrease with decreasing particle size. The most recent theoretical analyses suggest that for a given bubble size and the flotation rate constant (k),

$$k \propto d^N, \qquad [2]$$

where d is the particle diameter, and N is a constant between 1.5 and 2.0. This relationship has been verified experimentally in bench-scale and microflotation tests (Trahar, 1981; Collins and Jameson, 1976; Reay and Ratcliff, 1975).

In some of these hydrodynamic analyses, the collision efficiencies have been calculated assuming that particles

and bubbles in streamline flow collide with each other only by interception. Levich (1962) suggested, however, that large particles can deviate from the streamlines and strike the bubble by inertial impact. Fine particles, on the other hand, show no inertial effects and the collision efficiencies depend more critically on the bubble size (Flint and Howarth, 1971). Other factors affecting the collision efficiency, E_c, include diffusiophoretic motion (Derjaguin and Dukhin, 1960), Brownian motion (Reay and Ratcliff, 1973) and mechanical entrainment (Somasundaran, 1979; Trahar, 1981).

Several methods of improving the flotation of fine particles have been suggested in recent review articles (Trahar and Warren, 1981; Somasundaran, 1979; Fuerstenau, 1980; Trahar, 1981). These involve: 1) increasing the collision efficiency by increasing the effective size of the particles by aggregation, 2) increasing the adhesion efficiency by using selective chemisorbing collectors, and 3) increasing the collision efficiency by using fine bubbles. Since the present work is concerned with the improvement of flotation using fine bubbles, the third method will be discussed in more detail below.

There is overwhelming evidence, both theoretical and experimental, that the use of smaller bubbles should improve the recovery of fines. The hydrodynamic model of Reay and

Ratcliff (1973) suggests that the collision efficiency is proportional to $(1/D_b)^N$, where D_b is the bubble diameter and the exponent, N, is a function of the specific gravity (S.G.) of the particle to be floated: e.g., for glass beads of S.G. = 2.5, N = 2.05.

Since the flotation rate is proportional to the product of the collection efficiency and the volume swept by each bubble, one can derive a relationship between the rate constant, k, and the bubble diameter, D_b, as follows. The number of particles removed by a single bubble will be $E_c \pi (\frac{D_b}{2})^2 h(\frac{N_t}{V_c})$, in which h is the height of a flotation cell, N_t is the number of particles in the cell at time t and V_c is the cell volume. If Q is the volume flow rate of gas, $\frac{8Q}{\pi D_b^3}$ will be the number of bubbles produced per second. Therefore, the total number of particles removed per second will be:

$$- \frac{dN_t}{dt} = \frac{2QE_c h}{D_b V_c} N_t \qquad [3]$$

$$= kN_t \qquad [4]$$

Since $E_c \propto (\frac{1}{D_b})^{2.05}$ for the case of glass beads, the flotation rate constant, k, can be related to bubble diameter, D_b, as follows:

$$k \propto \left(\frac{1}{D_b}\right)^{3.05}, \qquad [5]$$

for a given gas flow rate, Q. According to Eq. [5], one can improve the flotation rate a thousand times by reducing the bubble size only ten times.

Flint and Howarth (1971) have presented a model that gives essentially the same relationship, i.e., $k \propto (1/D_b)^3$, for small particles. Sutherland's derivation (1948) suggests that k should vary as $(1/D_b)^2$ for larger particles, while recent experimental work done by Anfruns and Kitchener (1976, 1977; see also Jameson et al., 1977) shows that $k \propto (1/D_b)^{2.67}$. In summary, the exponent is closer to 3 with fine particles, suggesting a very striking effect due to bubble size, and becomes somewhat less than 3 for the flotation of larger particles.

Very little experimental work has been done to study the effect of bubble size on flotation, probably because it is difficult to control the bubble size during flotation. Nevertheless, the results reported in the literature generally show that Eq. [5] is valid (Reay and Ratcliff, 1975; Anfruns and Kitchener 1976, 1977). Bennett et al. (1958) measured the bubble size distribution in a flotation cell by means of a high-speed camera, and established a relationship, $k \propto (1/D_b)^{3-n}$, in which n has a value between 0.5 and 1.0 for coal flotation. Brown (1965) also found

that a reduction of mean bubble size resulted in higher flotation rates for coal particles.

Besides the probability of collision, E_c, the probability of the particle-bubble aggregate remaining stable until it reaches the concentrate, E_s, is also an important parameter in flotation. E_s is dependent on the force of adhesion between the particle and bubble, which in turn is directly related to the contact angle and inversely related to the particle size (Wark, 1933; Morris, 1952; Gaudin, 1957). Thus, for the flotation of large particles, the bubble-particle aggregate is stabilized by the interfacial energies represented by a finite contact angle.

Small particles, on the other hand, may be retained on the bubble by London dispersion forces without having to form the three-phase contact. This "contactless" flotation concept was put forth by Derjaguin and Dukhin (1981), noting that the tearing-off force of a 1-micron particle is 10^6 times less than that of a 100-micron particle. If contactless flotation is indeed the controlling mechanism for fine particle flotation, then one must conduct fine particle flotation under quiescent conditions. Roe (1980), in fact, has suggested that the flotation of particles of less than 5 microns in diameter requires quiescent conditions, which may support the concept of contactless flotation. The use of smaller bubbles will certainly contribute to minimizing the

turbulence around a bubble, and thus will help provide quiescent conditions.

Previous flotation work conducted with microbubbles on fine coal has shown that the use of these fine bubbles improves the separation efficiency by about 20% over that obtained with conventional flotation (Yoon and Miller, 1982; Sebba and Yoon, 1982; Halsey, Yoon and Sebba, 1982; Yoon, 1982). The process consisted of injecting a "cloud" of microbubbles into the bottom of a flotation column containing a coal slurry pre-conditioned with kerosene. The bubbles were generated with nonionic surfactants such as polypropylene glycol homologues and alcohols. Packham and Richards (1975) found that the probability of collision can be improved by using a "cloud" of sparsely dispersed microscopic air bubbles. The microbubbles used previously were generated using a glass aspirator, as described by Sebba (1971). This technique was inefficient, however, and cannot possibly be scaled up for industrial application. For this reason, new techniques of generating microbubbles have been developed in the present work.

1.3 Objectives

The objectives of this research have been 1) to investigate the possibility of improving the flotation of bituminous coal fines, and 2) to study the mechanisms

involved in generating small bubbles and floating fine particles using these microbubbles. Several different bituminous coal samples have been tested in the present work. Two nonionic frothers, i.e., methyl isobutyl carbinol (MIBC) and a polypropylene glycol (Dowfroth M150), that are most commonly used in the coal industry today, have been employed for generating microbubbles.

The results of the microbubble flotation tests are compared with those of conventional flotation tests using larger air bubbles. Emphasis is placed on the possibility of producing super-clean coal using the microbubble flotation process. The basic strategy of this technique is to pulverize the coal to micron sizes for liberation of mineral matter, and to float the hydrophobic coal particles with microbubbles.

In order to better understand the mechanisms involved, surface chemical experiments have been carried out to determine surface tensions, froth stabilities, electrophoretic mobilities of coal particles, streaming currents of microbubbles, contact angles, and the viscosities of frother solutions.

Success in this research may lead to a new technology of producing super-clean coal using a physical coal cleaning technique. The basic information gathered in the present

work will contribute to an increased understanding of fine particle flotation in general.

II. EXPERIMENTAL

2.1 Materials

2.1.1 Coal Samples

The coal seams used in the present work are given in Table I. Initially, each sample was crushed to -1/4 inch size using a laboratory hammer mill and then further pulverized using a small bench-scale hammer mill to -100 mesh. For batch flotation experiments, the -400 mesh fraction of this sample was taken by dry screening, riffled into 100-gram lots, and stored in a freezer in air-tight plastic bags.

In some flotation tests requiring a finer feed size distribution, samples were prepared by grinding the -100 mesh coal in an attrition mill using 1- and 2-mm diameter stainless steel balls. Figure 1 shows a typical size distribution of a sample ground in the attrition mill.

For electrophoretic measurements, a -1/4 inch +10 mesh sample from the Jawbone seam was cleaned in a magnetite suspension with a specific gravity of 1.3. Care was taken to remove the fine magnetite particles (-325 mesh) from the coal surface by repeatedly washing the sample with water. The clean coal was then ground with an agate mortar and pestle. The -3 micron fraction of the pulverized coal, as

Table I. Description of Coal Samples Used in the Present Work

Coal Seam	Location	Ash (%)
Harlan	Kentucky	35
Taggart	Virginia	40
Pittsburgh No. 8	West Virginia	11
Pittsburgh No. 8	Pennsylvania	3.5
Jawbone	Virginia	7
Pond Fork	West Virginia	5
Eagle Seam	Virginia	34

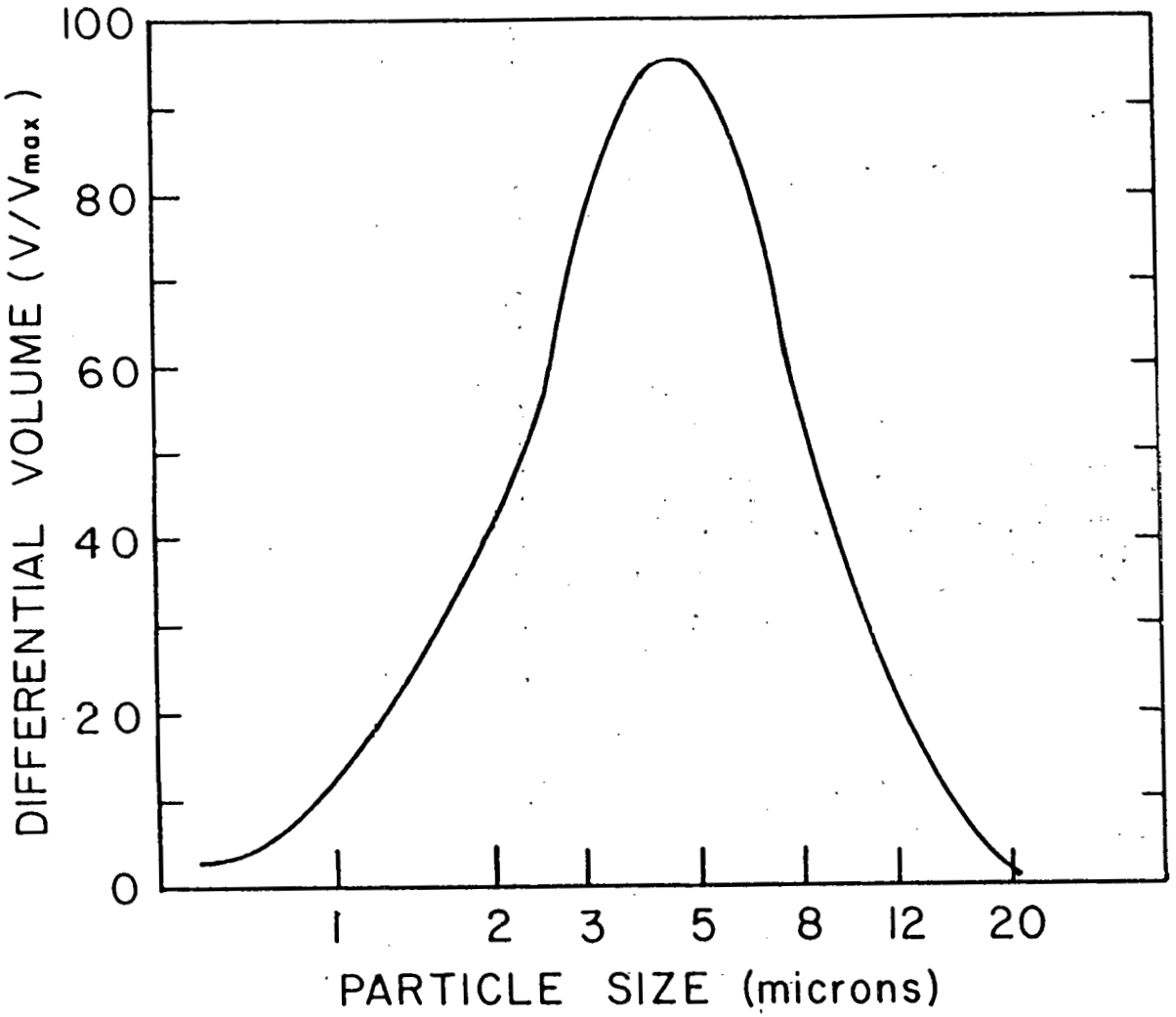

Figure 1. Volume-normalized particle size distribution of Harlan seam coal attrition-ground for 25 minutes.

obtained by sedimention using an Andreasen pipette, was used for microelectrophoresis. A pure quartz sample, purchased from Ward's Natural Science Establishment Inc., was also pulverized and sized in the same manner for electrophoretic measurements.

2.1.2 Reagents

Two different frothers were used in the present work: Dowfroth M150 (Propylene glycol, MW $\simeq$ 400), supplied by Dow Chemical Company, and MIBC (Methyl isobutyl carbinol, MW $\simeq$ 102), obtained from Union Carbide Company. Kerosene was used as a collector throughout this investigation. Hydrochloric acid (HCl) and sodium hydroxide (NaOH) were used for pH control.

2.2 Equipment

2.2.1 Microbubble Generator

Microbubbles were produced using a similar system as the one described by Yoon (1982). This earlier system utilized a microbubble generator made from ground glass joints (Sebba, 1971), but was considered to be impractical for use on the industrial scale. Therefore, a new microbubble generator was constructed and used in the present work.

The complete system used for the microbubble flotation tests is shown in Figure 2. Initially, a frother solution placed in the reservoir (R) is circulated through the microbubble generator (G) by means of a centrifugal pump (P). (For proprietary reasons, a more detailed description of the microbubble generator (G) is not given in this report.) The small size and large number of bubbles generated give a suspension of microbubbles with the appearance of milk. Microbubbles have also been generated using other techniques, as has been described previously (Halsey, Yoon and Sebba, 1982; Yoon and Miller, 1982).

Once a stable, dense microbubble suspension is formed, valve C and stopcock A are opened to allow microbubbles to be bled from the circuit and injected into a flotation cell or other apparatus.

2.2.2 Cell for Microbubble Stability Measurements

The stability of microbubble suspensions was determined using a specially designed cell, as shown in Figure 3. This cell consists of a 100-ml graduated cylinder with its top removed at the 100-ml volume mark and an inlet installed at the bottom of the cylinder.

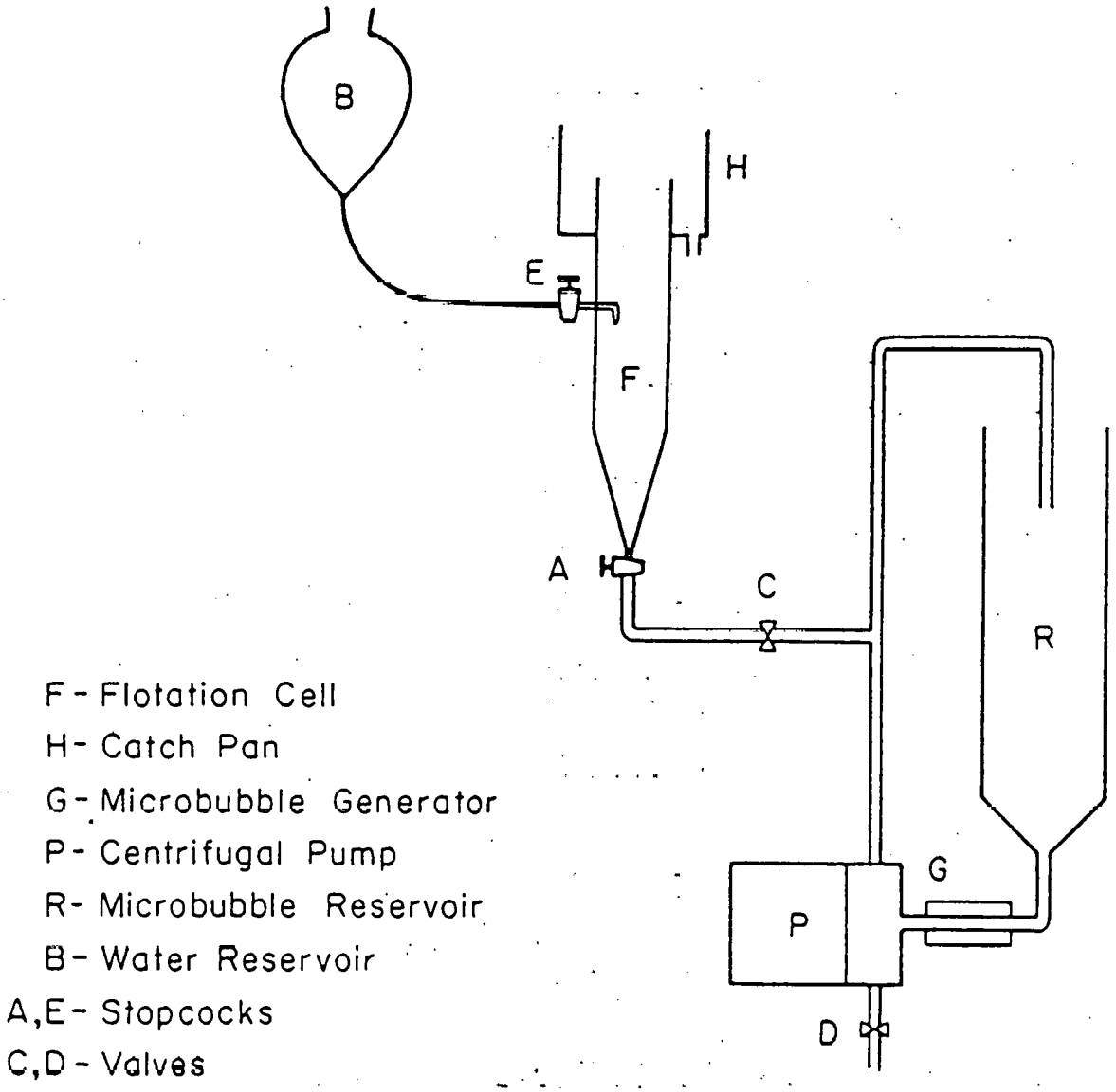

Figure 2. Schematic drawing of the microbubble flotation system.

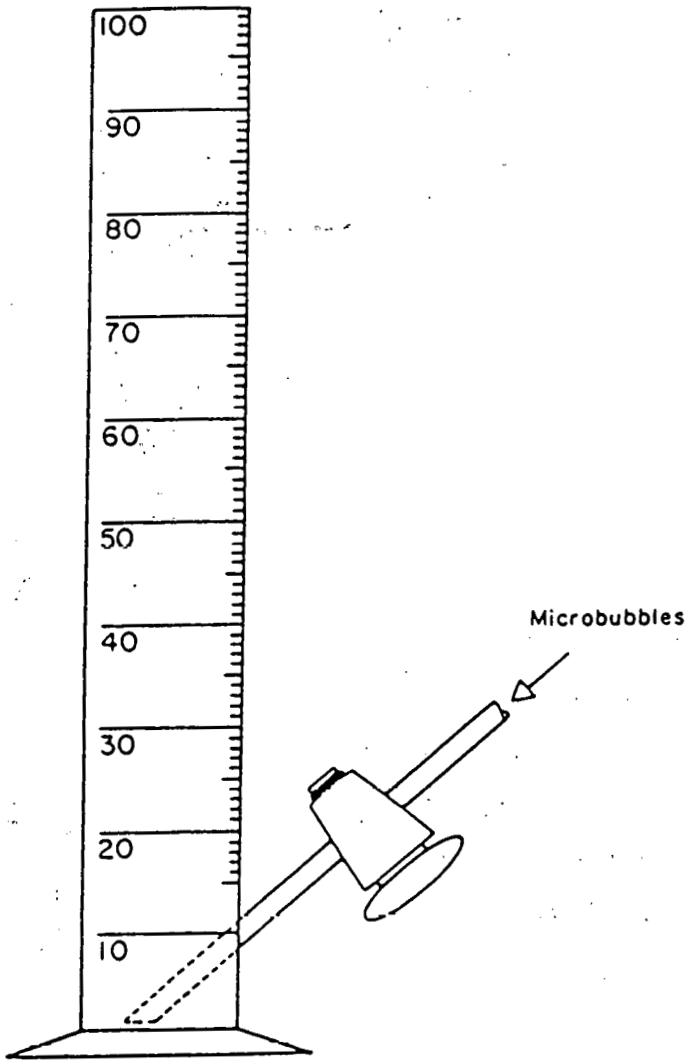

Figure 3. Cell used to determine the stability of microbubble suspensions.

2.2.3 Surface Tensiometer

Surface tension studies of frother solutions were conducted using the maximum bubble pressure technique. The apparatus, shown in Figure 4, is similar to that used by Brown (1932). This apparatus measures the maximum pressure necessary to blow a bubble in a liquid from the tip of a capillary. This pressure is measured with an oil manometer and used in the following equation in calculating surface tension:

$$\gamma = \frac{rg}{2} (hd_1 - \frac{2}{3} rd_2), \qquad [6]$$

where γ = surface tension (dynes/cm)

g = gravitional acceleration (981.2 cm/sec^2)

d_1 = density of manometer fluid (1.045 g/ml)

d_2 = density of test liquid (g/ml)

r = radius of capillary bore (0.09 mm)

h = maximum bubble pressure (cm of butyl phthalate).

2.2.4 Electrophoresis Apparatus

The electrophoretic mobilities of coal particles immersed in surfactant solutions were measured using a Rank Brothers Particle Micro-Electrophoresis Apparatus. All measurements were made using a flat cell made of fused

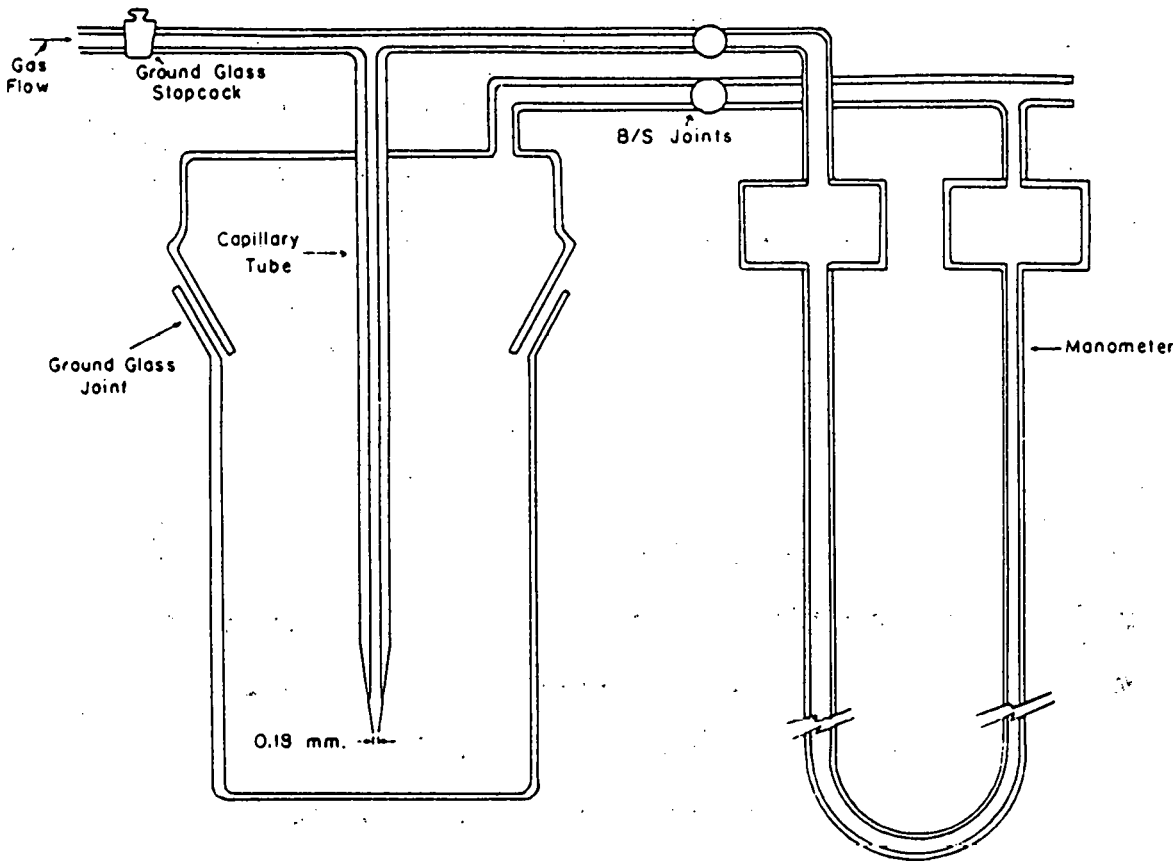

Figure 4. Surface tension apparatus.

quartz (Figure 5). A pair of platinized electrodes fit into the circular ground glass joints on both ends of the flat cell. The flat cell was immersed in a thermostatic bath which was controlled at 25 $\pm$ 1°C. The details of the calibration procedure for the equipment are given in Appendix I.

2.2.5 Streaming Current Apparatus

The cell used for determining the charge of micro-bubbles is shown in Figure 6. The technique involves sending the bubbles past a pair of Ag/AgCl electrodes while measuring the potential difference between them. The potential difference is then converted to current by knowing the resistance between the two electrodes. This streaming current technique, originally developed by Dibbs et al. (1974), suffered from convective currents due to the large cell dimensions. The cell used in the present work (Figure 6) is made of small diameter glass tubing to minimize this problem.

2.2.6 Contact Angle Apparatus

Figure 7 shows the contact angle apparatus used in the present work. A leveled microscope stage fitted with a

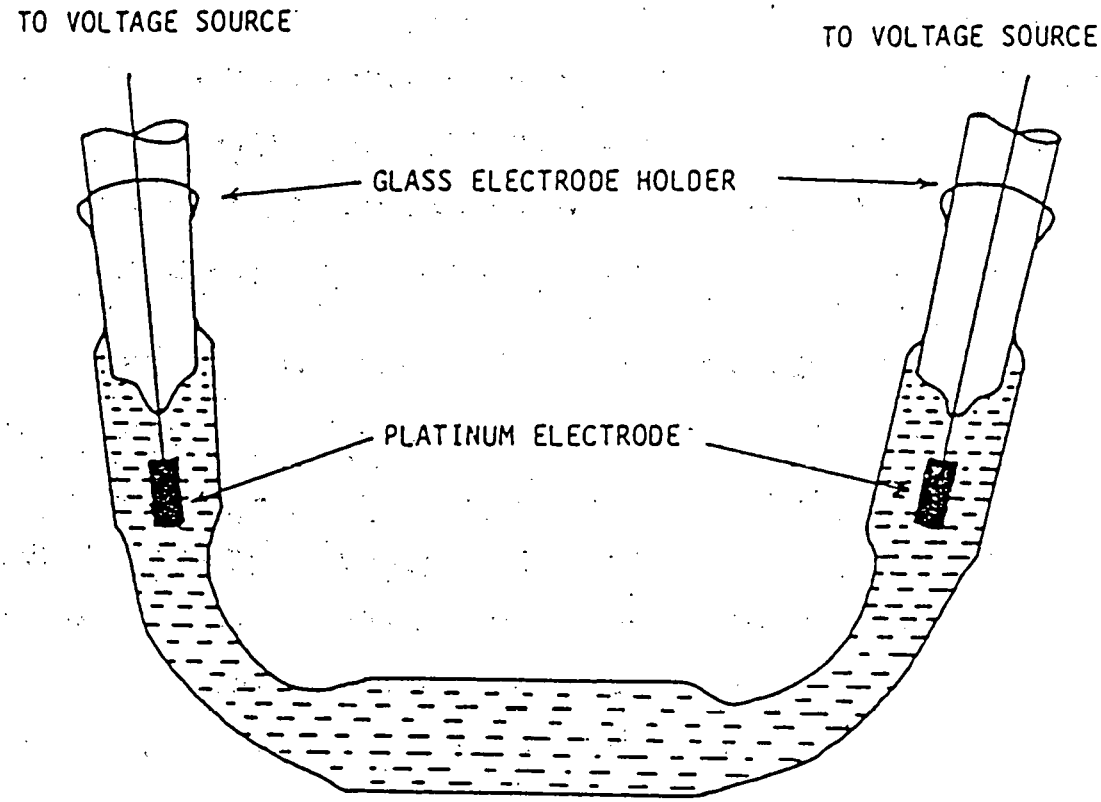

Figure 5. Flat cell used for electrophoretic measurements.

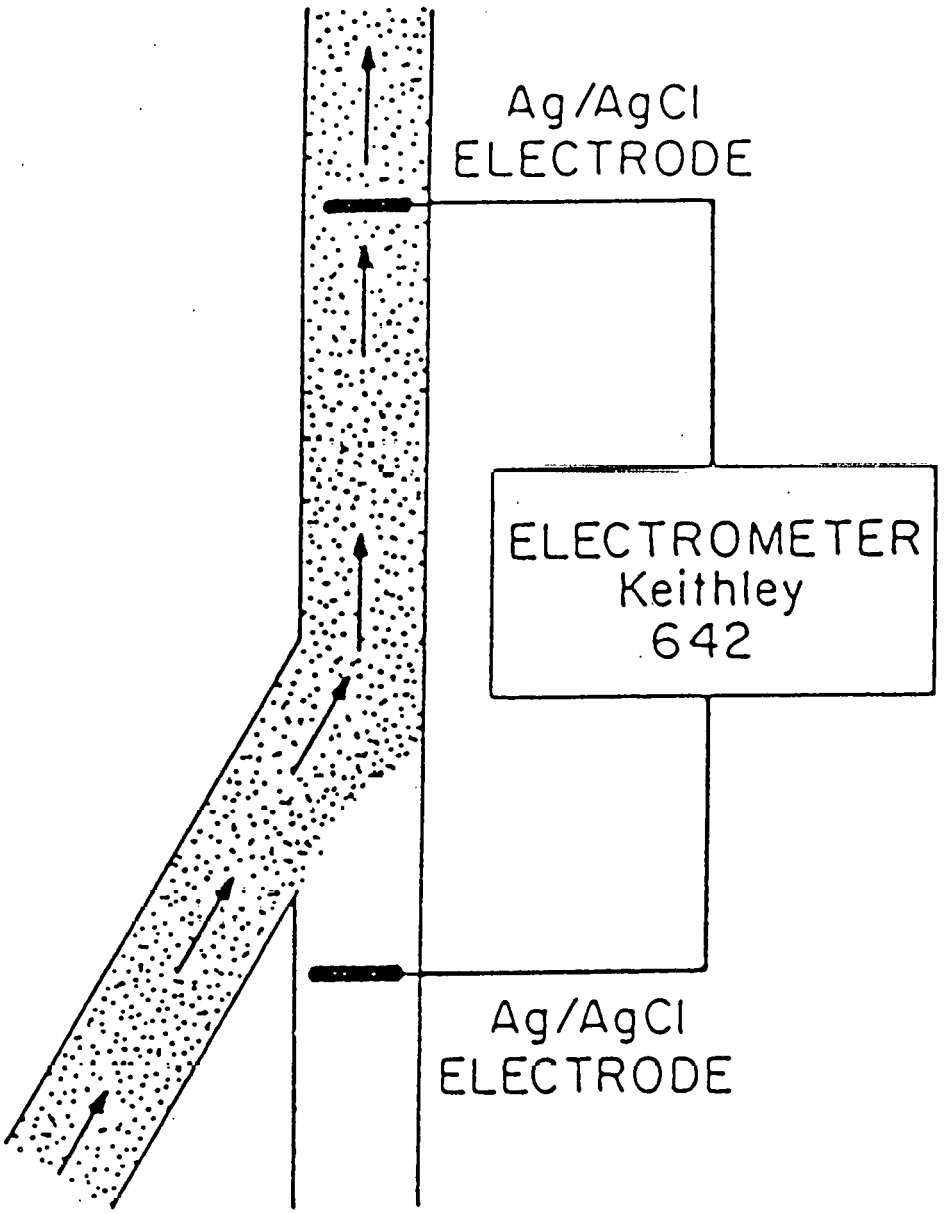

Figure 6. Schematic drawing of the apparatus used to determine streaming currents of microbubbles

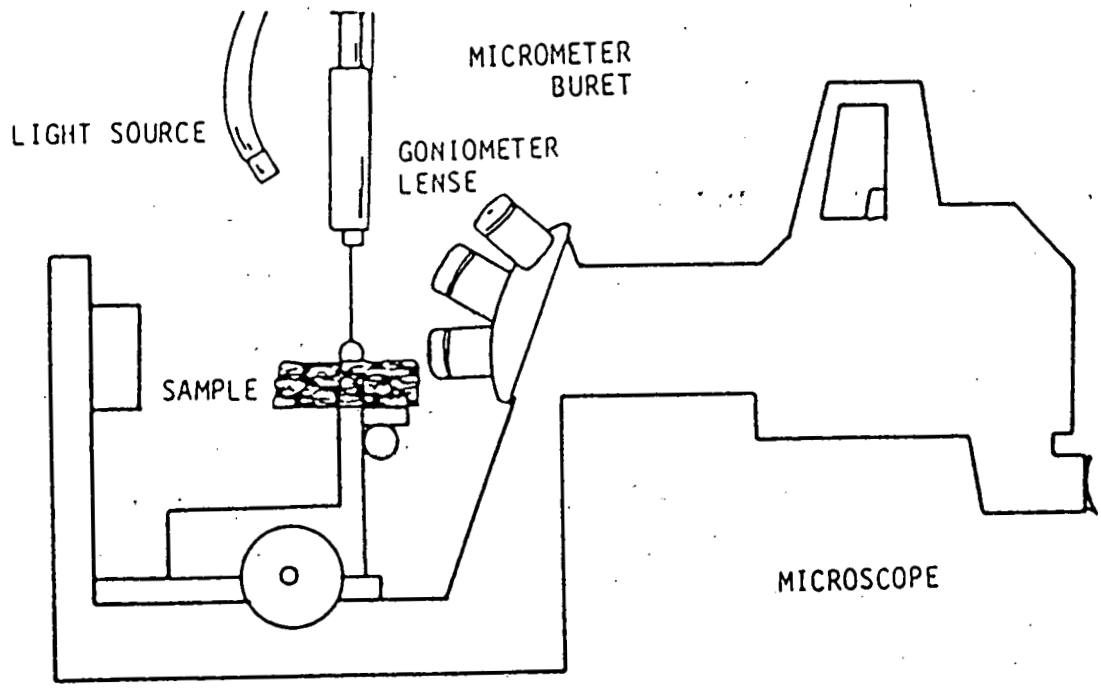

Figure 7. Contact angle apparatus.

goniometer lens was used to measure the equilibrium contact angles.

2.2.7 Viscometer

The viscosity of surfactant solutions was measured using a Thomas-Stormer Viscometer (9730-F10 series), as shown in Figure 8. Viscosities were calculated on the basis of the time required for 100 revolutions of a rotor in the surfactant solution.

2.2.8 Laboratory Flotation Machine

Conventional flotation tests were conducted in an automated Denver laboratory flotation machine (Model D-12), as reported by Luttrell and Yoon (1983). This equipment is designed to reduce human error by automatically controlling the froth level, air flow rate, froth removal rate and impeller speeds. Figure 9 shows the schematics of the apparatus.

2.3 Procedures

2.3.1 Microbubble Stability Measurements

A microbubble suspension was pumped into the bottom of the microbubble stability measuring cell (Figure 3) and

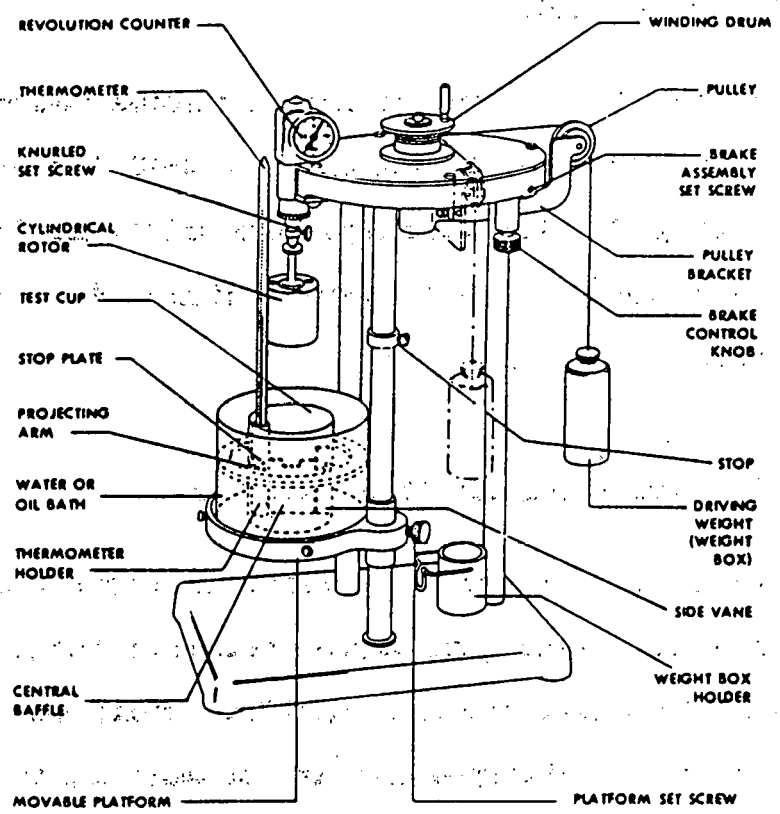

Figure 8. Schematic drawing of viscometer.

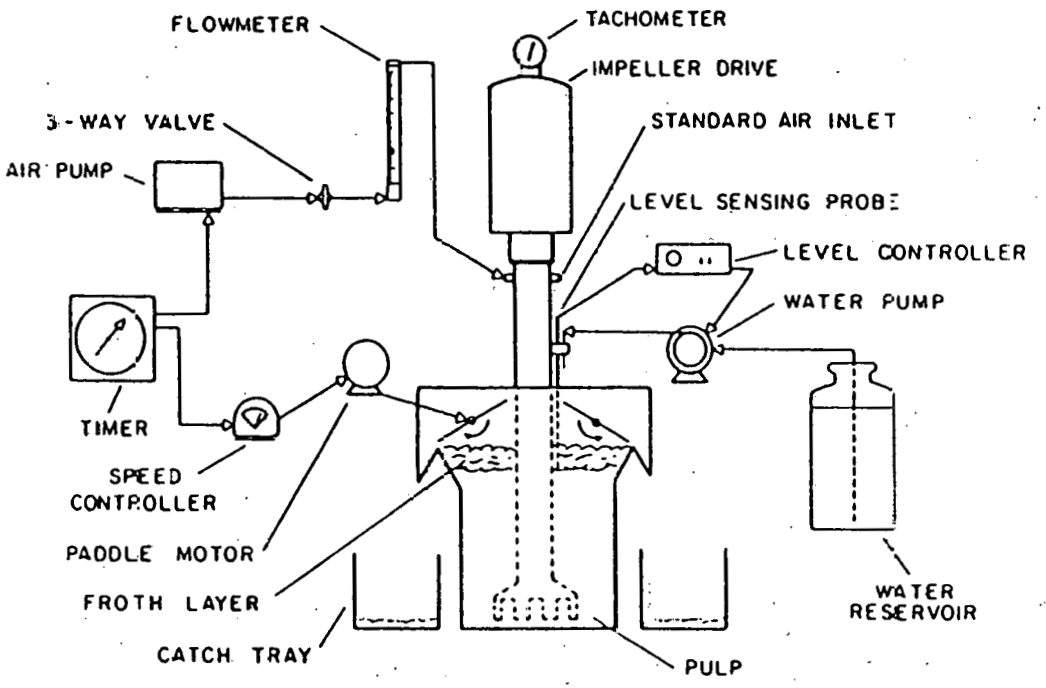

Figure 9. Schematic drawing of the automated laboratory flotation machine used for the conventional flotation tests (from Luttrell and Yoon, 1983).

allowed to overflow the top for approximately one-half minute before the flow was stopped. This procedure was necessary to ensure that at time t = 0, 100 ml of the microbubble suspension was contained uniformly in the column. The volume of clear solution that formed under the rising microbubbles was then measured as a function of time. At the end of each measurement, the total volume of the clear solution was also recorded and used to determine the volume fraction of air in the microbubble suspension. All tests were conducted at ambient temperature and natural pH.

2.3.2 Surface Tension Measurements

A fixed volume (40.5 ml) of each surfactant solution was placed in the bubble chamber for each measurement. This was necessary to position the tip of the capillary within the surface of the liquid, and to eliminate the necessity of making a correction for the hydrostatic pressure depending on the depth of the capillary below the surface. A positive pressure was maintained in the system to prevent a capillary rise of solution into the capillary bore.

Once the solution was in place, the gas flow (nitrogen) was increased until a bubble formation frequency of approximately one per second was obtained. The maximum pressure necessary to blow a bubble through the surface of the liquid

was then measured with a manometer (in centimeters of butyl phthalate).

Several readings were made for each solution to ensure reproducibility. The measurements were carried out at ambient temperature. After each test, the apparatus was washed with chromic acid and then with double-distilled water and allowed to dry.

2.3.3 Electrophoretic Mobility Measurements

The electrophoretic mobilities of the coal particles were measured using a Rank Brothers Particle Micro-Electrophoresis Apparatus, Mark II. The size of the coal particles used for electrophoresis was -3 microns and was calculated using the Stokes equation:

$$t = \frac{18h\eta}{d_t^2(\rho_s - \rho_f)g}, \qquad [7]$$

in which η is the viscosity, ρ_s is the density of the solid, ρ_f is the density of the fluid, g is the gravitional acceration, and d_t is the diameter of particles settling at distance h in time t.

A quantity of surfactant was added to the suspension containing -3 micron coal particles to obtain a desired concentration. The pH of the slurry was adjusted using HCl

and NaOH. The pulp was then conditioned for 30 minutes while being agitated prior to the electrophoretic measurements.

After the conditioning, a portion of the slurry was transferred to the flat cell (Figure 5) and the electrodes were placed in the cell. The cell was then immersed in the thermostatic bath at 25 $\pm$ 1°C. Twelve readings were made at each frother concentration and averaged to calculate each mobility.

2.3.4 Streaming Current Measurements

Frother solutions were prepared by adding a quantity of surfactant to double-distilled water and adjusting the pH using HCl and NaOH. A steady stream of frother solution, in which no microbubbles were dispersed, was first passed through the working electrode to obtain a steady baseline on a strip-chart recorder. Then, a stream of microbubbles was passed through the working electrode to obtain another constant potential value with the reference electrode immersed in the same frother solution but without contact with the microbubbles. The difference between the two base-lines was taken as the potential due to the bubbles streaming past the electrode. Knowing this potential difference and the resistance between the electrodes, the

streaming current was calculated.

2.3.5 Contact Angle Measurements

Polished sections of lump coal samples (Pittsburg No. 8 seam) were prepared using 600-grit sand paper, followed by polishing with 1.0-, 0.3-, and then 0.05-micron alumina powder. Surfactant solutions were prepared with double-distilled water and the pH was adjusted using HCl and NaOH. The temperature was maintained at 25 $\pm$ 1°C. A specimen was then mounted on the mobile stage, and a 4-microliter drop of surfactant solution was placed on its surface, and the contact angle was measured. At least 3 drops were placed on each specimen, and the measured contact angles were averaged.

2.3.6 Viscosity Measurements

The movable platform on the viscometer (Figure 8) was positioned so that the rotor, when lowered, was centered inside the test cup. The test cup was then filled with a solution to 1/4 inch above the rotor. The time required for 100 revolutions of the rotor in the liquid, as indicated by the revolution counter, was then measured with a stopwatch. A calibration curve was first constructed by measuring the time per 100 revolutions of the rotor in solutions of known

viscosity. The viscosities of the test samples were read from this curve.

2.3.7 Flotation Tests

a. Microbubble Flotation Tests

After grinding, a coal sample was split into representative portions. Samples that were attrition-ground were split in slurry form, while those that were dry-ground were riffled.

The coal samples were agitated for three minutes in a Waring blender with approximately 300 ml of tap water at the highest rpm (approximately 16,000 rpm). This procedure was necessary to ensure that all the coal particles were completely wet. A volume of kerosene was then added by means of a microliter syringe and the agitation was continued for another three minutes. After this conditioning period, the slurry was transferred to a flotation cell.

A microbubble suspension was prepared by circulating a frother solution for at least 50 seconds through the generator to ensure the formation of a dense microbubble suspension. A known volume of the microbubble suspension was then pumped into the bottom of the flotation cell. After this injection, the slurry was allowed to stand for four minutes, during which time the microbubbles rose to the surface of

the pulp, carrying coal particles and forming a stable froth. The froth was removed by slowly pumping water through the side (stopcock E, Figure 2) of the column, thus flooding the froth product over into the catchpan. The sink product (refuse) was drained through the bottom of the column by opening stopcock A after the froth was removed. Usually, the froth product from the first stage was repulped in the blender and floated again. After each test, the products were filtered, dried and analyzed for ash.

b. Conventional Flotation Tests

Each test was conducted on a 100-gram coal sample in a 2-liter flotation cell using tap water. The pulp was agitated at 900 rpm for three minutes to wet the coal sample, and conditioned for another three minutes after adding a measured volume of kerosene. Following this, a known amount of frother was added and the pulp was further conditioned for three minutes. Flotation commenced upon opening the air valve to provide 4.5 l/min of air. Both the first- and second-stage flotation were conducted for four minutes. The flotation products were filtered, dried and analyzed for ash.

c. Oil Agglomeration Tests

In each test, a 50-gram sample was agitated for five minutes in a blender with 500 ml of tap water. A volume of kerosene was then added and the slurry was conditioned for five minutes at the highest rpm. The resulting agglomerates were washed on a screen by spraying with fine streams of water. The mesh size of the washing screen was chosen so that it corresponded to the top size of the feed coal. The products were filtered, dried and analyzed for ash.

d. Flotation Kinetics Tests Using Different Bubble Sizes

In order to determine the effect of bubble size on flotation rate, batch kinetics tests were carried out using bubbles of three different size consists at a constant gas flow rate. The apparatus used for these experiments was essentially the same as shown in Figure 2, except for minor modifications to change bubble size. After a microbubble flotation test, the stopcock (A) at the bottom of the flotation cell was replaced with glass frits of two different porosities, i.e., 4-8 micron and 145-175 micron. This was done to generate larger bubbles by a sparging mechanism and to use them for flotation. It is also noted that microbubbles were generated using a glass aspirator, as described by Sebba (1971), instead of the generator (G in Figure 2) developed in the present work for flotation tests.

Two series of kinetics tests were conducted using -100 mesh and -500 mesh Eagle seam coal samples. The -500 mesh coal was prepared by pulverizing the -100 mesh coal in a stirred ball mill for 25 minutes. Each series consists of flotation tests using i) microbubbles, ii) bubbles generated using 4-8 micron frit and iii) bubbles generated using 145-175 micron frit. The gas flow rate during the microbubble flotation test was calculated by multiplying the volume flow rate of the microbubble suspension with the volume fraction of air in the suspension. The froth products overflowed continuously into the catch pan and were collected in beakers at predetermined time intervals. Each timed-cut sample was filtered, dried and analyzed for ash.

III. RESULTS

3.1 Frother Characteristics

Halsey, Yoon and Sebba (1982) reported the results of using two different frothers in the microbubble flotation of coal. They showed that MIBC was the more selective of the two, but gave low yields even at high concentrations. More promising results were obtained using Dowfroth M150. This frother produced much higher yields than MIBC, but the selectivity was relatively poor. In the present work, characteristics of these two frothers have been studied in an effort to better understand the mechanisms involved in producing microbubbles and using them in the flotation of fine coal.

3.1.1 Stability of Microbubbles

Figure 10 compares the stability of microbubble suspensions produced with Dowfroth M150 to those generated using MIBC at reagent concentrations of 250 mg/l. The final volume of clear solution remaining after each test is given at the end of each curve.

The bubbles generated using Dowfroth M150 rose through the column at a rate of 0.40 cm/sec, while those generated using MIBC rose at a rate of 0.88 cm/sec. These results

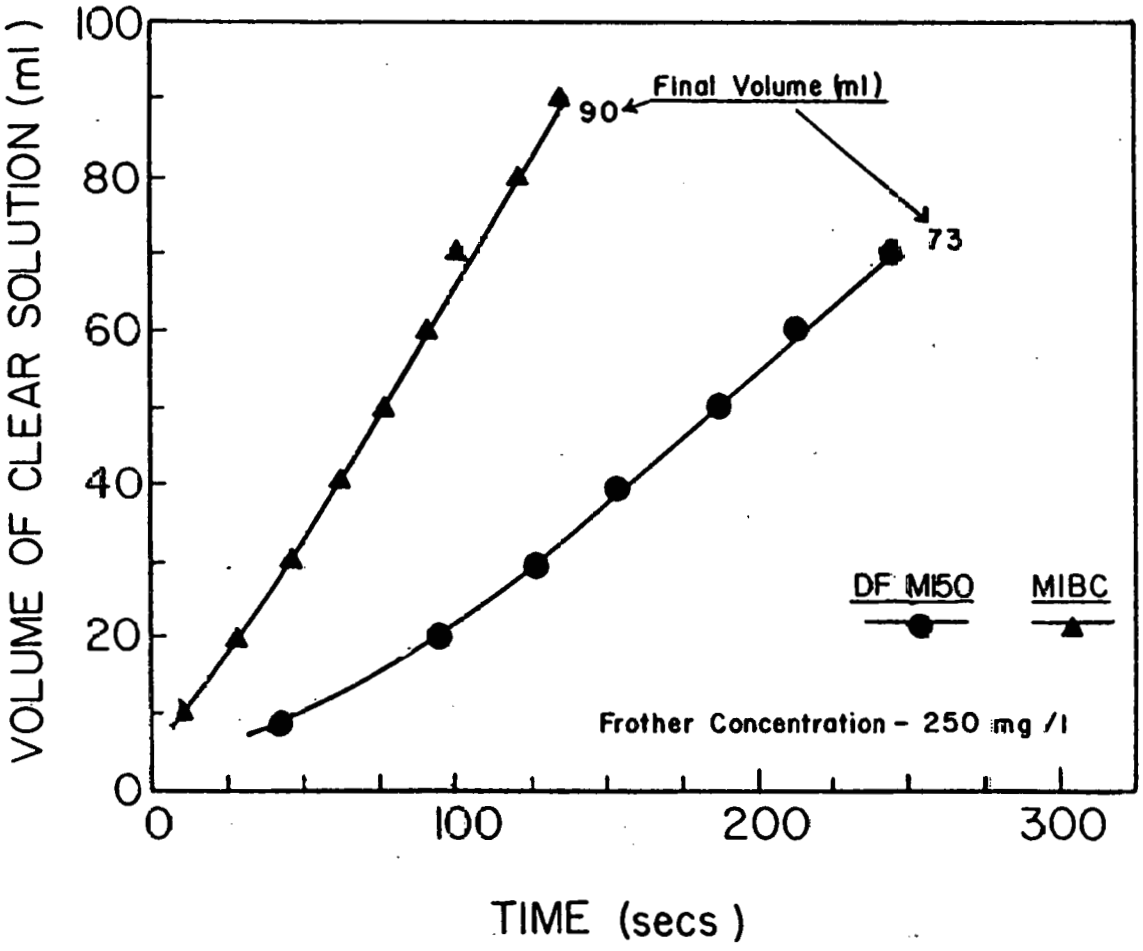

Figure 10. Stability of microbubble suspensions produced with Dowfroth M150 and MIBC.

indicate that Dowfroth M150 produces microbubble suspensions twice as stable as those produced with MIBC.

The microbubbles generated using Dowfroth M150 also contained a larger percentage of air than those produced using MIBC. The volume fraction of air for Dowfroth M150 was 27% and only 10% for MIBC.

3.1.2 Surface Tension of Dowfroth M150 and MIBC Solutions

Figure 11 shows the surface tension of aqueous solutions of Dowfroth M150 and MIBC as a function of concentration. Dowfroth M150 gave a lower surface tension than MIBC over the concentration range tested, and the slope of the curve, $d\gamma/d \log c$, was larger with Dowfroth M150. It has been shown that the stability of froth produced by alcohol increases as $d\gamma/d \log c$ increases (Whelan and Mainhood, 1955; Booth et al., 1962). Therefore, the results shown in Figure 11 suggest that Dowfroth M150 is a stronger surfactant than MIBC.

3.1.3 Electrophoretic Mobilities of Coal and Quartz Particles

Figure 12 shows the electrophoretic mobilities of coal and quartz particles as a function of frother concentration at pH 7. Both coal and quartz particles become more

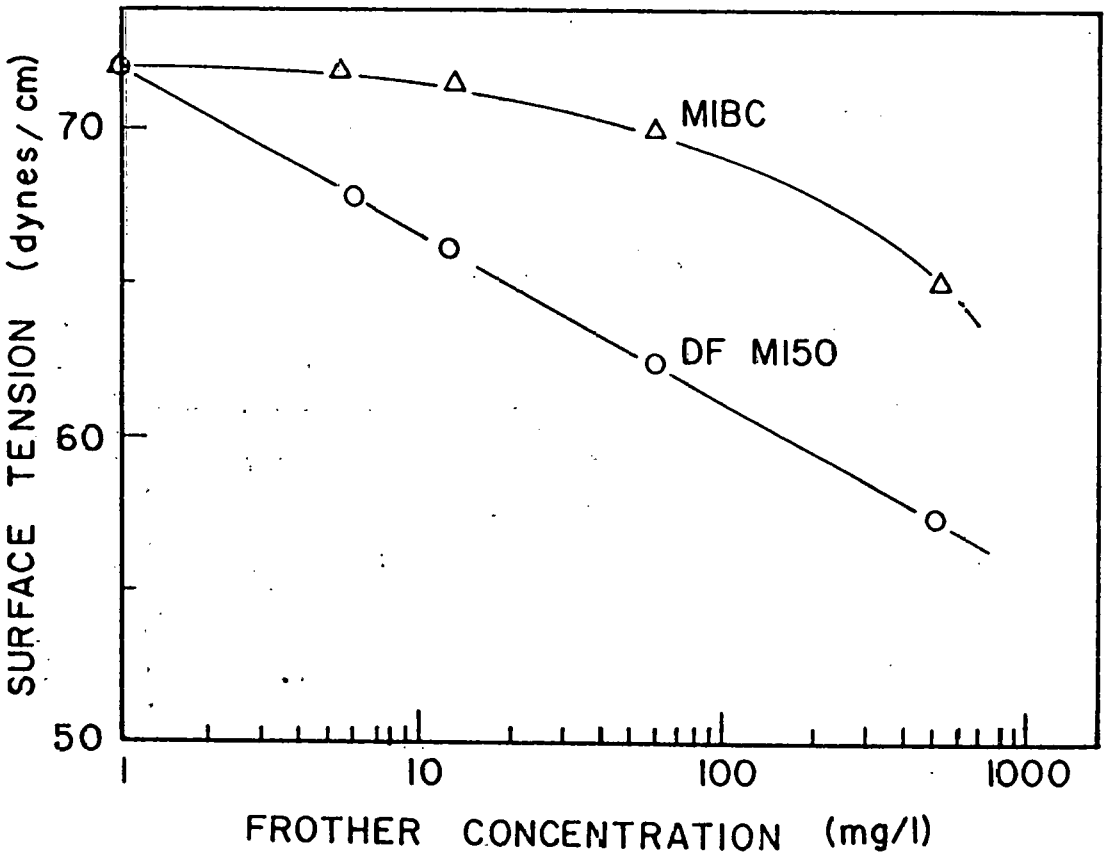

Figure 11. Surface tension of Dowfroth M150 and MIBC solutions as a function of concentration.

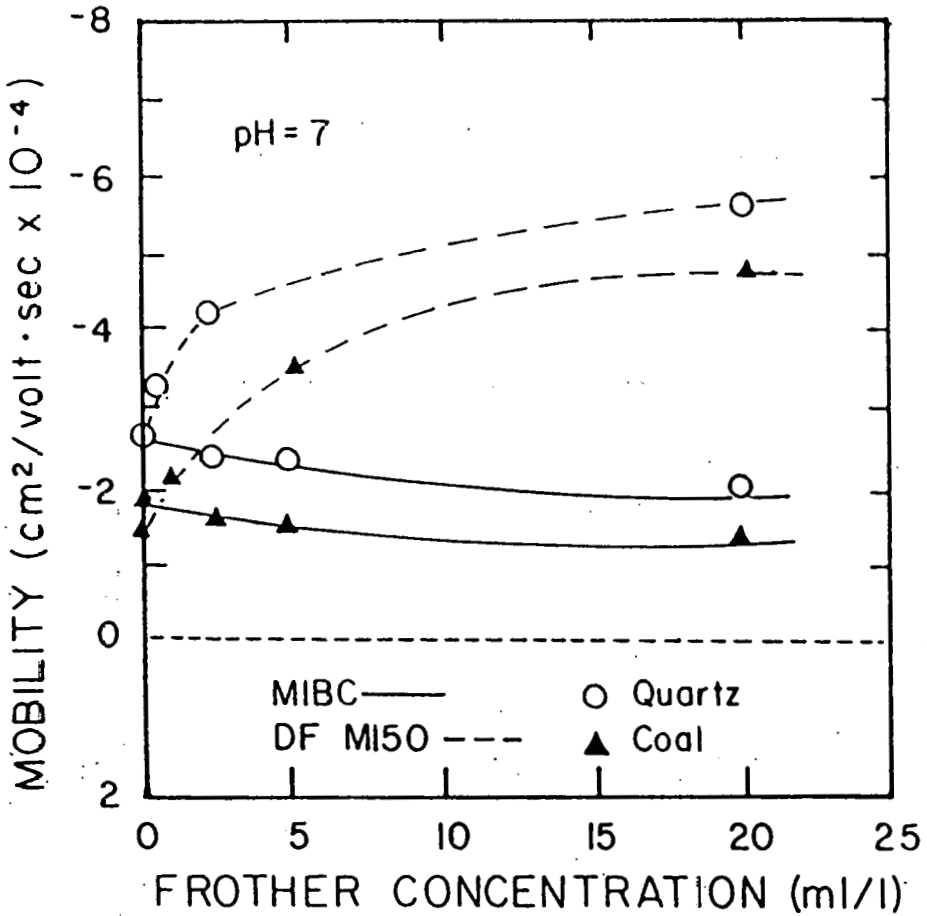

Figure 12. Electrophoretic mobility of coal and quartz particles as a function of frother concentration at pH 7.

negative with increasing Dowfroth M150 concentration. In the presence of MIBC, however, the mobilities do not change significantly. These results may suggest that Dowfroth M150 adsorbs significantly on both coal and quartz, while MIBC does not. However, it is possible that MIBC adsorption on these solids may not result in a modification of the charge characteristics.

3.1.4 Charge Characteristics of Microbubbles

Figure 13 shows the results of streaming current measurements conducted on the microbubble suspensions produced with Dowfroth M150 and MIBC at pH 7. The bubbles generated with Dowfroth M150 are shown to be negatively charged throughout the concentration range tested. Thus, the adsorption of Dowfroth M150 at the air/water interface appears to produce a net negative charge, as is the case at the coal/water and quartz/water interfaces. The increasing streaming current in the vicinity of 0.15 ml/l might indicate the formation of molecular aggregates such as micelles. However, the surface tension results shown in Figure 11 do not indicate the formation of micelles for Dowfroth M150 at the concentrations tested.

Low concentrations of MIBC appear to give a positive charge on the surface of the bubbles. Above 0.17 ml/l, however, the bubble charge was negative. At low pH values,

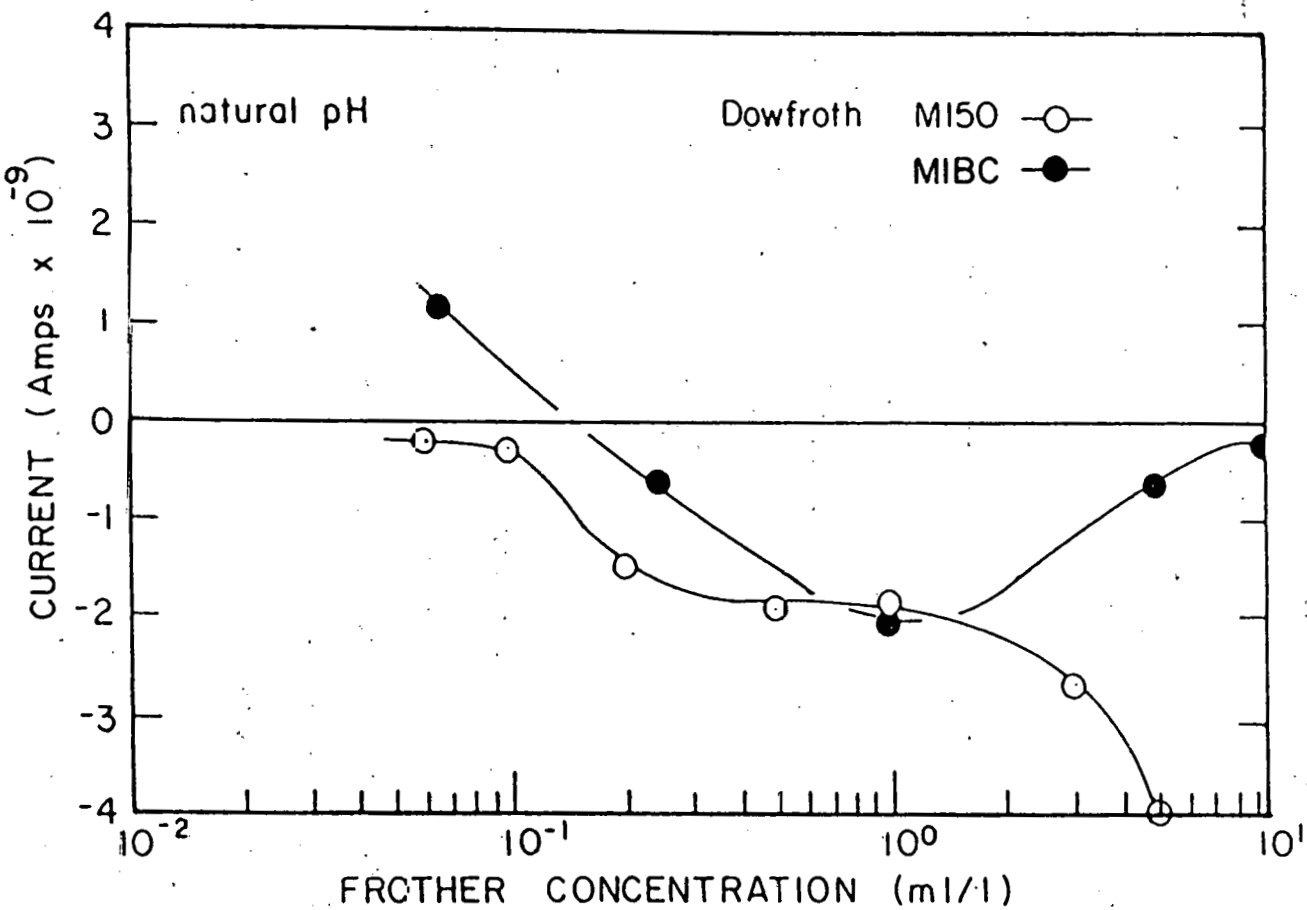

Figure 13. Streaming current of microbubbles as a function of frother (Dowfroth M150 and MIBC) concentration.

bubbles produced in Dowfroth M150 solutions exhibit positive charge, as shown in Figure 14. The isoelectric point for these bubbles occurs at pH 4.8.

3.1.5 Contact Angle Measurements

Figure 15 shows the results of contact angle measurements made on the Pittsburgh No. 8 seam coal as a function of frother concentration. A contact angle of approximately 70 degrees has been measured in the absence of surfactant, and increases with increasing frother concentration up to 90 degrees. Note that Dowfroth M150 gives lower contact angles than MIBC, despite the fact that the electrophoretic measurements (Figure 12) suggest a stronger adsorption of Dowfroth M150 on coal. However, electrophoresis does not necessarily indicate an adsorption of surfactants, as has already been noted.

3.1.6 Viscosity Measurements

Figure 16 shows the viscosity of surfactant solutions as a function of concentration. Here it can be seen that solutions of Dowfroth M150 are more viscous than MIBC solutions, especially at high concentrations. These results may be related to the froth stability and foam drainage, which may significantly affect the flotation recovery and

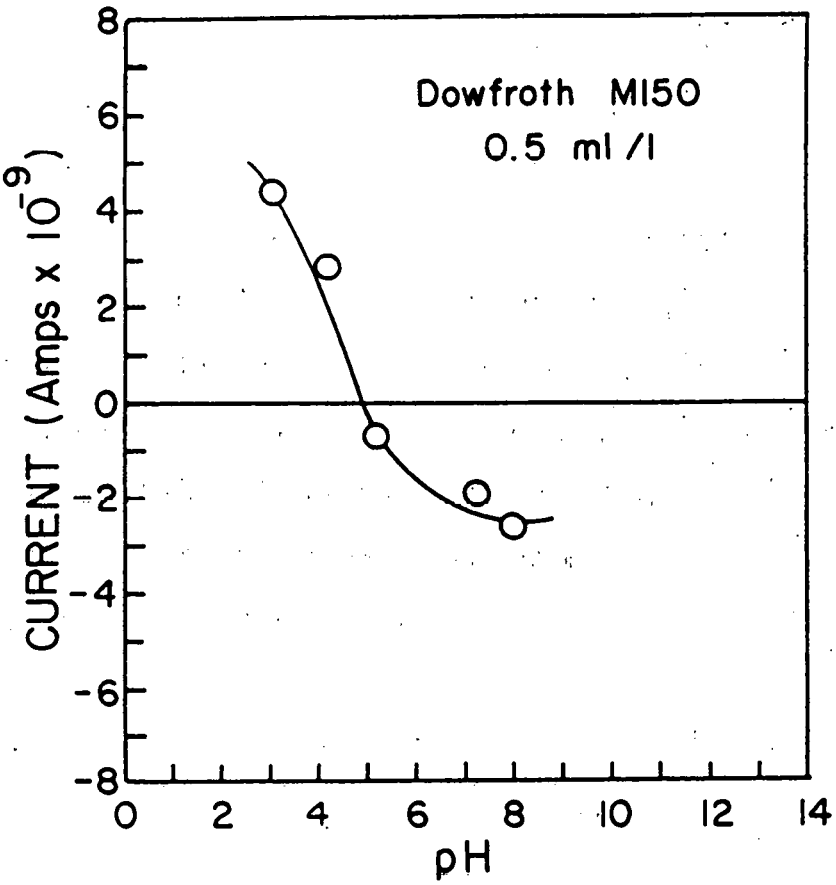

Figure 14. Streaming current of microbubbles produced with Dowfroth M150 as a function of pH.

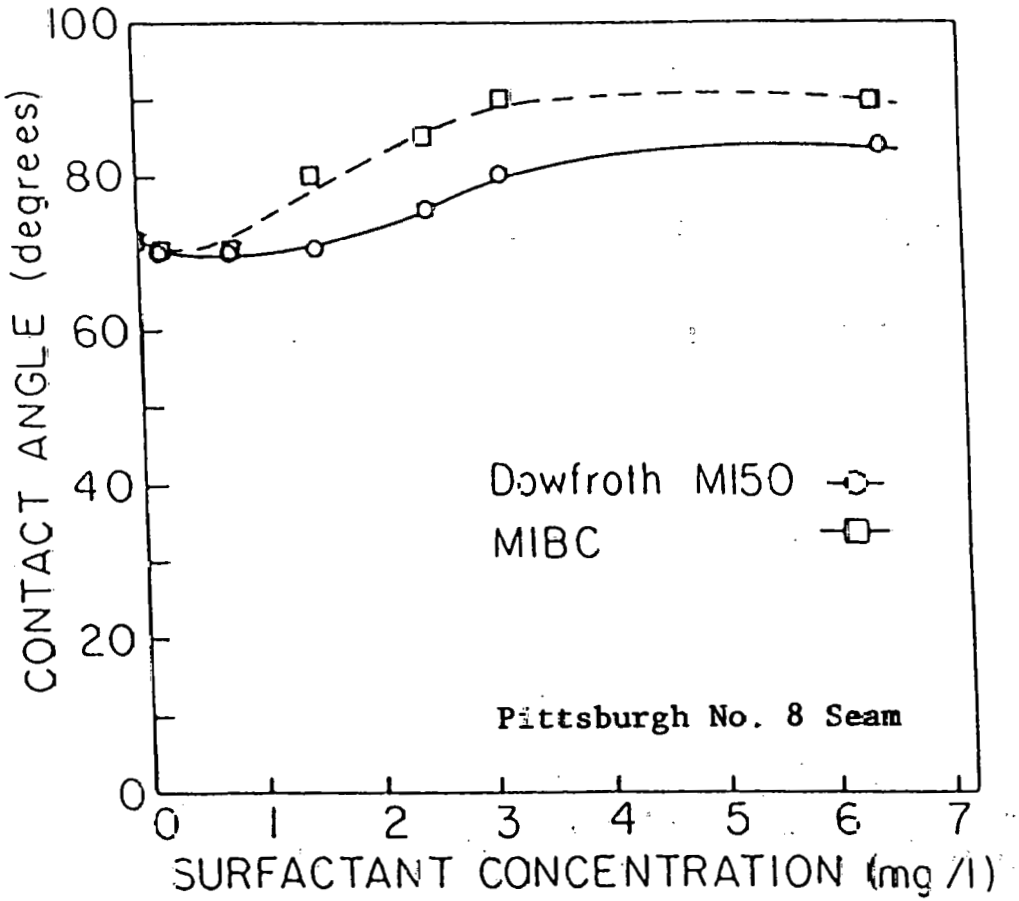

Figure 15. Contact angles of sessile drops of frother solutions on Pittsburgh No. 8 seam coal as a function of concentration.

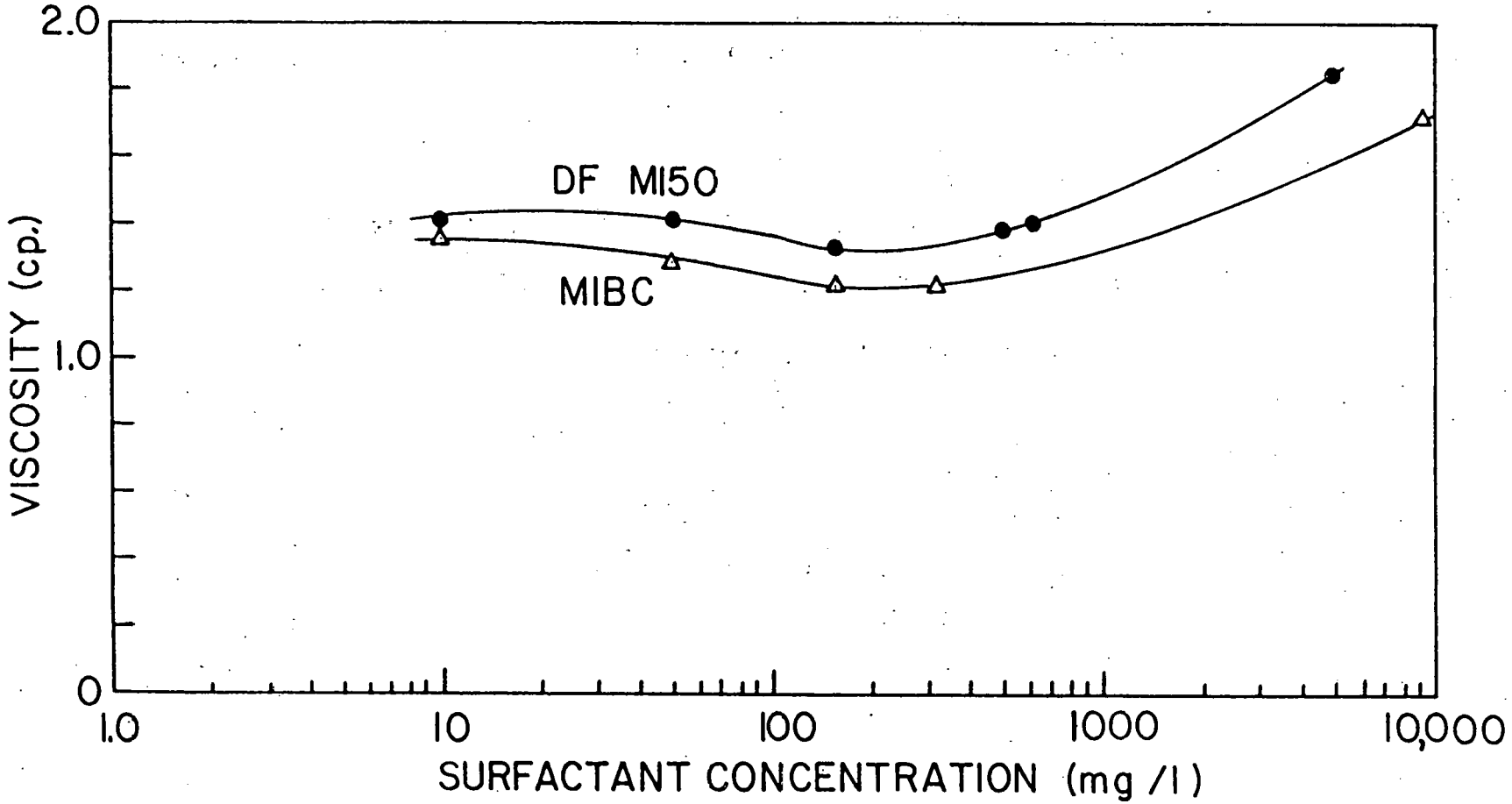

Figure 16. Viscosity of frother (Dowfroth M150 and MIBC) solutions as a function of concentration.

selectivity. The larger viscosity of Dowfroth M150 solution may be due to the large molecular weight of the reagent.

3.2 Flotation of Coal

3.2.1 Effects of Frothers

The results of two series of flotation tests conducted on the Harlan seam coal (-400 mesh) with 37% feed ash, using microbubbles generated with varying amounts of MIBC and Dowfroth M150, are compared in Figure 17. In each series, 3 lb/ton kerosene was used and the frother concentration was varied from 1 to 6 lb/ton. As shown, Dowfroth M150 produced a maximum yield of 80%, whereas the yields obtained with MIBC were only 30% maximum. MIBC was more selective, however, than Dowfroth M150 at higher concentrations, producing clean coals assaying less than 12% ash compared to 20% ash for those produced with Dowfroth M150. These results are similar to those reported by Halsey, Yoon and Sebba (1982).

Figures 18, 19 and 20 show the results of two-stage microbubble flotation tests conducted on three different coal samples. In the first stage, varying amounts of Dowfroth M150 were used, while the frother addition was fixed in the second stage. The tests shown in Figure 18 were conducted on the Harlan seam coal (-400 mesh) which

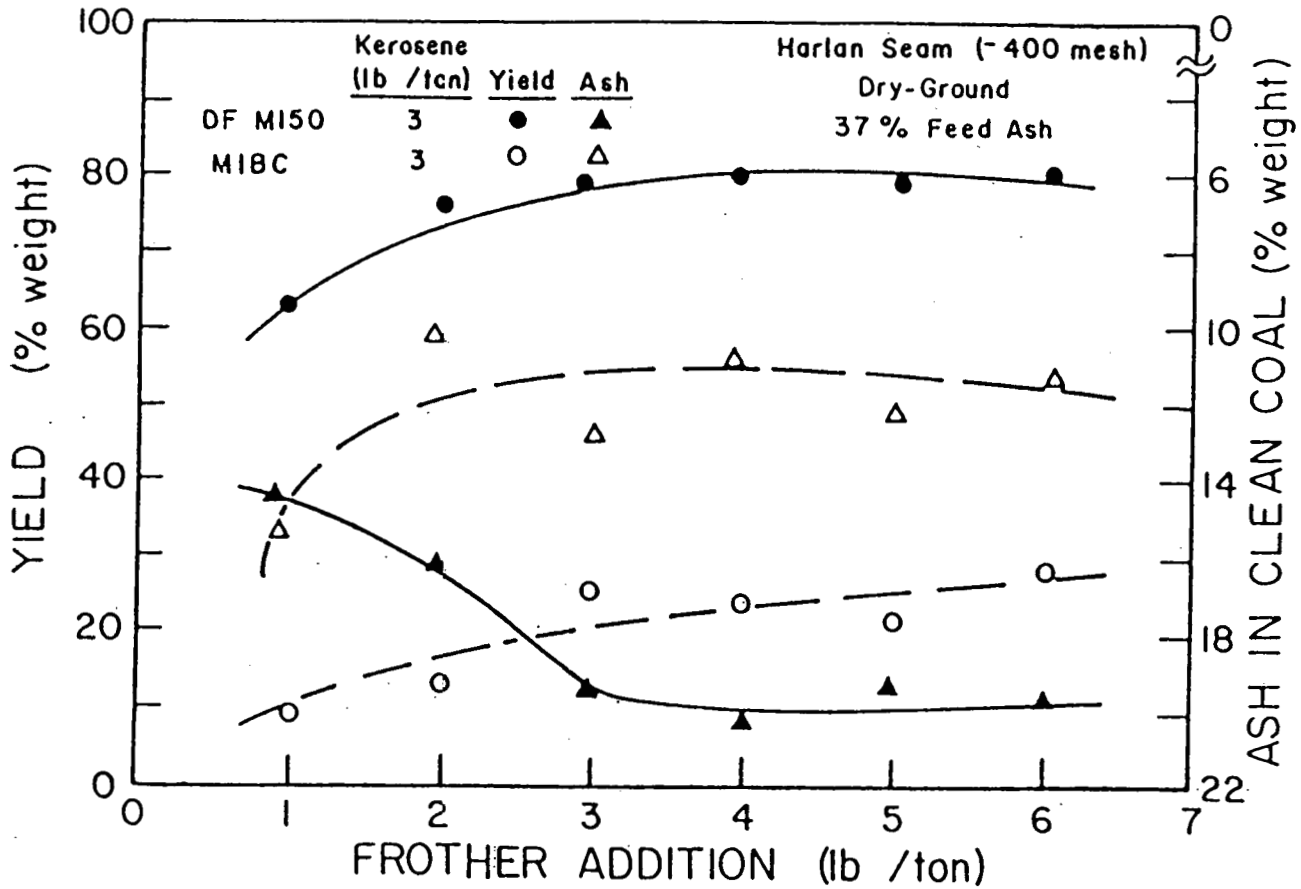

Figure 17. Results of single-stage microbubble flotation tests conducted on Harlan seam coal (-400 mesh) as a function of frother (Dowfroth M150 and MIBC) addition.

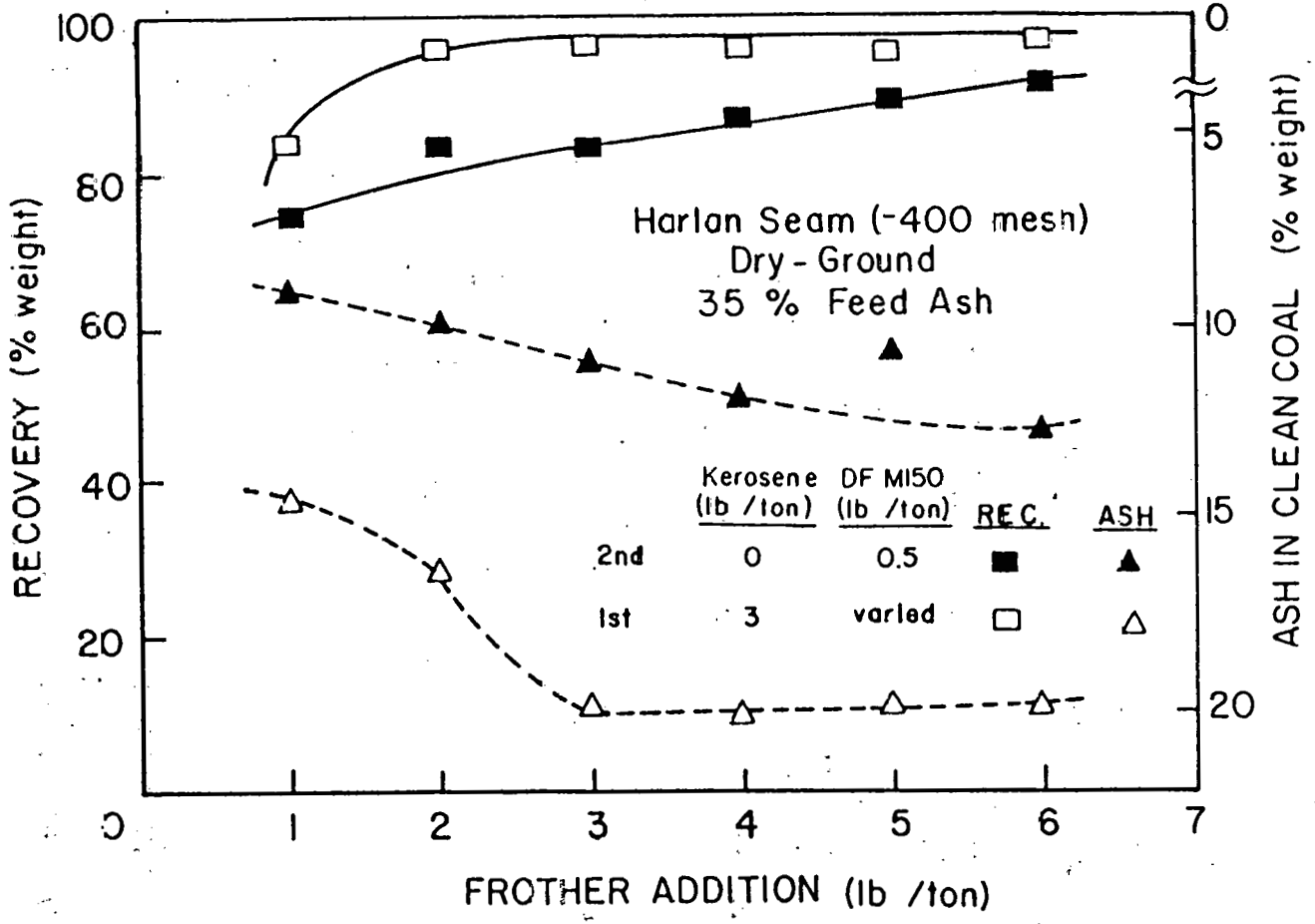

Figure 18. Results of two-stage microbubble flotation tests conducted on Harlan seam coal (-400 mesh) as a function of frother (Dowfroth M150) addition in the first stage.

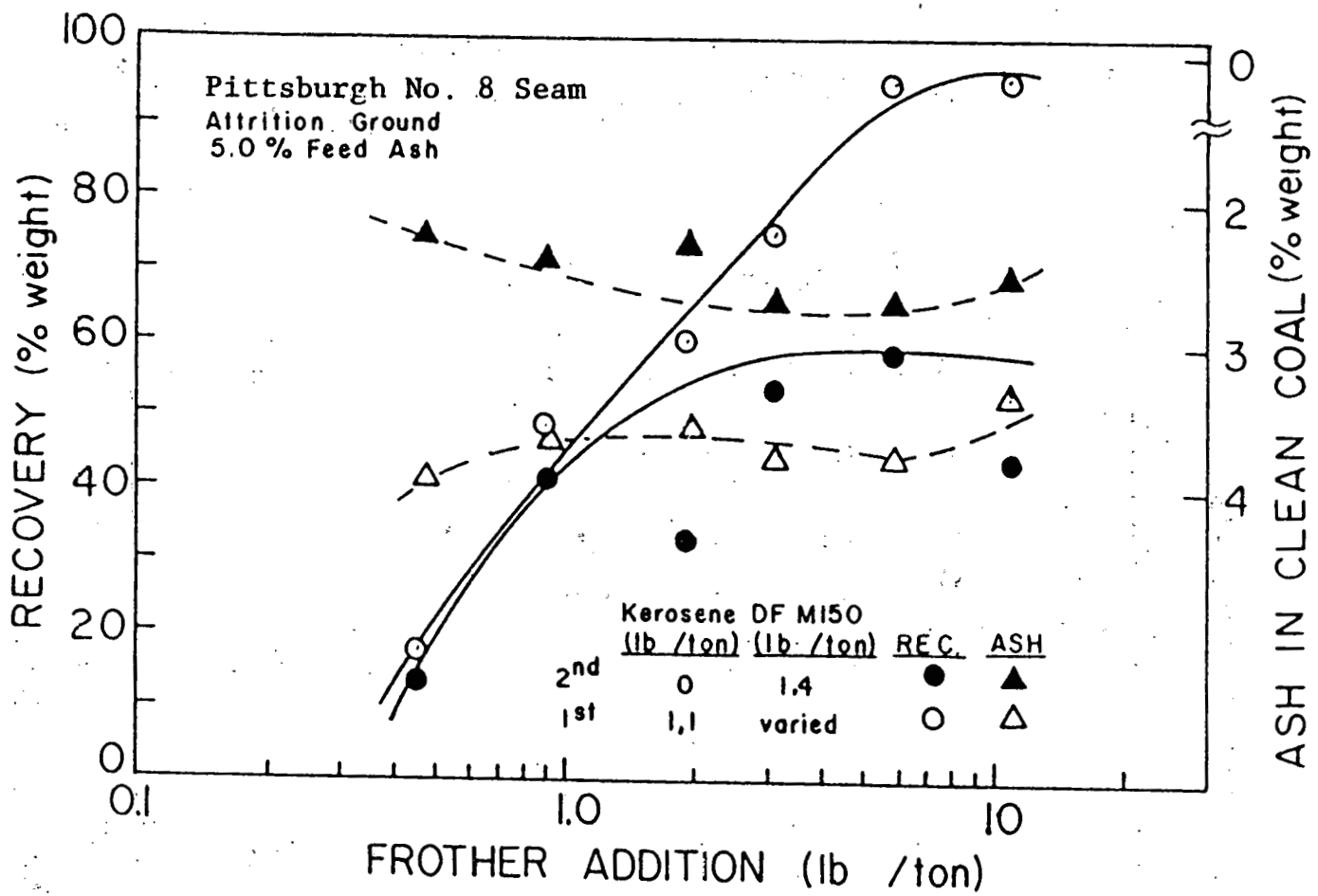

Figure 19. Results of microbubble flotation tests conducted on the attrition-ground Pittsburgh No. 8 seam coal as a function of frother (Dowfroth M150) addition in the first stage.

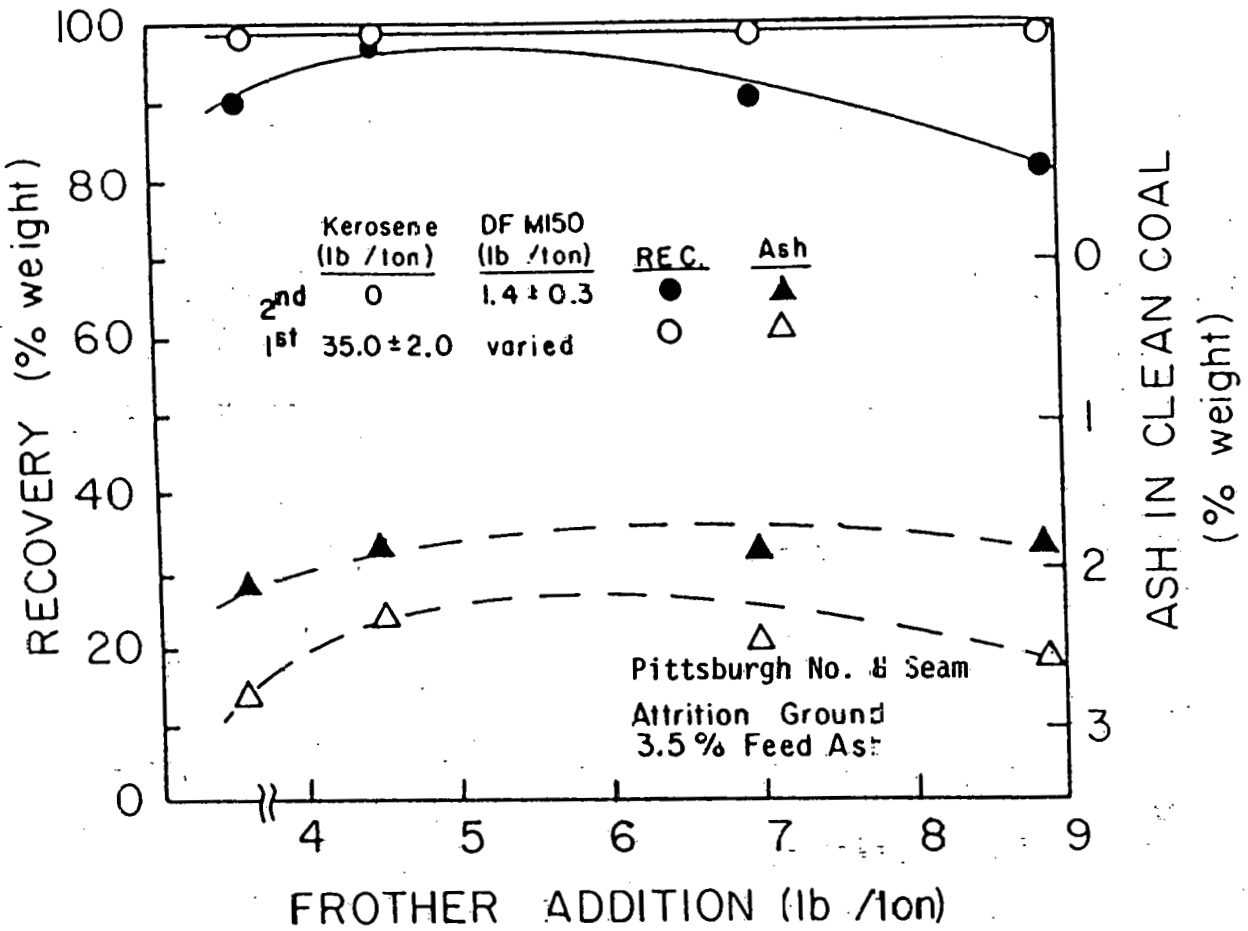

Figure 20. Results of microbubble flotation tests conducted on the attrition-ground Pittsburgh No. 8 seam coal as a function of frother (Dowfroth M150) addition in the first stage.

contained approximately 35% feed ash. Three lb/ton kerosene was used to condition the coal prior to the first stage of flotation and 0.5 lb/ton Dowfroth M150 was used in the second stage. When using 1 lb/ton Dowfroth M150, the first-stage flotation produced a clean coal product assaying 14.5% ash with 84% recovery. After the second stage flotation, the ash content was reduced to 9.0%, although at the expense of a lower recovery (75%). At higher frother concentrations, recoveries as high as 97% were obtained, but the percent ash of the froth products increased with increasing frother additions. This may be attributed to the entrainment and/or entrapment of ash particles, which appeared to increase with increasing frother additions and, hence, with the increasing number of bubbles per unit volume of flotation pulp.

Figure 19 shows the effect of frother addition in the first stage on the flotation of a low-ash (5% feed ash) Pittsburgh No. 8 seam coal. The sample was attrition-ground for 25 minutes to produce a flotation feed with a mean particle size of 4-5 microns (see Figure 1). The results show that when using only 1.1 lb/ton kerosene on this ultrafine coal sample, between 3 and 4 lb/ton Dowfroth M150 was required to produce recoveries over 80% in the first stage. The second-stage flotation cleaned this coal to 2.2% ash at lower frother concentrations, but the recovery was lower.

Figure 20 shows that at a much higher kerosene addition (35 lb/ton), recoveries as high as 99% can be obtained with less than 4 lb/ton Dowfroth M150. After the second-stage flotation, using only 1.4 lb/ton Dowfroth M150, a clean coal product assaying as low as 1.8% ash was produced (3.5% feed ash), with 85% coal recovery.

Figures 21, 22 and 23 illustrate the effects of Dowfroth M150 additions in the second stage. The results shown in Figures 21 and 22 were from tests conducted on Harlan seam coal (-400 mesh) under identical conditions, except that 1 lb/ton kerosene was used in the second-stage flotation in the latter. The kerosene addition in the second stage improved both the recovery and the ash rejection at lower frother additions, but at higher frother additions higher ash froth products were produced, most likely due to entrainment.

The effect of frother additions in the second stage is shown in Figure 23, which gives the results of the tests conducted on the Pittsburgh No. 8 seam coal attrition-ground for 25 minutes. Because of the longer grinding time, the flotation feed had a much finer size distribution than in the previous tests (Figures 21 and 22). Only 1 lb/ton kerosene was used in the first-stage flotation, but a large amount (5.5 lb/ton) of Dowfroth M150 was used. Despite the small amount of kerosene used, very high

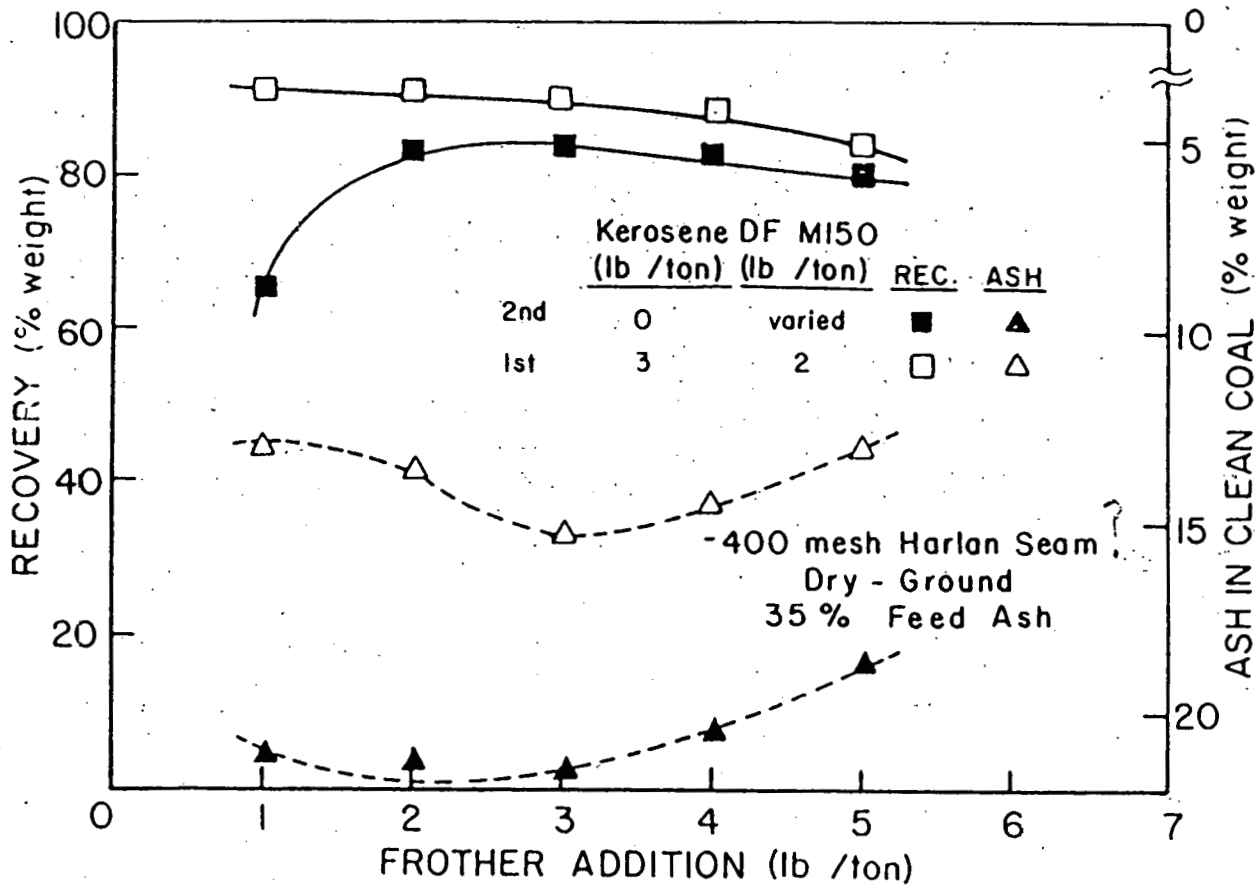

Figure 21. Results of microbubble flotation tests conducted on the Harlan seam coal (-400 mesh) as a function of frother (Dowfroth M150) addition in the second stage.

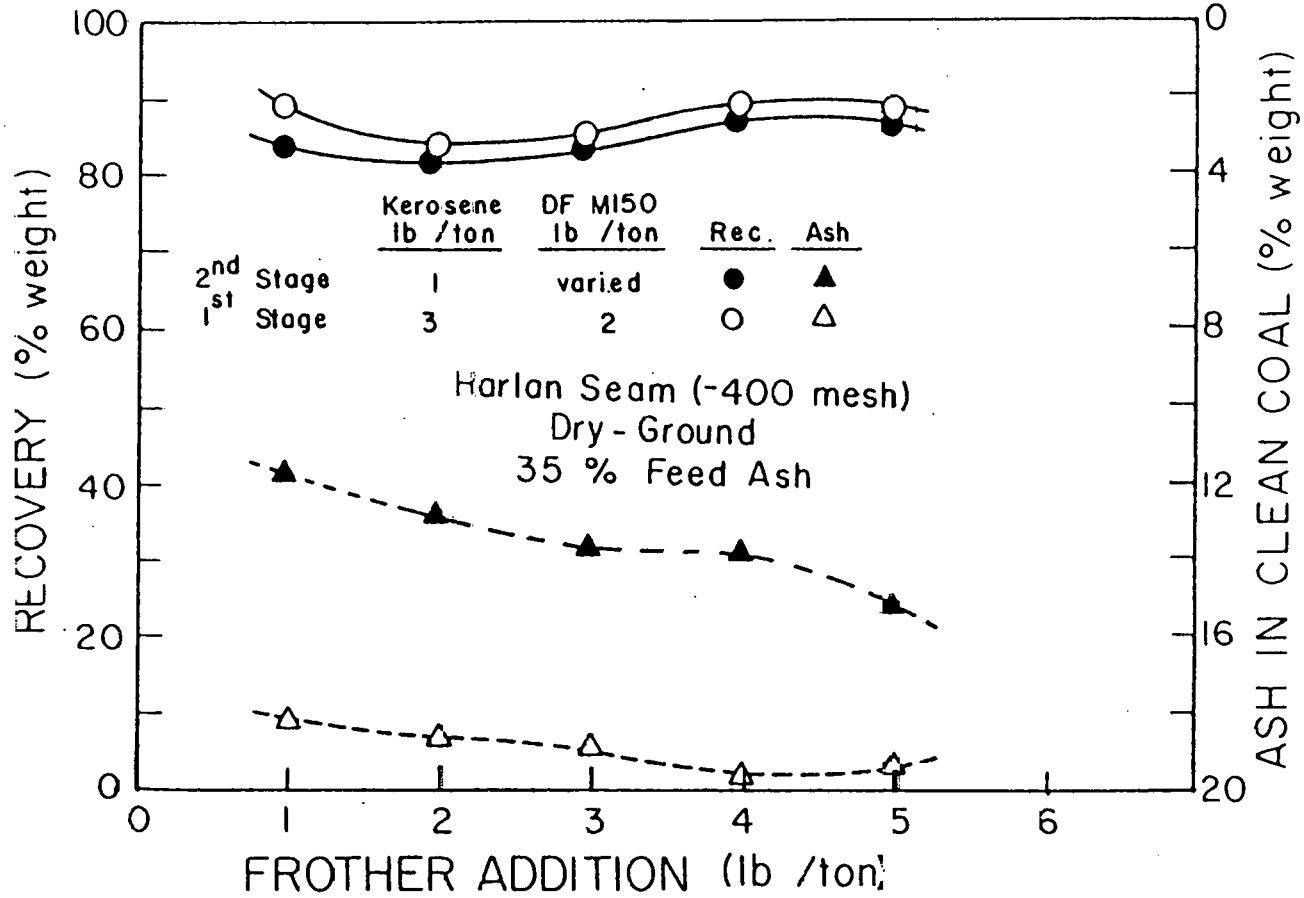

Figure 22. Results of microbubble flotation tests conducted on the Harlan seam coal (-400 mesh) as a function of frother (Dowfroth M150) addition in the second stage. Kerosene was also used in the second stage.

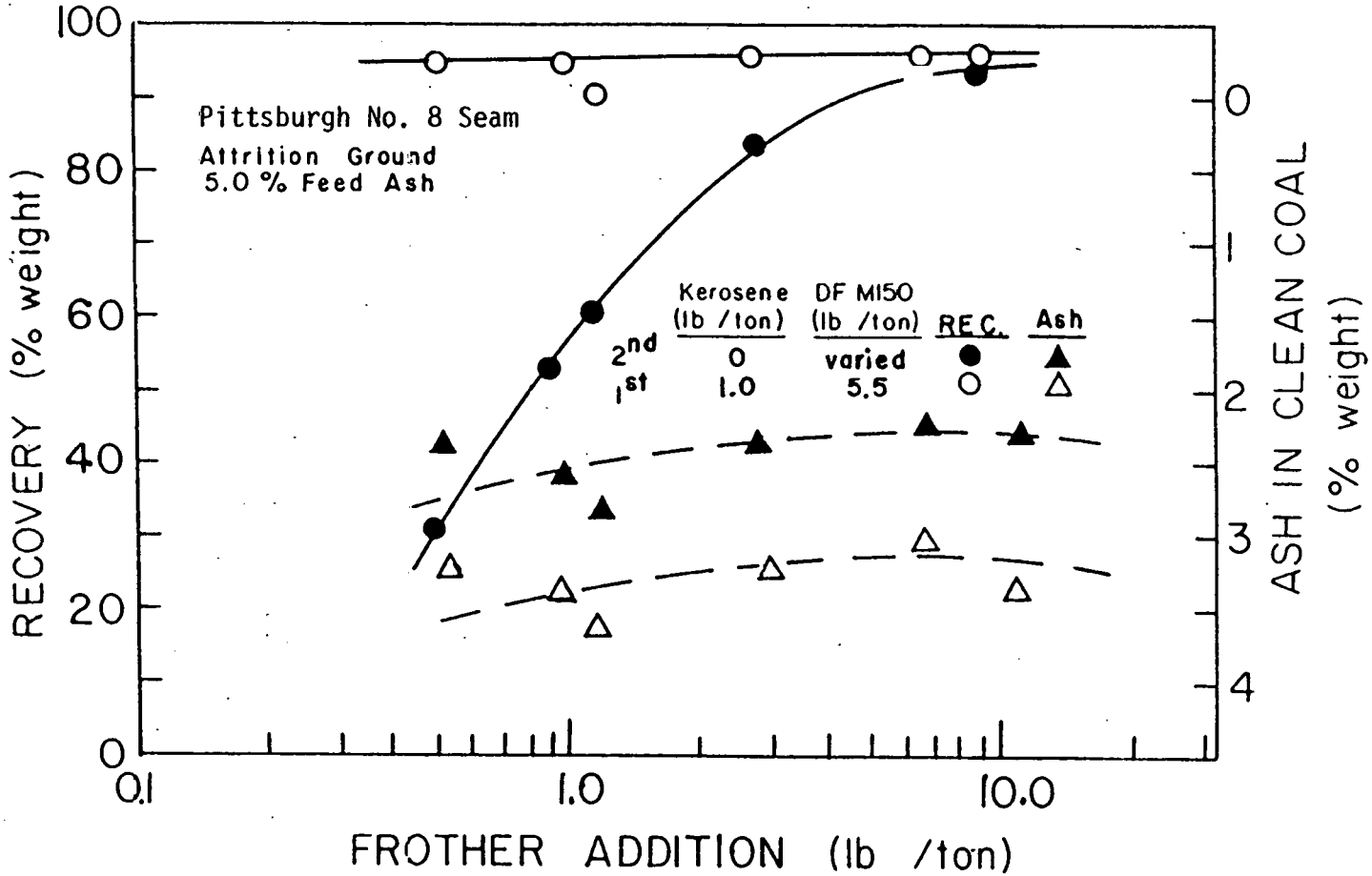

Figure 23. Results of microbubble flotation tests conducted on the attrition-ground Pittsburgh No. 8 seam coal as a function of frother (Dowfroth M150) addition in the second stage.

coal recoveries were obtained with low ash contents in the froth products. In the second-stage flotation, however, as much as 6 lb/ton Dowfroth M150 was needed to obtain over 90% recovery. The large amounts of frother might have contributed most significantly to obtaining high recoveries by producing smaller air bubbles, while the smaller kerosene dosage minimized the ash entrainment.

3.2.2 Effects of Kerosene

Figure 24 shows the results of microbubble flotation tests conducted on the Harlan seam coal (-400 mesh). The sample was prepared by dry-pulverization using a laboratory hammer mill, and the -400 mesh fraction was taken as the flotation feed. In this series, varying amounts of kerosene were used in the first stage and none was added in the second stage. The amounts of Dowfroth M150 used were 2 lb/ton in the first stage and 1 lb/ton in the second stage.

With no kerosene, the recoveries of the first- and second-stage flotation were 75% and 53%, respectively. Upon the addition of kerosene, the recovery increased up to 97% in the first stage and 91% in the second stage, with 3 lb/ton kerosene. The percent ash of the second-stage froth products decreased with the addition of kerosene to its lowest value of 7.7% at 2 lb/ton. Above this dosage, the

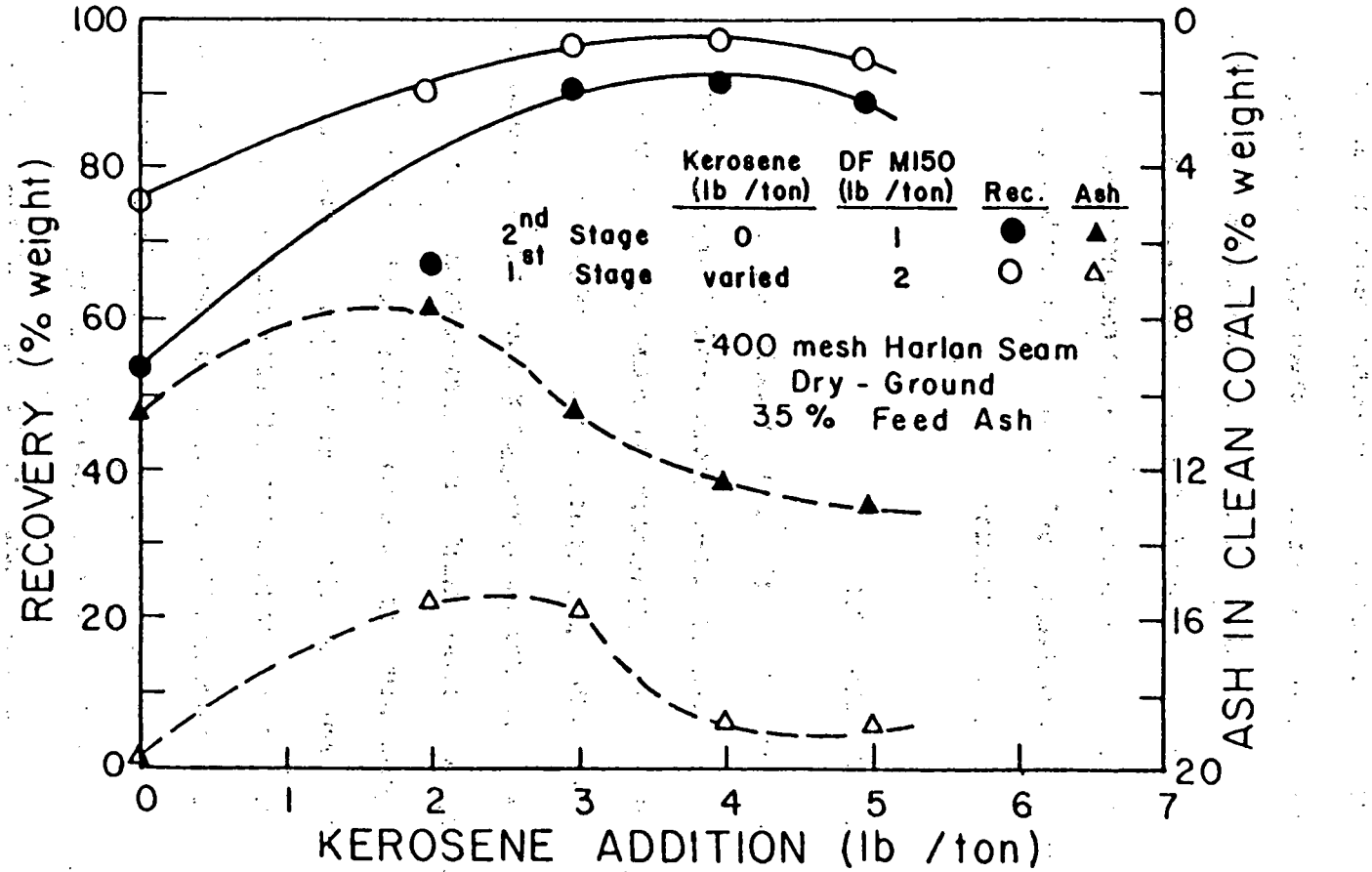

Figure 24. Results of microbubble flotation tests conducted on the Harlan seam coal (-400 mesh) as a function of kerosene addition in the first stage.

percent ash of the final product increased, possibly as a result of recovering composite particles of higher ash content at higher kerosene additions.

Figure 25 shows the results of flotation tests conducted on the Pittsburgh No. 8 coal (4.4% ash) by varying the kerosene additions in the first stage. The flotation feeds were prepared by grinding the -100 mesh coal in an attrition mill for 25 minutes to further liberate the ash particles from the coal. Frother additions of 5.7 and 3.0 lb/ton were used in the first and second stages, respectively. Under these conditions, second-stage recoveries higher than 90% were obtained with as little as 0.3 lb/ton kerosene. At higher kerosene additions, the recovery reached as high as 98%. With this ultrafine coal, the percent ash in the second-stage froth product remained constant up to 3 lb/ton kerosene and decreased to a minimum of 2% at approximately 30 lb/ton.

Note here that with the -400 mesh Harlan seam coal (Figure 24), the percent ash increased with increasing kerosene additions at larger dosages, whereas with the attrition-ground Pittsburgh No. 8 coal, a reverse trend was observed. This may be explained by the possibility that with the ultrafine coal (Figure 25), liberated coal particles were recovered at higher kerosene additions, while with the coarser flotation feeds (Figure 24), composite

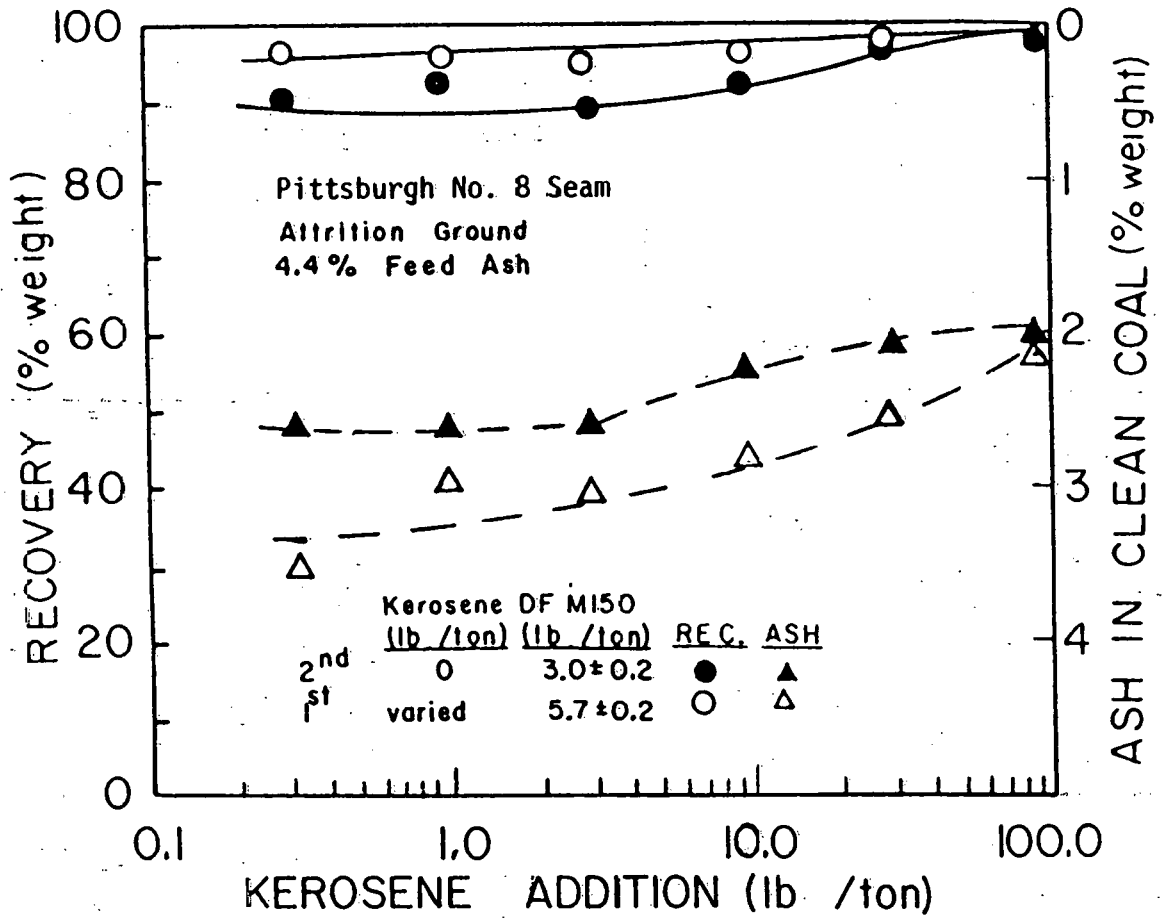

Figure 25. Results of microbubble flotation tests conducted on the attrition-ground Pittsburgh No. 8 seam coal as a function of kerosene addition in the first stage.

particles containing ash were recovered. However, had larger amounts of kerosene been used with the Harlan seam coal, a similar trend might have been observed.

3.2.3 Effect of Using Varying Volumes of Microbubble Suspensions

The major problem associated with fine particle flotation is probably the entrainment and/or entrapment of unwanted gangue particles. In an effort to minimize this problem, the froth product from a flotation test has been repulped and floated again using smaller amounts of reagents. This two-stage flotation process has been found to improve the ash rejection substantially, as has been demonstrated in Figures 17-25. Another method that has been found to improve the ash rejection is to use more dilute microbubble suspensions. By reducing the number of bubbles in a given volume, one can reduce the entrapment and improve the ash rejection.

Figure 26 gives the results of two series of flotation tests; in one, 300 ml of microbubble suspension was injected into the bottom of the flotation cell containing 25 grams of coal sample (-100 mesh, Eagle seam) assaying 36% ash, and in the other, 500 ml of microbubble suspension was used. For a given frother addition, the latter series used a more dilute microbubble suspension and produced froth

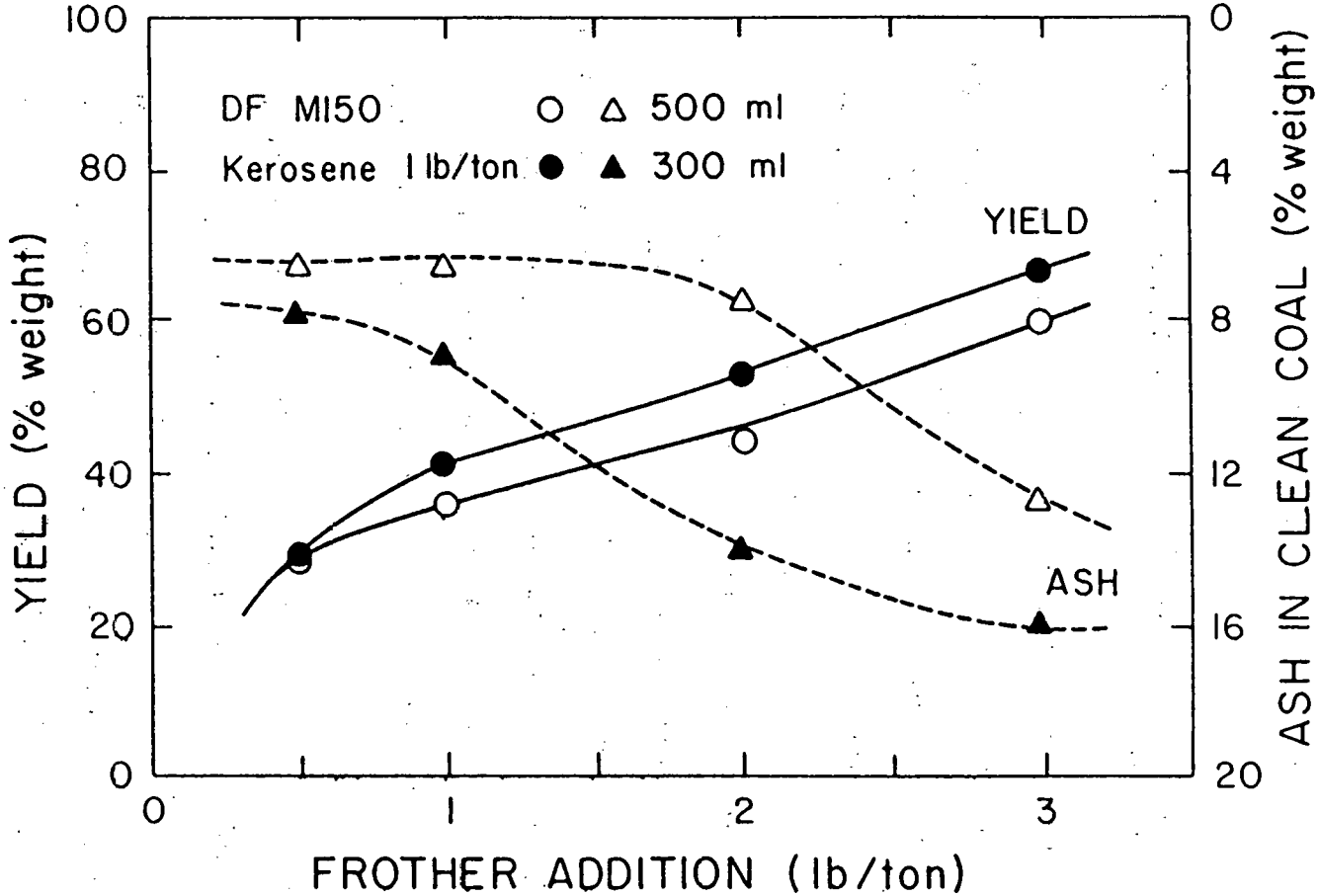

Figure 26. Effect of using different volumes (300 and 500 ml) of microbubble suspensions for the flotation of Eagle seam coal (-100 mesh, 36% ash).

products containing less than 8% ash without a second-stage cleaning. Figure 26 also shows that at higher frother additions the ash content of the froth product increased, partly due to an excessive number of bubbles.

Figure 27 gives the results of another series of tests conducted on an ultrafine coal, varying the volume of the microbubble suspension injected. In these tests, however, the concentration of Dowfroth M150 was kept constant at 0.08 ml/l, so that the density of bubbles injected was kept constant. The results show an increasing ash content in the product with an increasing volume of microbubble suspension and recovery. This finding may be attributed to the excess amount of frother used.

3.2.4 Effects of pH

The results shown in Figure 28 illustrate the effects of pH on the microbubble flotation of a Pittsburgh No. 8 seam coal sample that was attrition-ground for 25 minutes to produce ultrafine coal. The pH values of both the coal slurry and the frother solution were adjusted to a desired value using NaOH and HCl. The best recoveries were obtained between pH 6 and 9, while the percent ash in the concentrate was the lowest between pH 7 and 8. These results are similar to those reported by Zimmerman (1979) and Halsey, Yoon and Sebba (1982). It is noted here that most flotation

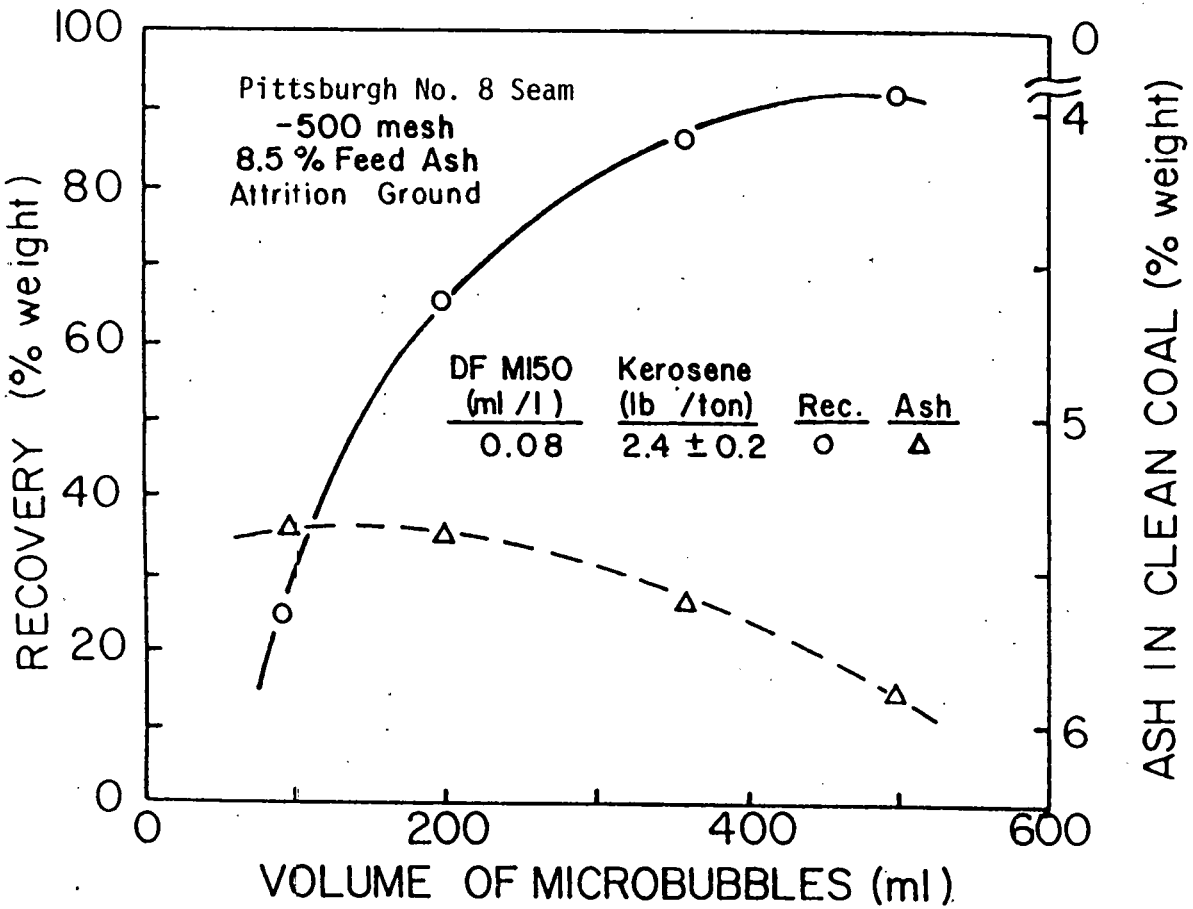

Figure 27. Effect of using different volumes of microbubble suspension for the flotation of Pittsburgh No. 8 seam coal (-500 mesh) at a constant frother concentration.

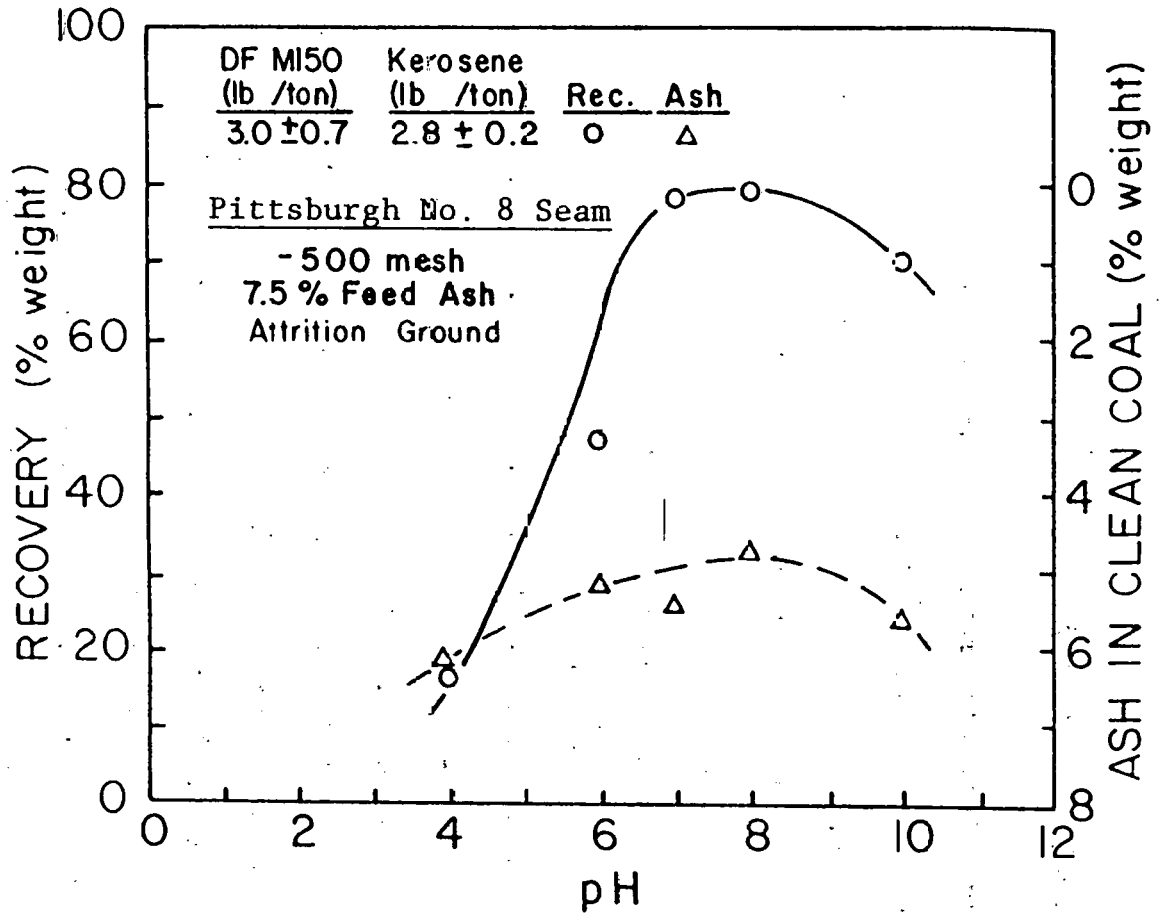

Figure 28. Effect of pH on the flotation of Pittsburgh No. 8 seam coal (-500 mesh).

experiments in the present work were carried out without pH adjustment, but the natural pH usually ranged between 7 and 8, which corresponds to the optimum flotation pH.

3.2.5 Effects of Pulp Density

Another method of minimizing the ash entrapment problem would be to conduct flotation tests at a low pulp density. Figure 29 shows the results of microbubble flotation tests conducted by varying the pulp density. The feed coal (Pittsburgh No. 8 seam) was ground for 25 minutes in an attrition mill. Recoveries of approximately 90% were obtained at pulp densities greater than 3%, below which the recoveries dropped sharply. Note, however, that cleaner products were obtained at pulp densities below 3%.

Current U.S. practice in coal flotation plants shows the percent solids to average 3-4% (Aplan, 1976). Cleaner products are usually obtained with lower pulp densities as a consequence of reduced mechanical entrapment of gangue in the froth and less coagulation of liberated particles with composite particles containing high percentages of ash. Coal recovery is higher, however, with higher pulp densities (Brown, 1962). In this regard, Tomlinson and Fleming (1965) characterized two types of flotation, i.e., "inhibited" flotation that occurs at high pulp densities when all air

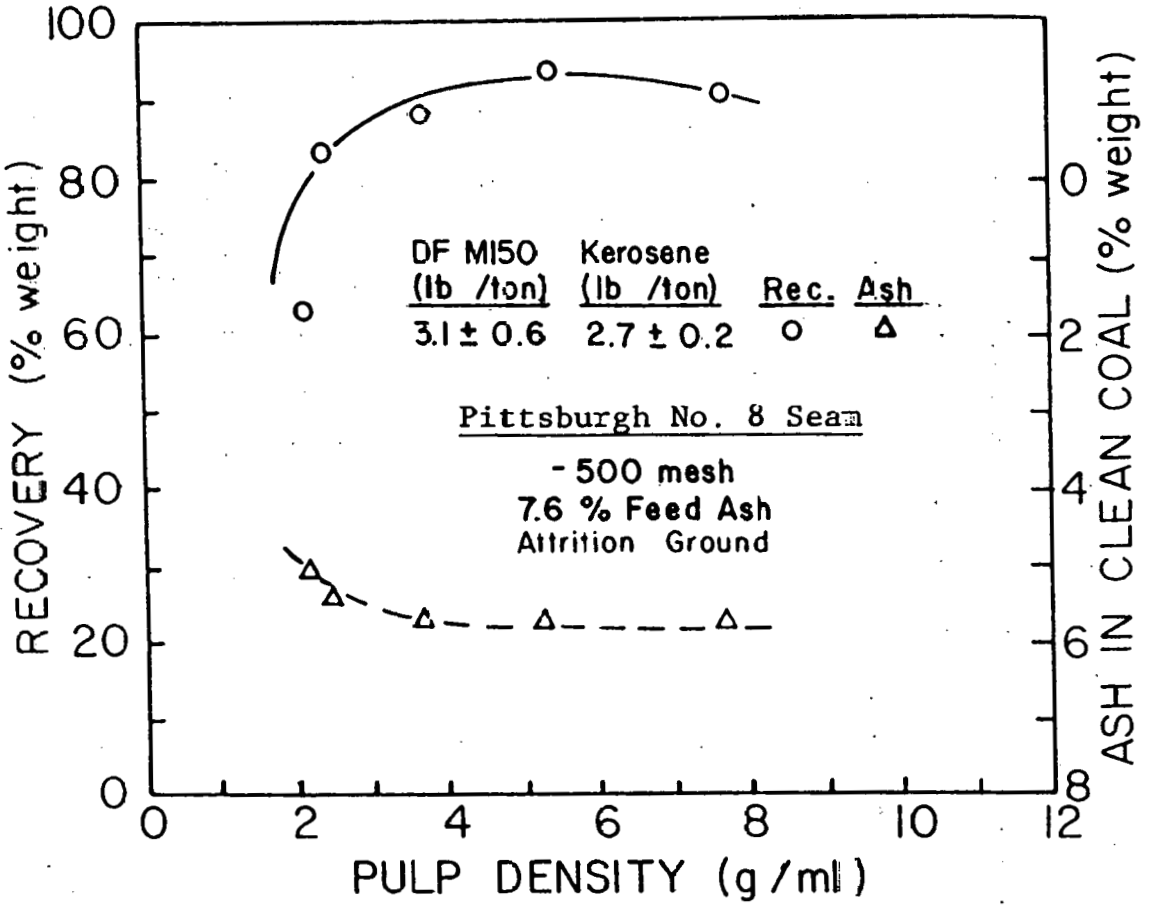

Figure 29. Effect of pulp density on the flotation of Pittsburgh No. 8 seam coal (-500 mesh).

bubbles that reach the froth are saturated with particles, and "free" flotation that occurs at lower pulp densities when the bubbles are sparsely coated with particles.

3.2.6 Effect of Water Recovery on Ash Entrainment

Lynch et al. (1974) found a direct correlation between the recovery rate of silicious gangue and the water recovery rate in the flotation of sulfide minerals. Trahar (1981) also found that the recovery of fine quartz was related to the water recovery in the concentrate, which amounted to as much as 60% in some cases. Two series of single-stage microbubble flotation tests were conducted in the present work on an attrition-ground coal sample (Pittsburgh No. 8), and the results are presented to show the ash recovery in relation to the water recovery at different frother dosages.

The results given in Figure 30a show that the water recovery increased only slightly from 6.9% at 1 lb/ton frother to a maximum of 11% at 4 lb/ton frother, while the ash recovery increased steadily from 36% at 1 lb/ton frother to 60% at 82 lb/ton frother.

In the second series (Figure 30b), the percentage of water in the froth remained practically constant at approximately 82% at all frother concentrations, but the ash recovery increased significantly with increasing frother addition. These results suggest that in microbubble

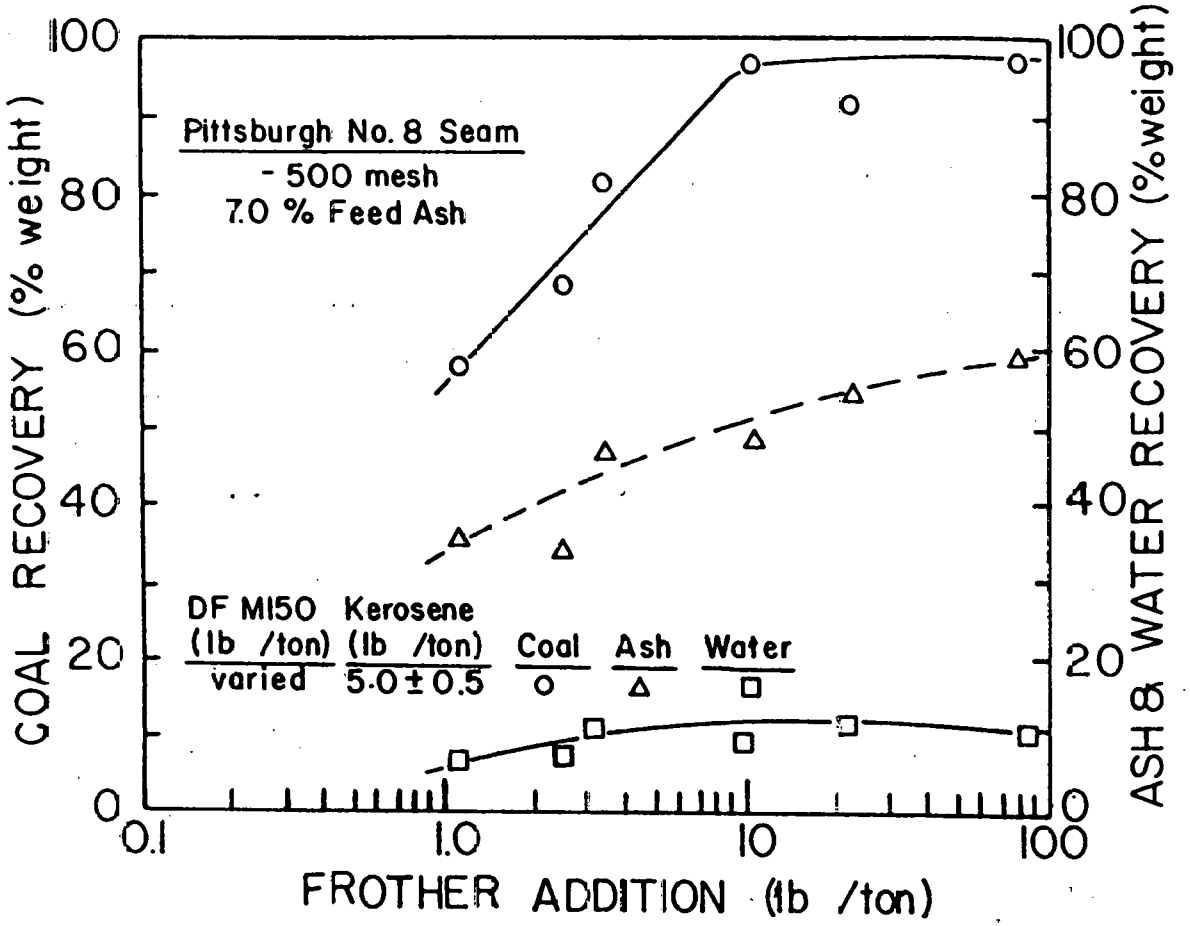

Figure 30a. Results of flotation tests conducted on the Pittsburgh No. 8 seam coal (-500 mesh) showing the relationship between coal recovery, ash recovery and water recovery.

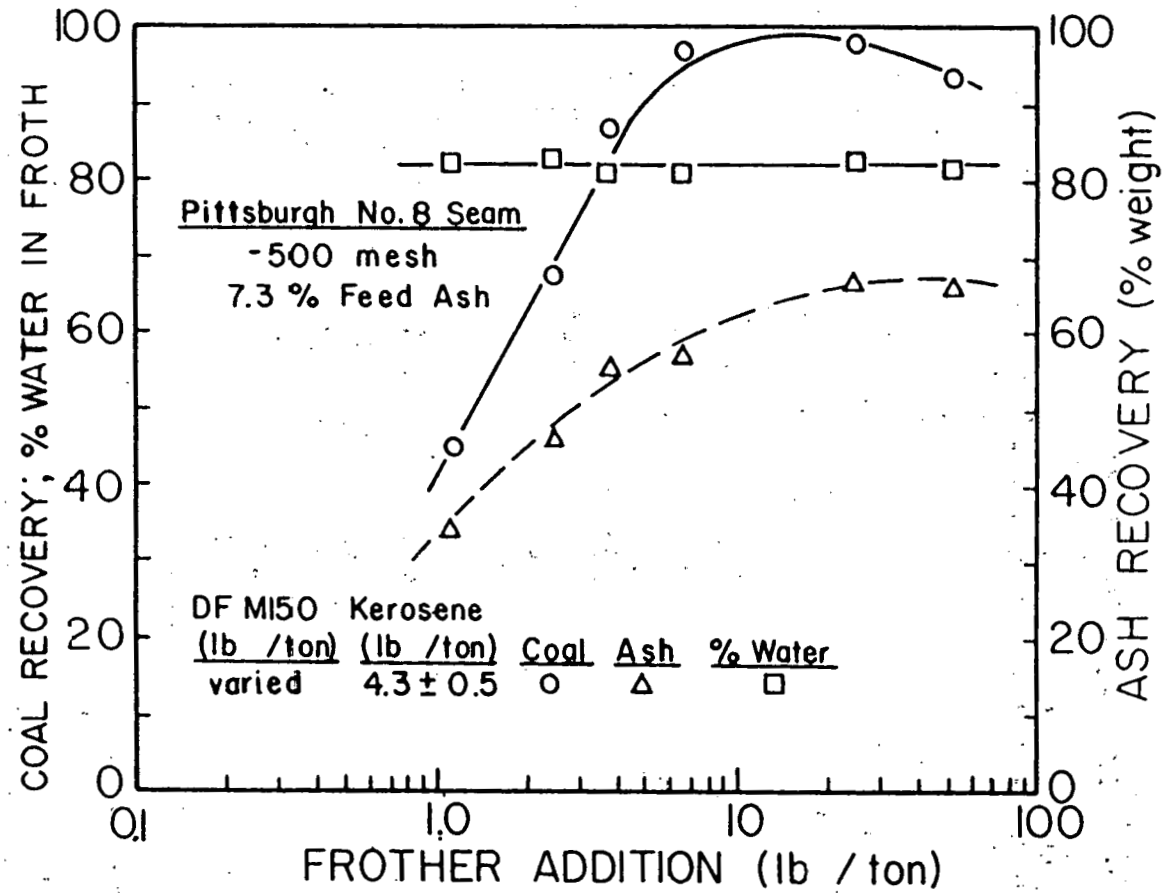

Figure 30b. Results of flotation tests conducted on the Pittsburgh No. 8 seam coal (-500 mesh) showing the relationship between coal recovery, ash recovery and percent water in the froth.

flotation, the ash recovery is not as directly related to the water recovery as in conventional flotation. It appears that in microbubble flotation, ash particles are mechanically entrapped in the froth due to the larger number of bubbles produced at higher frother concentrations.

3.2.7 Methods to Reduce Ash Entrapment

Several different techniques were employed to improve the selectivity of microbubble flotation. Table II shows the results of the microbubble flotation tests in which the froth was sprayed with water continuously during flotation in an effort to wash the ash particles from the bubbles. Two sets of flotation tests were conducted: one on the -500 mesh Harlan seam coal prepared by wet attrition grinding and the other on -100 mesh coal. The amounts of reagents used in both are comparable.

With the -100 mesh sample, the water spray seemed to be effective in reducing the ash entrapped in the froth without detriment to the recoveries. The percent ash was reduced during the second-stage flotation to 8.8% from 12.2% ash by the water spray without a significant loss of recovery. When no water spray was employed, however, the percent ash was reduced to only 10.5% from 11.9%.

Table II. Results of Microbubble Flotation Tests Conducted on Harlan Seam Coal Samples of Different Feed Sizes

Feed Size	Products	Without Sprayer Recovery (%)	Without Sprayer Ash (%)	With Sprayer Recovery (%)	With Sprayer Ash (%)	Reagents (lb/ton) Kerosene	Reagents (lb/ton) Dowfroth M150
-500 mesh	2nd stage	68.3	4.2	8.9	6.8	1.8±0.1	2.5±0.3
	1st stage	81.8	10.9	18.2	13.9	4.7±0.2	4.6±0.2
	Feed	100.0	30.8	100.0	33.0		
-100 mesh	2nd stage	92.1	10.5	94.2	8.8	1.8±0.1	2.2±0.1
	1st stage	94.4	11.9	96.5	12.2	4.7±0.2	4.1±0.1
	Feed	100.0	23.0	100.0	21.1		

The test results obtained with the -500 mesh sample show that the froth loaded with ultrafine particles was much less stable. The recoveries in both stages of flotation dropped by more than 60% when the froth was sprayed with water. This possibly resulted from ultrafine particles held to the bubbles via van der Waals forces or other weak attractive forces, whereas the coarser particles are held more strongly to the bubbles by means of a three-phase contact. The possibility that fine particles are held to a bubble by weak van der Waals forces has been suggested by Derjaguin and Dukhin (1981) in their discussion of contactless flotation.

Note also that the cleaned, ultrafine coal contained only 4.2% ash, which may be attributed to the improved liberation of ash particles. The feed ash of the -500 mesh coal was higher than that of the -100 mesh coal because of the wear of the grinding media during attrition grinding.

Similar results were obtained when applying a mechanical stirrer to the froth, as shown in Table III. With the stirrer, a second-stage recovery of 99.4% with 4.5% ash was obtained on the -200 mesh sample from the Pond Fork seam. With the -500 mesh sample prepared by grinding the -200 mesh coal for 18 hours in a ball mill, the second-stage recovery was only 24.7%, although the ash content of the froth product was as low as 1.8%.

Figure 31 shows the results of a series of microbubble

Table III. Results of Microbubble Flotation Tests Conducted Using a Mechanical Stirrer on Pond Fork Seam Coal

Feed Size	Products	Recovery (%)	Ash (%)	Reagents (lb/ton)	
				Kerosene	Dowfroth M150
-200 mesh	2nd stage	99.4	4.5	1	3
	1st stage	99.4	4.5	4	5
	Feed	100.0	4.89		
-500 mesh	2nd stage	24.7	1.8	1	3
	1st stage	27.4	2.9	4	5
	Feed	100.0	7.3		

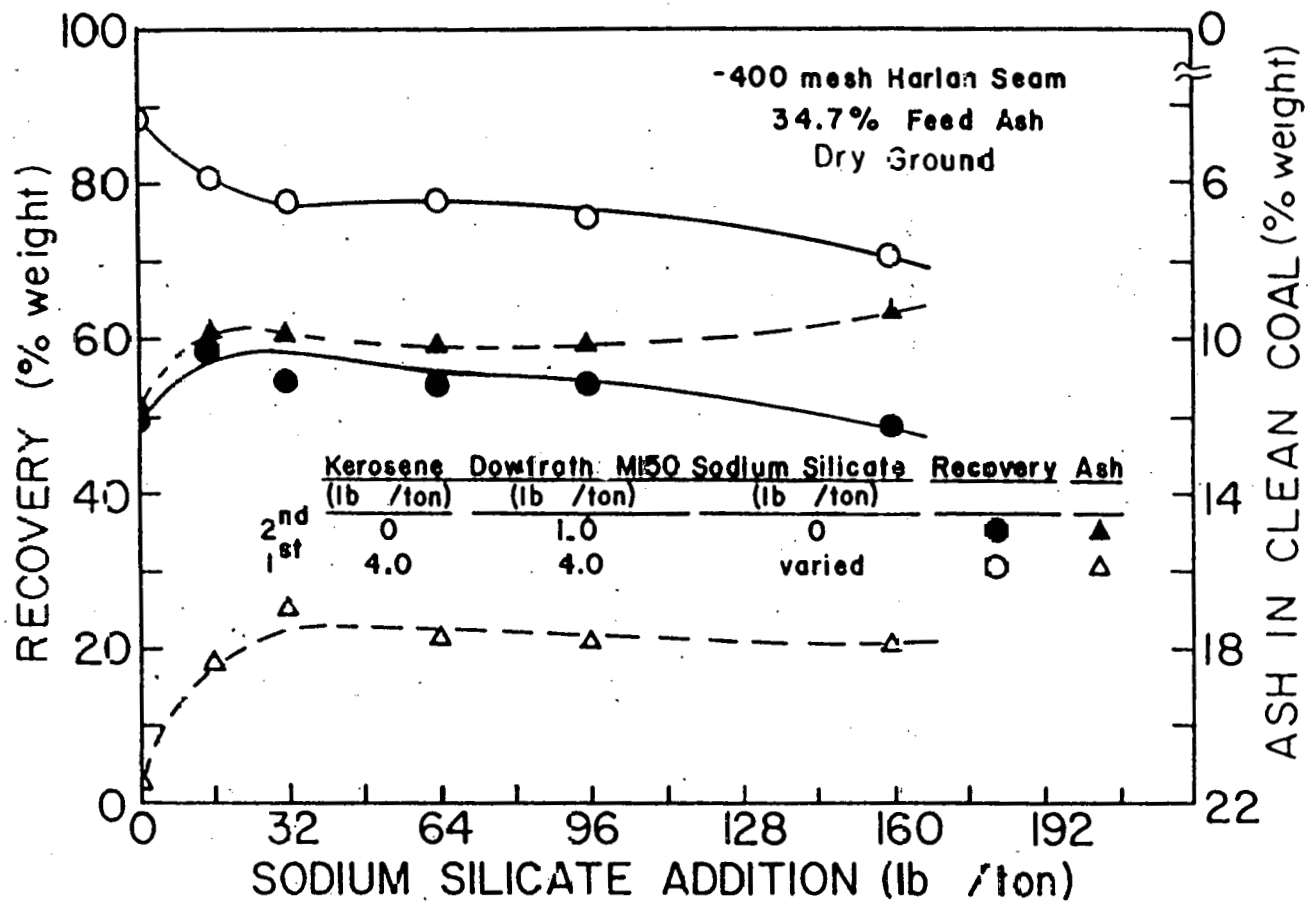

Figure 31. Effect of sodium silicate addition on the flotation of Harlan seam coal (-400 mesh).

flotation tests in which the coal samples were conditioned with varying amounts of sodium silicate prior to flotation. The addition of 32 lb/ton sodium silicate reduced the ash content by about 4% in the first-stage flotation and by about 2% in the second stage. Thus, the use of a dispersant improved the ash rejection, although at the expense of the recovery.

3.2.8 Ash Content Along the Froth Depth

In order to examine the changes in ash content along the froth depth, a single-stage microbubble flotation test was conducted while taking the froth at different depths and assaying each segment separately. The coal sample was from the Pittsburgh No. 8 seam and had been attrition-ground for 25 minutes. One lb/ton kerosene was used to condition the coal and 2.1 lb/ton Dowfroth M150 was used to produce the microbubbles. The first segment of the froth (top 1.5 cm) was not removed until four minutes after the microbubble injection. During this time, the total froth height was decreased from 5.80 cm to 5.45 cm.

Figure 32 shows the percent ash profile along the froth depth. The percent ash remained at approximately 4% in the top 3.5 cm of the froth, but increased to above 5% in the bottom 2 cm. This may be explained by the drainage of liquid lamellae between the bubbles, which takes the loosely

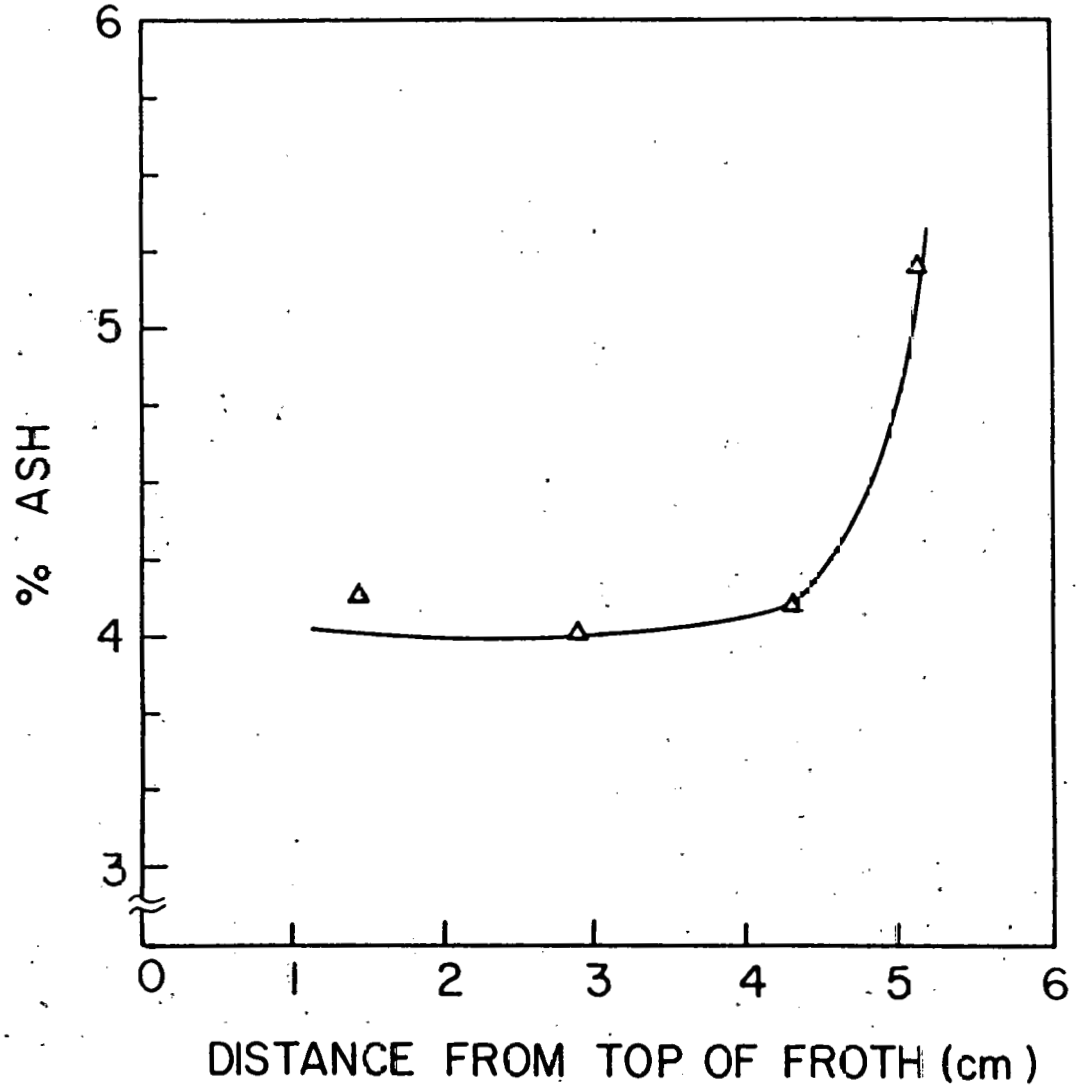

Figure 32. Ash content along the depth of the froth formed during the microbubble flotation conducted on the Pittsburgh No. 8 seam coal.

held ash particles to the bottom of the froth.

3.2.9 Effect of Grinding Time

In order to compare the effects of particle size on both conventional and microbubble flotation, the Pittsburgh No. 8 seam (-100 mesh) coal was attrition-ground for various lengths of time at a pulp density of 40% solids. Each flotation test was conducted using 2.8 lb/ton kerosene and 3.2 lb/ton Dowfroth M150 in the first stage. In the second stage, 2.2 lb/ton Dowfroth M150 was used without additional kerosene. The results are shown in Figures 33 and 34.

The second-stage recoveries obtained in the microbubble flotation tests varied from 95% with 0 grinding time to 65% with a 25-minute grinding time. These results were superior to the ones obtained with conventional flotation, which ranged from 85% to 20%. In both series of tests, the ash contents of the clean coal products decreased significantly with increased grinding time. This may be attributed primarily to the improved liberation with increased grinding time, but it may also be due simply to the drop in recovery. The conventional flotation technique gave a final product containing only 2% ash after 15 minutes of grinding time. The microbubble process, on the other hand, produced a clean coal product assaying 3% ash, but with a significantly

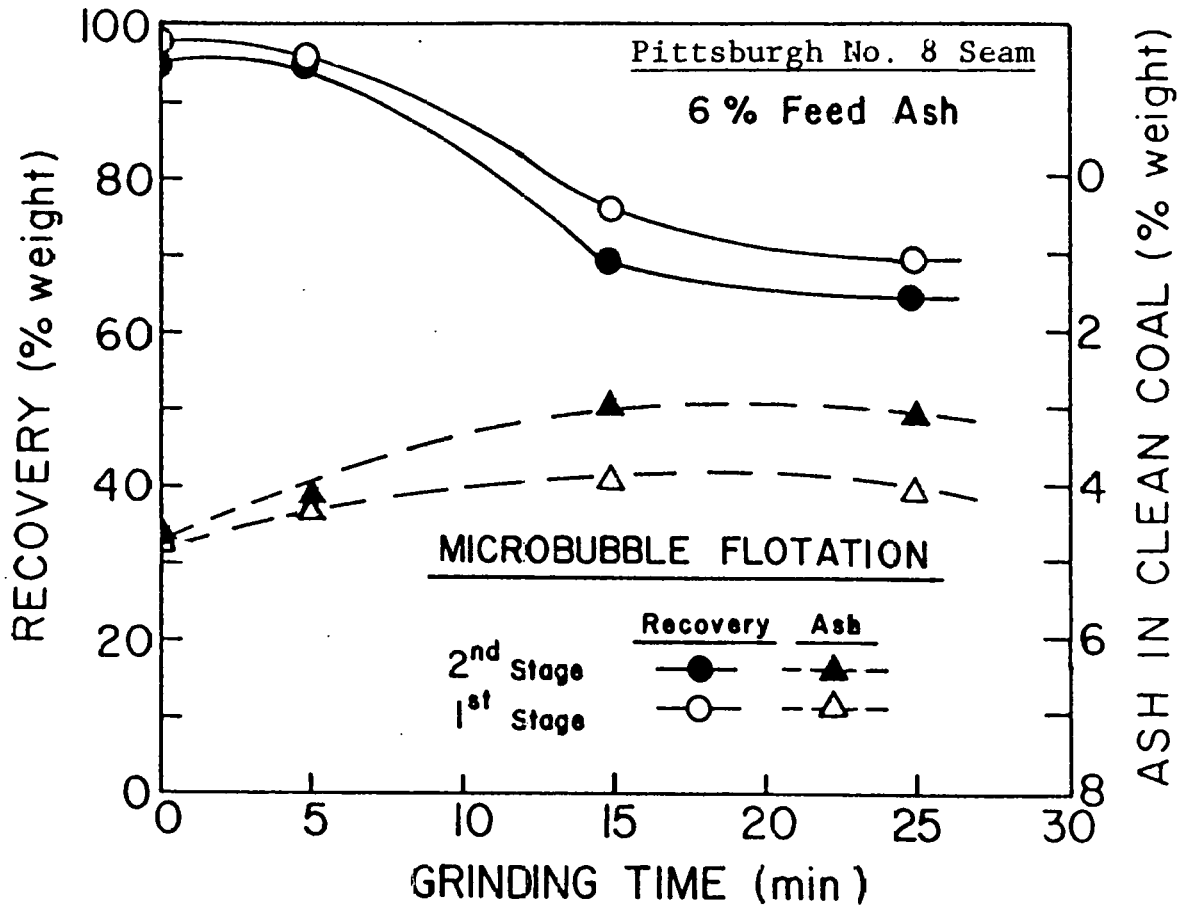

Figure 33. Results of microbubble flotation tests conducted on the Pittsburgh No. 8 seam coal as a function of grinding time.

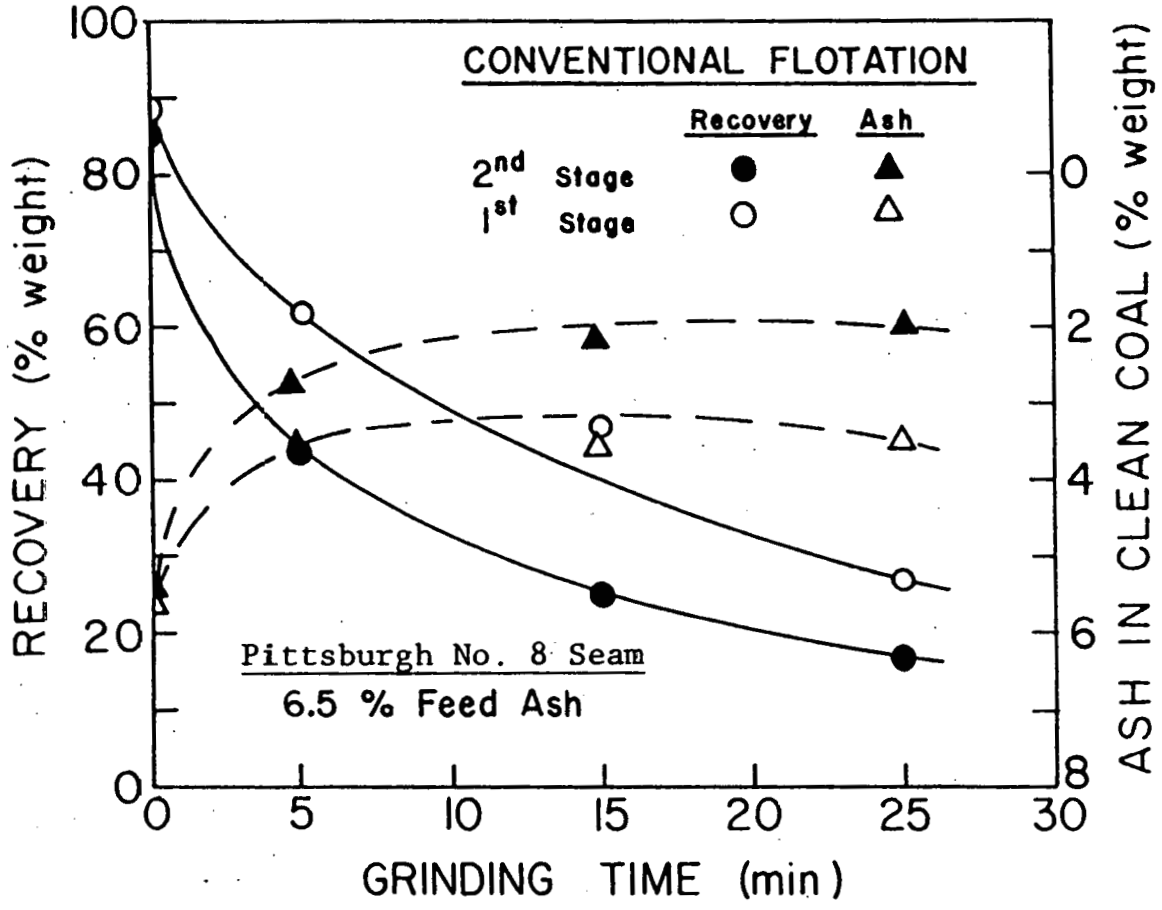

Figure 34. Results of conventional flotation tests conducted on the Pittsburgh No. 8 seam coal as a function of grinding time.

higher recovery by as much as 45%.

3.2.10 Comparison of Microbubble Flotation, Conventional Flotation and Oil Agglomeration Test Results

Table IV compares the results of microbubble flotation tests with those of conventional flotation tests conducted on the -400 mesh Harlan seam coal. The sample was prepared by dry-pulverization in a hammer mill and the tests were conducted using identical reagent dosages. In the first stage, the microbubble flotation produced a froth product assaying 16.3% ash with 96.1% recovery, while the conventional flotation gave a froth product assaying 26.1% with 91.7% recovery. In the second-stage flotation, the microbubble flotation gave only 9.9% ash in the froth product, while in the conventional flotation the ash content was as high as 21.6%. The separation efficiencies of the microbubble flotation process were significantly higher than those of the conventional process in both stages, suggesting that the microbubble flotation process was more selective. It is pointed out, however, that the 2 lb/ton of frother used in the conventional flotation might have been excessive, resulting in poor selectivity.

Table V shows the test results obtained on the same Harlan seam coal using three different fine coal cleaning techniques, i.e., conventional flotation, microbubble

Table IV. Comparison of Conventional and Microbubble Flotation Test Results Obtained on a -400 Mesh Harlan Seam Coal Using Identical Amounts of Reagents

Products	Conventional Flotation Recovery (%)	Ash (%)	S.E.*	Microbubble Flotation Recovery (%)	Ash (%)	S.E.	Reagents (lb/ton) Kerosene	Dowfroth M150
2nd stage	89.4	21.6	43.26	83.4	9.9	65.69	0	0.5
1st stage	91.7	26.1	31.05	96.1	16.3	59.79	3	2
Feed	100.0	34.5		100.0	34.5			

*Separation Efficiency

Table V. Comparison of Flotation Tests Conducted on -500 Mesh R-O-M Harlan Seam Coal

Products	Conventional Flotation		Oil Agglomeration		Microbubble Flotation			
					Test 1*		Test 2**	
	Recovery (%)	Ash (%)	Recovery (%)	Ash (%)	Recovery (%)	Ash (%)	Recovery (%)	Ash (%)
2nd stage	9.1	5.9	37.1	10.6	91.0	8.8	83.5	4.6
1st stage	16.3	17.0	94.2	16.0	98.2	23.1	93.1	10.9
Feed	100.0	25.3	100.0	23.3	100.0	30.2	100.0	25.0
	Reagents (lb/ton)							
Kerosene	4		300		4		4	
Dowfroth M150	1		0		5		6	

*Ball mill ground, 48 hours, 100% -500 mesh
**Attrition mill ground, 10 minutes, 100% -500 mesh

flotation and oil agglomeration. The oil agglomeration test was included in this series of experiments because it is generally recognized as one of the best physical cleaning techniques for fine coal, although it requires large amounts of oil. Note that the feed size for these tests was much smaller than those shown in Table IV. The flotation feeds were prepared by wet-grinding the R-O-M coal in a laboratory ball mill for 48 hours using small grinding media, except for Test No. 2 of the microbubble flotation. In this test, the sample was attrition-ground for ten minutes using a stirred ball mill. All of the sample passed through a 500-mesh screen after grinding.

For the first three tests shown in Table IV, the pulverized coal was filtered for the purpose of sample dividing and repulped prior to flotation, while Test No. 2 of the microbubble tests was performed without filtration. The variation in the feed ash of these samples is due mostly to differential media wear during grinding.

With the ultrafine coal, conventional flotation using large air bubbles produced very poor results (9.1% recovery with 5.9% ash). The oil agglomeration technique gave a much improved recovery (87.1%), but with a relatively high ash content (10.6%). The microbubble flotation (Test No. 1) produced the best results (91.0% recovery with 8.8% ash) using relatively little kerosene compared to the amount

used in the oil agglomeration test. In the other microbubble flotation test (Test No. 2), the ash content was only 4.6%, while a respectable recovery (83.5%) was maintained. This improved ash rejection might be attributed to the attrition grinding, which could have produced smaller and, thus, more liberated coal particles. However, a more likely reason is that the pulverized coal was not filtered prior to flotation for the purpose of sample dividing. It is possible that during filtration ash particles adhere to coal particles by some capillary forces and cannot readily be dispersed during the repulping procedure.

Table VI shows the results of another series of tests similar to those presented in Table V. Note, however, that in this microbubble test, a stirrer was inserted into the froth layer to help reduce the amount of ash recovered in the froth. The coal sample used was a clean coal product from a dense medium separator treating Pittsburgh No. 8 seam coal. The mechanical stirrer did indeed help reduce the ash content to 6.5%, but at the expense of the recovery (only 57.5% in the second stage). Nevertheless, the results of the microbubble flotation test are much better than those of the conventional flotation test and the ash rejection was better than that obtained with oil agglomeration.

Table VII shows similar results obtained on the Taggart seam coal pulverized in an attrition mill. This coal sample

Table VI. Comparison of Flotation Tests Conducted on the -500 Mesh Pittsburgh No. 8 Seam Coal

	Conventional Flotation		Microbubble Flotation*		Oil Agglomeration	
Products	Recovery (%)	Ash (%)	Recovery (%)	Ash (%)	Recovery (%)	Ash (%)
2nd stage	28.5	8.1	57.5	6.5	90.4	8.5
1st stage	36.0	9.6	70.2	8.8	95.2	8.9
Feed	100.0	11.3	100.0	11.0	100.0	10.2
	Reagents (lb/ton)					
Kerosene	4		10		300	
Dowfroth M150	1		5		0	

*a stirrer was used

Table VII. Comparison of Flotation Tests Conducted on the -500 Mesh R-O-M Taggart Seam Coal

	Conventional Flotation		Microbubble Flotation*		Oil Agglomeration	
Products	Recovery (%)	Ash (%)	Recovery (%)	Ash (%)	Recovery (%)	Ash (%)
2nd stage	13.7	5.4	60.2	4.7	95.1	4.1
1st stage	17.1	22.3	74.7	11.3	95.6	7.8
Feed	100.0	40.7	100.0	41.4	100.0	39.8
	Reagents (lb/ton)					
Kerosene	4		8		300	
Dowfroth M150	2		10		0	

*a stirrer was used

contained a much higher percentage of ash than those shown in Tables V and VI. Again, a stirrer was used with the microbubble flotation tests, which helped produce a low ash coal (4.7% ash). The recovery was only 60.2%, however, due to excessive stirring. The oil agglomeration technique produced the best results with this coal, the clean coal assaying only 4.1% ash with 95.1% recovery. However, as much as 300 lb/ton oil was used in the oil agglomeration process.

3.2.11 Bubble Size Versus Flotation Kinetics

Figure 35 shows the results of the kinetics tests conducted on the -100 mesh Eagle seam coal (34% ash) using bubbles of three different sizes. Each test was conducted at a 42 ml/min gas (nitrogen) flow rate using 20 grams of coal conditioned with 3 lb/ton kerosene. This flow rate was chosen on the basis of the unique procedure of the microbubble flotation technique; that is, instead of bubbling inside a flotation cell as in conventional flotation, microbubbles are injected as a suspension. A 330-ml volume of the microbubble suspension, prepared from 0.082 ml/l of Dowfroth M150 and containing 7.8% gas volume, was injected into the bottom of the flotation cell for 37 seconds, which corresponded to the gas flow rate of 42

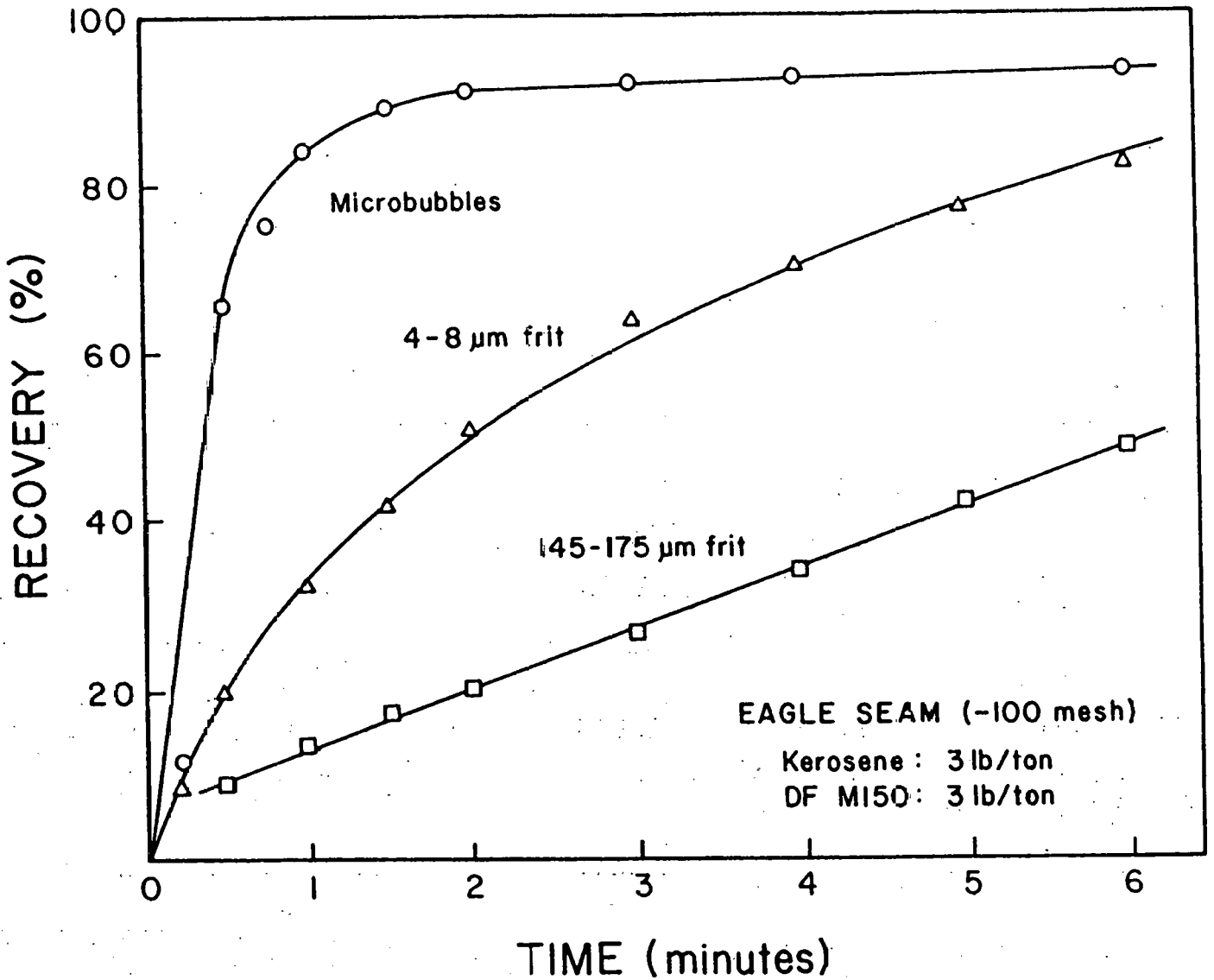

Figure 35. Results of flotation kinetics experiments conducted on the Eagle seam coal (-100 mesh) as a function of bubble size.

ml/min for a period of 37 seconds. Although the microbubble suspension was injected for only 42 seconds, the flotation time took much longer as the bubbles rose very slowly due to their small size. When using larger bubbles generated by the frits, the gas flow rate of 42 ml/min was maintained throughout the entire flotation period. Thus, the total volumes of gas used in these experiments were much larger than that of the microbubble flotation.

A comparison of the test results given in Figure 35 clearly demonstrates a drastic improvement in flotation rate brought about by the use of microbubbles. Qualitatively, this finding is in agreement with Eq. [5] which relates the flotation rate constant to the bubble diameter. It is unfortunate that the bubble size measurements have not been made in the present work due to a lack of proper facilities; however, work is currently underway to verify Eq. [5] in a more quantitative manner.

Figure 36 represents the kinetics results obtained on the -500 mesh Eagle seam coal (37.5% ash). The experimental conditions were essentially the same as the other series except that the gas flow rate was 46 ml/min. With this ultrafine coal, the slopes of the curves are much reduced compared to those of Figure 35, indicating slower kinetics. It is not certain whether these slow kinetics were due to the small particle size or to the high surface area. It is

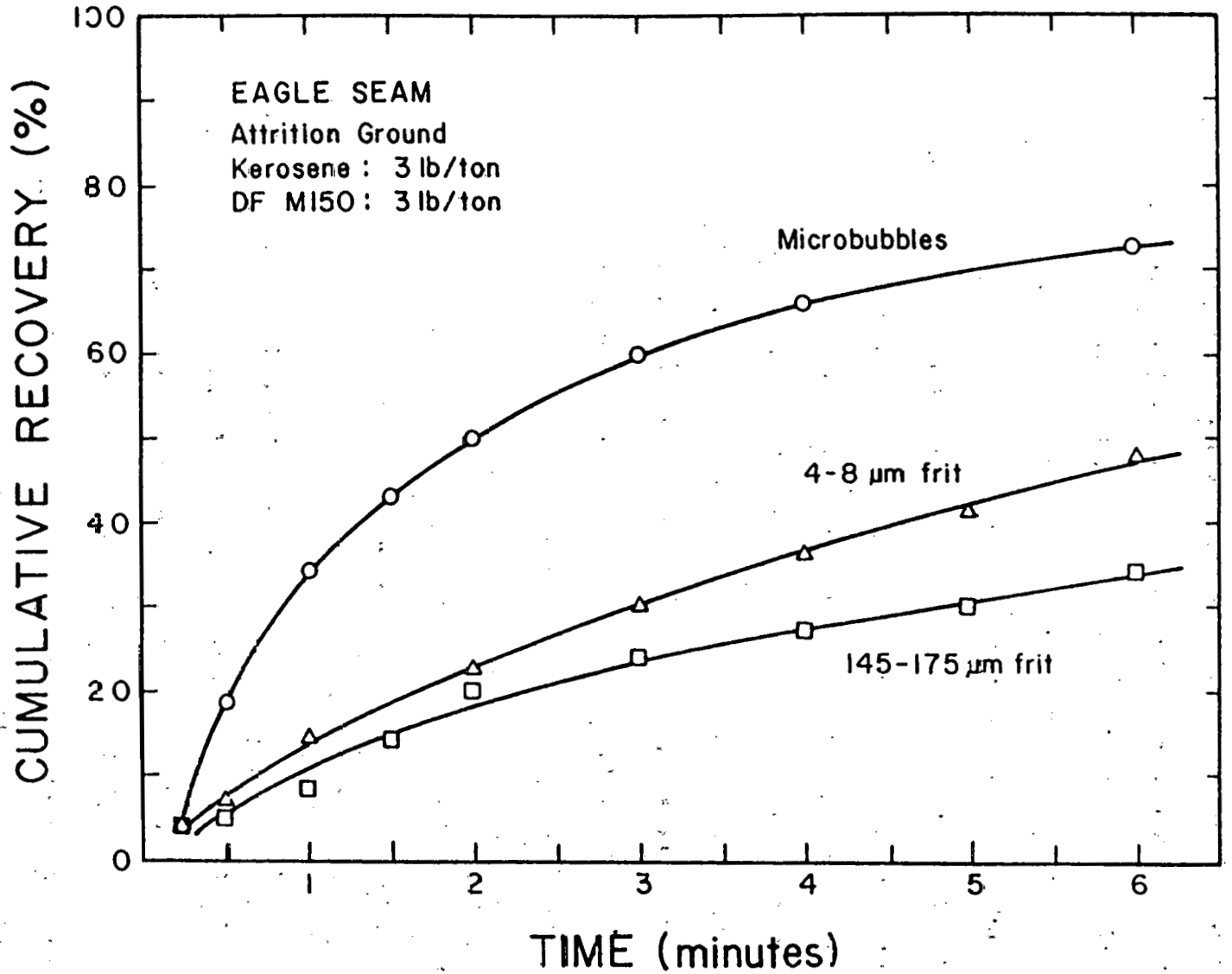

Figure 36. Results of flotation kinetics experiments conducted on the Eagle seam coal (-500 mesh) as a function of bubble size.

possible that 3 lb/ton kerosene and 3 lb/ton Dowfroth M150 were not enough for a good flotation of ultrafine coal. Nevertheless, the microbubble flotation exhibited significantly faster flotation rates than the others using larger bubbles, even with this ultrafine coal.

The most intriguing finding from these kinetics experiments is that the froth products of the microbubble flotation test contained significantly less ash than those of the other tests, as shown in Figures 37 and 38. With this ultrafine coal, the larger bubbles generated by the frits did not show much selectivity. In fact, the froth products contained only a few percent less ash than the feed coal (37.5% ash), which may be a good example showing that when using larger bubbles, flotation occurs largely due to an entrainment mechanism rather than to true flotation. It appears, therefore, that microbubble flotation can not only give higher recovery, but also improved ash rejection in cleaning ultrafine coal.

For the flotation of -100 mesh coal (see Figure 35), however, the same cannot be said. In fact, the froth products obtained by using larger bubbles contained significantly less ash than those of the microbubble flotation (see Appendix II). This merely indicates that larger bubbles can still float coal particles as large as -100 or -200 mesh with some selectivity. Microbubbles, on the other

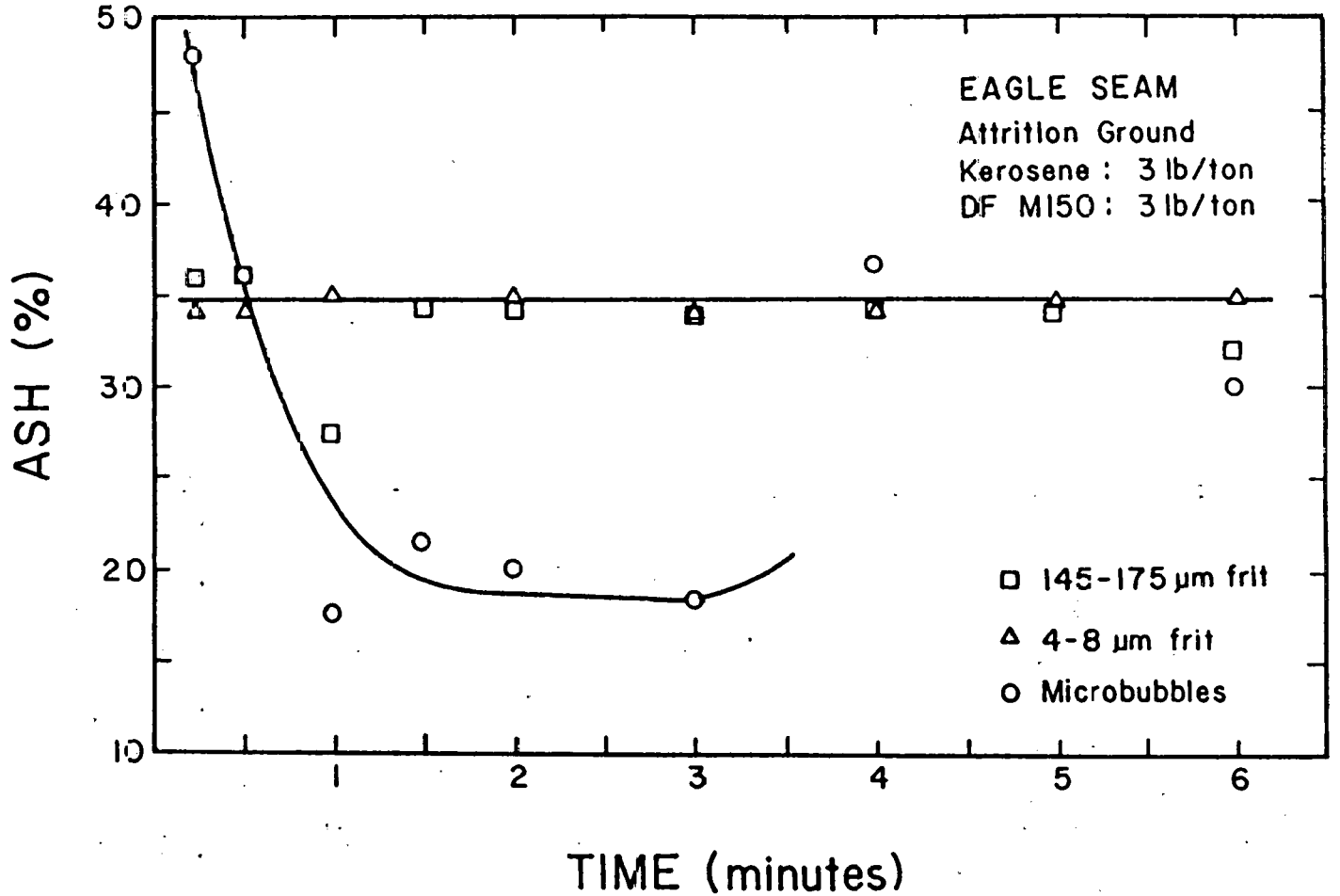

Figure 37. Ash contents of the timed-cut froth products from the kinetics experiments conducted on the Eagle seam coal (-500 mesh).

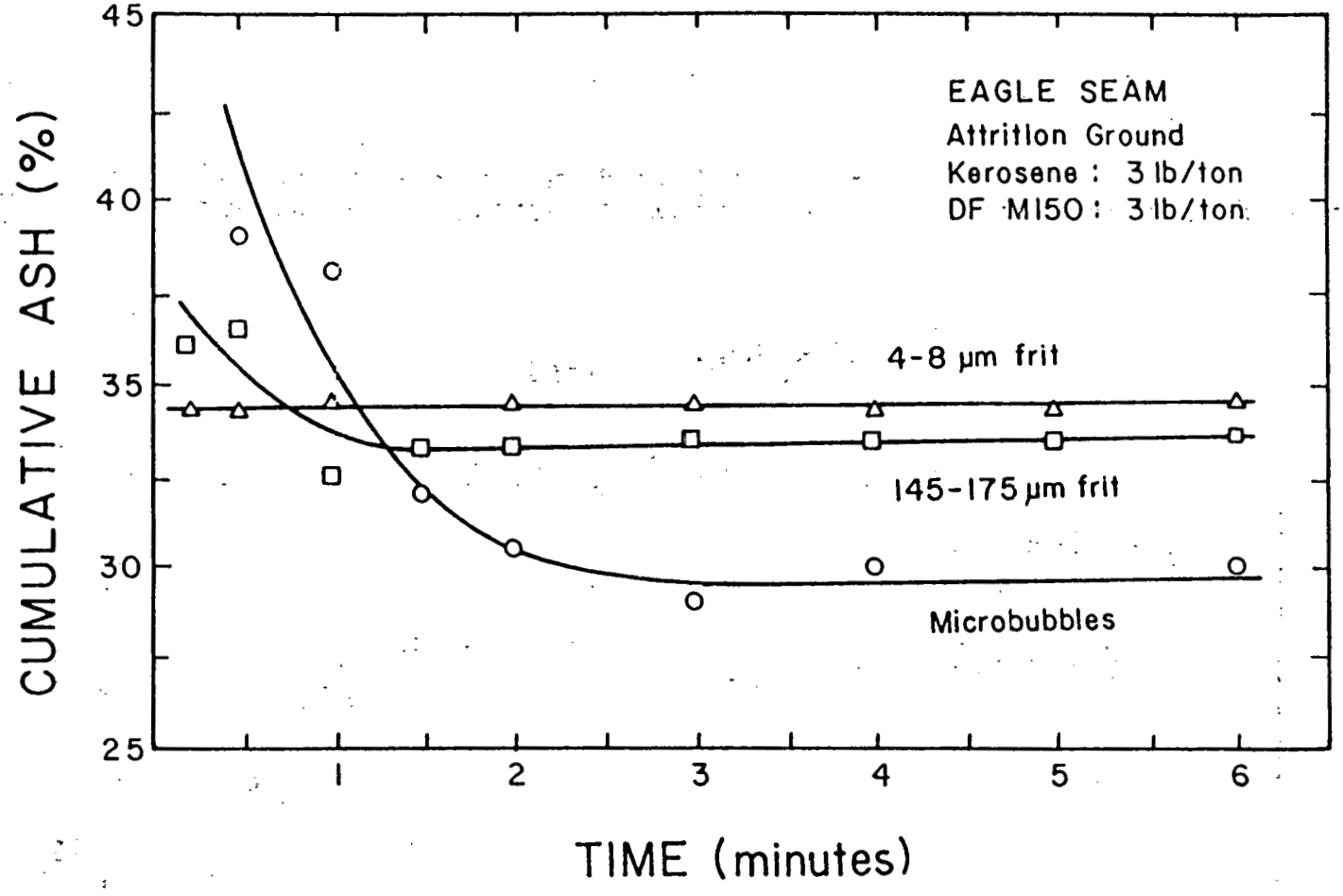

Figure 38. Cumulative ash contents of the froth products from the kinetics experiments conducted on the Eagle seam coal (-500 mesh).

hand, can cause entrapment due to their large number, resulting in inferior ash rejection although with much improved recovery and kinetics, as shown in Figure 35.

IV. DISCUSSION

4.1 General

It has been found in the present work that small air bubbles in the 50-100 micron size range are effective in cleaning ultrafine coal with a mean particle size as fine as 5 microns. The microbubble flotation process can produce clean coal containing less than 2% ash with over 85% recovery. Two nonionic frothers, i.e., MIBC and Dowfroth M150, have been used to produce the microbubbles. It would be of interest to discuss the surface chemistry of these surfactants prior to attempting to discuss the complex flotation mechanism.

4.2 Characteristics of Dowfroth M150 and MIBC and Their Effect on Flotation

The following represents the molecular structure of MIBC (F.W. = 102):

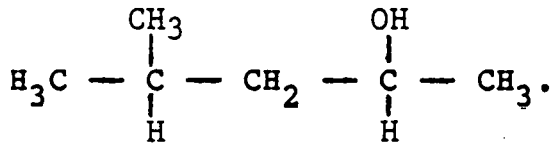

Dowfroth M150 is a polypropylene glycol which has the following molecular configuration:

$$CH_3 — (O — C_3H_6)_n — OH.$$

It has an average molecular weight of 400, n being approximately 6. Thus, the total number of carbon atoms in the molecule is about 19. Reagents employed in flotation usually possess hydrocarbon chains containing 6-20 carbon atoms. The reagents that have less than 6 carbons do not exhibit enough surface activity, while those with more than 20 are too insoluble for most flotation purposes.

In view of the large difference in molecular weights of the two frothers used, one may expect that Dowfroth M150 would be more surface active than MIBC. The surface tension data shown in Figure 11 indeed shows this to be the case: the surface tension of the Dowfroth M150 solution decreases more sharply than that of the MIBC solution. From the slopes ($d\gamma/d \log C$) of the surface tension versus concentration curves, one can determine the surface excess of these reagents at the air/water interface using the Gibbs adsorption equation:

$$\Gamma = \frac{-1}{2.3\ RT} \frac{d\gamma}{d \log C}, \qquad [8]$$

where Γ = surface excess (moles/cm^2)

γ = surface tension

C = surfactant concentration

R = gas constant

T = temperature (^{o}K).

Table VIII summarizes the results of the surface excess calculation made at 50 mg/l. This concentration has been chosen for the calculation because the microbubbles were prepared with frother solutions usually in the 25-100 mg/l range.

Table VIII. Surface Excess Concentrations and Area/Molecule for Dowfroth M150 and MIBC

Surfactant	Slopes at 50 mg/l (dynes·cm^{-1})	Surface Excess, Γ (moles/cm^2)	Area/Molecule (A^2)
Dowfroth M150	-14.8	2.6×10^{-10}	64.0
MIBC	- 3.1	5.43×10^{-11}	306.0

As shown, Dowfroth M150 gives much higher surface excess than MIBC. The area occupied per molecule of frother is rather small (64.0 $\mathring{A}^2$) for Dowfroth M150, but this may

suggest that the frother molecules are adsorbed at the air/water interface forming multi-layers. One can see, on the contrary, that MIBC molecules are sparsely distributed at the air/water interface.

The large difference in surface activities of the two reagents may account for the following observations: i) Dowfroth M150 is a much better frothing agent than MIBC for generating microbubble suspensions containing a higher volume fraction of air and producing a more stable froth during flotation, ii) higher flotation recovery is obtained using Dowfroth M150 as a frother although at the expense of the selectivity, and iii) higher streaming currents of the microbubbles are generated using Dowfroth M150.

The stability of the froth produced during flotation may also be related to the viscosity of the frother solutions. A froth would be unstable when the liquid lamellae between bubbles drains too quickly. As shown in Figure 16, Dowfroth M150 solutions are somewhat more viscous than MIBC solutions, which may explain the higher stability of the froth produced by Dowfroth M150 and, hence, the higher coal recovery. It should be noted, however, that if a froth is too stable, a high degree of ash entrapment can occur, resulting in inferior coal products. For this reason, the froth products obtained using Dowfroth M150 are not as clean as those obtained using MIBC.

Figure 32 shows the percent ash profile of the froth layer. The higher ash contents at the bottom of the froth may indicate the cleaning mechanism by drainage. During the process of drainage, both coal and ash particles will move downward, but the ash particles are likely to trickle down more readily than the hydrophobic coal particles that may cling to the air bubbles more strongly. This will result in the removal of entrained ash particles from the upper portion of a froth layer. Thus, it may be advantageous to build up a thick froth layer and remove only the top portion of the froth. In a continuous operation, it would be of interest to determine the residence times for both ash and coal particles as functions of particle size, froth height, pulp density, pedal speed, etc.

4.3 Bubble Size Calculations Using the Stokes Equation Modified for Hindered Settling Conditions

From the measurements of stability of microbubble suspensions, the volume fraction of air in the microbubble suspensions has been determined. This is shown as a function of frother concentration in Figure 39. Also shown in this figure is the time required for the moving boundary between the cloudy microbubble suspension and the clear water to reach the 70-ml mark (12.6 cm height from the

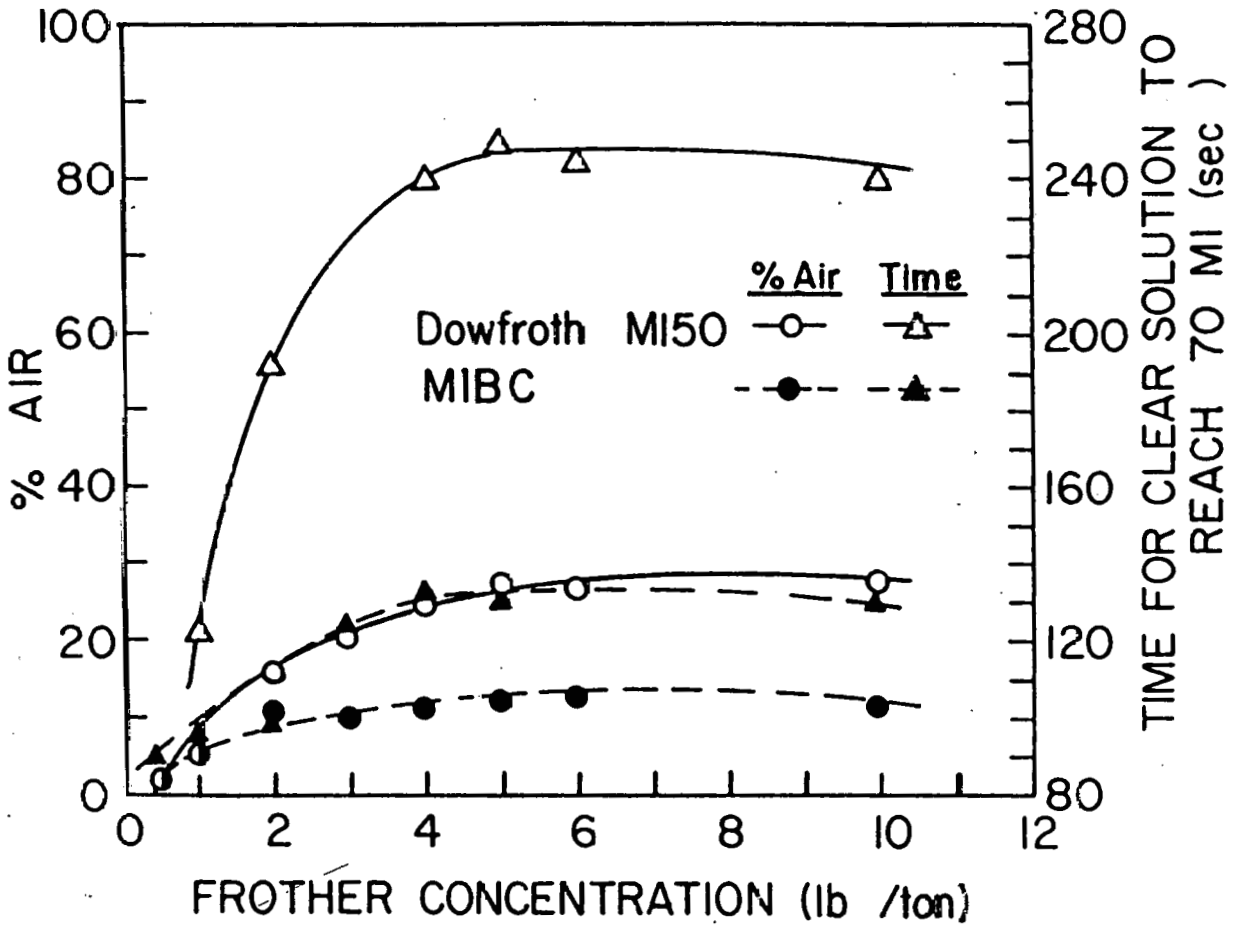

Figure 39. Stability of microbubble suspensions prepared with Dowfroth M150 and MI3C as a function of concentration.

bottom) of the graduated cylinder modified for the stability measurements (Figure 3).

The microbubbles produced with Dowfroth M150 contain up to 28% air, as compared to 13% for those bubbles generated with MIBC. Also, the moving boundary under the microbubbles produced with Dowfroth M150 requires almost twice as much time to reach the 70-ml mark on the graduated cylinder. From the rate of the moving boundary rising through the column, the diameters of the microbubbles have been calculated using the Stokes equation modified for the hindered settling of particles (McCabe and Smith, 1976; Yoon, 1982):

$$u = \frac{gD_b^2 \varepsilon e^{-4.19(1-\varepsilon)} (\rho_1 - \rho_2)}{18\eta} \qquad [9]$$

where u is the terminal velocity, g the gravitational acceleration, ε the porosity (or the fractional volume of the suspension occupied by the liquid), ρ_1 the density of air, ρ_2 the density of the medium, η the viscosity of the liquid, and D_b the spherical bubble diameter. The results of these calculations are shown in Table IX. The velocities of the moving boundaries used in these calculations are those for higher frother concentrations given in Figure 39.

Table IX. Results of Bubble Diameter Calculations Using the Stokes Equation for Hindered Settling Conditions

Reagent	u (cm/sec)	ε (%)	η (cp)	ρ_1 (g/cm^3)	ρ_2 (g/cm^3)	D (μm)
Dowfroth M150	0.053	75	1.32	1.2×10^{-3}	0.75	80.3
MIBC	0.096	89	1.21	1.2×10^{-3}	0.89	65.2

It is surprising to see that despite the large difference in the velocities of rising bubbles, i.e., 0.0525 cm/sec for Dowfroth M150 and 0.0955 for MIBC, the calculated bubble sizes show little difference. In fact, the bubbles generated with MIBC are somewhat smaller than those generated with Dowfroth M150. In view of the Stokes equation (Eq. [9]), the porosity (ε) of the microbubble suspension significantly affects the velocity of rising bubbles. This implies that when there are too many bubbles, the bubbles are hindering each other's rising velocities. The large volume fraction of air in the microbubble suspension prepared using Dowfroth M150 may, therefore, be considered most responsible for the slow rising velocity.

It should be pointed out, however, that the application of Eq. [9] for the bubble size calculation is questionable, and the results are only approximate at best. Further work is in progress for direct measurements of bubble size.

4.4 Advantages of Microbubble Flotation

As has been discussed in Section 1.2, the major advantage to using microbubbles for flotation may be found in the flotation rate. According to Eq. [5], a tenfold reduction in bubble size can bring about a $10^{3.05}$ times larger flotation rate constant. This advantage has been manifested in the kinetics experiments (Figures 35 and 36), which show that the use of smaller bubbles greatly increases the flotation rate. The increase in flotation rate is more dramatic with the -100 mesh coal (Eagle seam) than with the micronized coal (-10 micron), but the increase is still substantial even with the ultrafine coal. This may account for the improved recoveries obtained in most of the microbubble flotation tests conducted in the present work compared to the conventional flotation tests using larger bubbles.

Conceptually, the improved flotation rates with the use of small bubbles can be attributed to the improved

streamline conditions around smaller bubbles, resulting in improved collision efficiency (E_c). According to Reay and Ratcliff (1973),

$$E_c \propto \left(\frac{1}{D_b}\right)^{2.05} \qquad [5]$$

for the case of glass beads. Furthermore, Flint and Howarth (1971) suggested that when a cloud of bubbles is used for flotation, the streamlines around the bubbles are compressed, resulting in improved collision efficiencies.

In addition, fine bubbles can provide a larger surface area to carry the particles. Recently, G. J. Jameson (1983; personal communication) has taken pictures of bubbles carrying coal particles in an industrial flotation cell. The photographs show that the bubbles are of relatively uniform size (3 mm in diameter) and carry maximum loading, even in the last cell of a flotation bank. This finding is an illustration that a lot of coal is lost due to the small surface area of bubbles generated in conventional flotation processes. By simply reducing the bubble size and, hence, increasing the bubble surface area at a given gas flow rate, coal recovery can be improved significantly.

One of the most intriguing findings of the present work is the fact that the microbubble flotation appears to be considerably more selective than the conventional flotation

process. For example, with the -400 mesh Harlan seam coal, the conventional flotation process gave 89.4% recovery with 21.6% ash in the froth product (Table IV). Using identical amounts of reagents, the microbubble flotation produced a froth product assaying only 9.9% ash and 83.4% recovery. The separation efficiencies (S.E.) of these two processes are 43.3 and 65.7%, in favor of the microbubble flotation. The S.E. is defined here as the percent distribution of combustible material in the froth product minus the percent distribution of noncombustible material in the same product.

Other test results given in Tables V, VI and VII also show significant improvements in selectivity with the use of the microbubble flotation technique. Usually an increase in recovery results in a corresponding decrease in grade in conventional flotation processes, but some of the microbubble flotation tests gave not only an increase in recovery, but also a reduction in ash content in the froth product. Much of this is due to the techniques employed to reduce the ash entrapment, e.g., water spraying and mechanical agitation. However, there may be reasons to believe that microbubble flotation can be intrinsically more selective than the conventional process.

Two hydrodynamic reasons may be given for the improved selectivity exhibited by the microbubble flotation process. The first is the fact that a microbubble carries little or

no turbulent wake volume behind it. Figure 40 shows the relationship between the dimensionless wake volume and the bubble size in relation to the Reynolds number. The curves shown in this figure are from Kalra and Uhlherr's (1971) measurements of wake volume behind rigid spheres as a function of the Reynolds number. From the Reynolds number, the bubble diameter has been calculated using the following relationship:

$$D_b = \left(\frac{18\eta^2 Re}{g\rho(\rho - \rho_g)} \right)^{1/3} \qquad [10]$$

in which η is the kinematic viscosity, Re the Reynolds number, ρ the density of liquid, ρ_g the density of gas in the bubble, and g the gravitational acceleration.

Theoretically, for $Re < 1$, no eddy wake is formed because of the viscous, streamlined flow past a sphere. One can then calculate the theoretical bubble diameter, below which no wake is formed, by substituting $Re = 1$ into Eq. [10]. At 20°C, Eq. [10] gives D_b = 123 microns. The bubble size used in the present work is smaller than this value and, therefore, the wake volume may be insignificant. It is likely that the presence of a wake may be responsible for the entrainment of ash particles during flotation. Currently, the concentration gradient of particles across

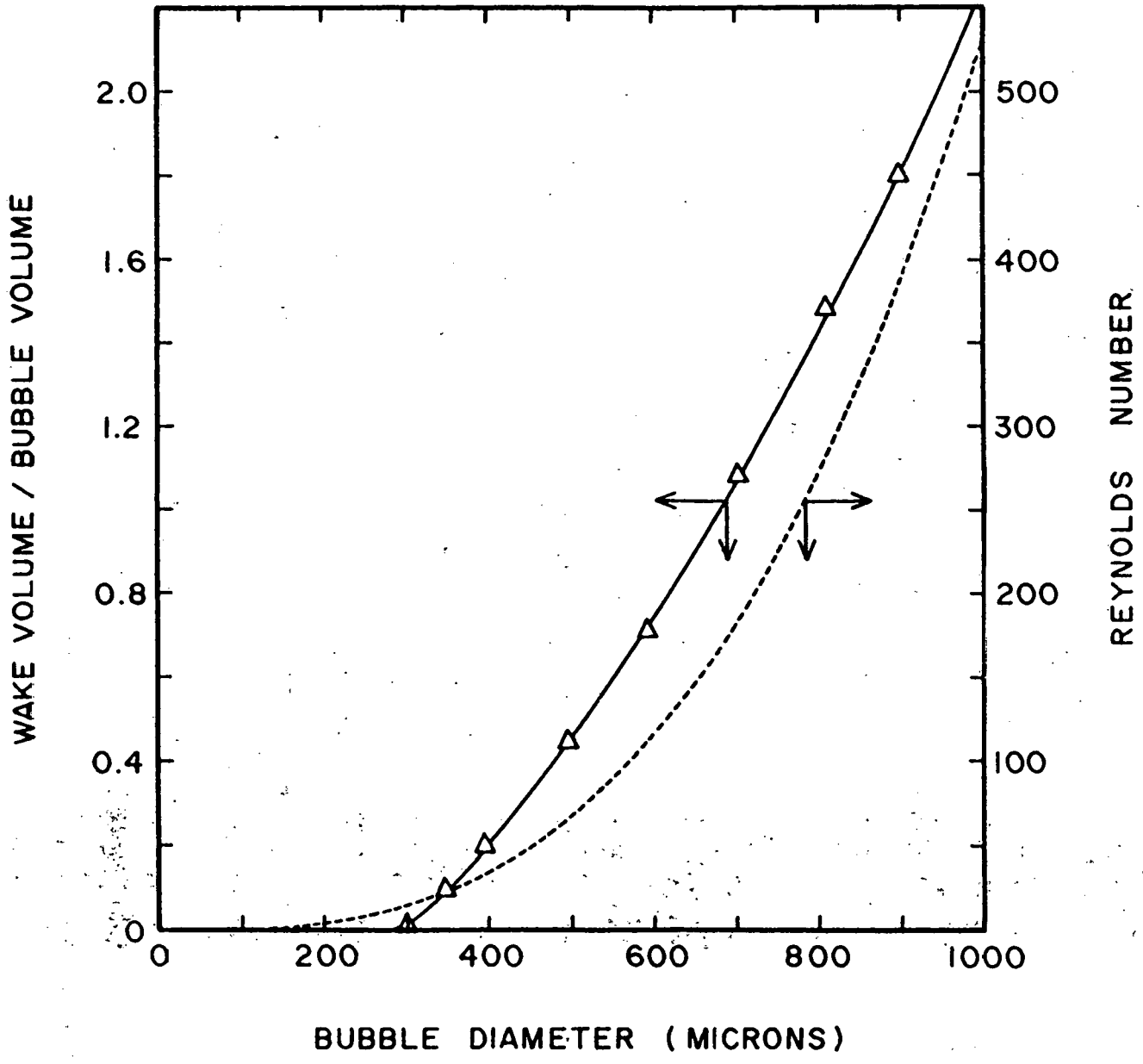

Figure 40. Dimensionless wake volume and Reynolds number as a function of bubble diameter.

the wake volume behind a solid sphere is being determined.

The improved selectivity of the microbubble flotation may also be related to bubble loading. Kiefer and Wilson (1980) have developed a mathematical model to show that the effective bubble loading, which is defined here as the surface area (S_c) of a bubble that is covered by particles divided by the volume (V) of the bubble, decreases exponentially with increasing bubble size. This finding can explain the improved flotation recovery with decreasing bubble size, but may also be used for improved selectivity as discussed below.

Let us consider a small bubble that is fully covered by particles in a monolayer form. Some of the particles on the bubble may be ash particles which are entrapped between two hydrophobic particles. During flotation, some of the ash particles which must be more weakly held to the bubble than the hydrophobic coal particles may be readily detached from the bubble surface by the drag force. When a mechanical force of proper amplitude is applied to the bubble, the detachment of ash particles will be facilitated and the flotation process will become more selective. In some of the microbubble flotation tests, water spray and mechanical agitation have been employed to achieve improved selectivity.

When larger bubbles are employed for flotation, the effective bubble loading would be small, as predicted by Kiefer and Wilson (1980). It is possible, however, that the particle attachment to the bubble is not limited to the monolayer. The particles colliding with the bubble will be quickly swept to the back of the bubble and attach themselves to the particles that are already on the surface. In other words, the particles may adhere to the bubble in multi-layer form. Figure 41 may show such an example. In this case, the detachment of the entrained ash particles from the bubble during the short flotation time would be more difficult than in the case of a smaller bubble covered by a monolayer or particles, and as a result, the flotation process would be less selective.

In an effort to minimize the ash entrapment during flotation, the froth layer was sprayed with water or agitated with a mechanical stirrer. It was observed during these experiments that when finer particles were used for flotation, the froth was much less stable than when coarser particles were used. It is likely that large particles can penetrate the thin films around the bubbles and stop the drainage of lamellae, while the small particles follow the movement of the liquid during drainage.

As has already been discussed in Section 1.2, Derjaguin and Dukhin (1981) have put forth a concept of 'contactless

Figure 41. Coal particles adhering to a large bubble.

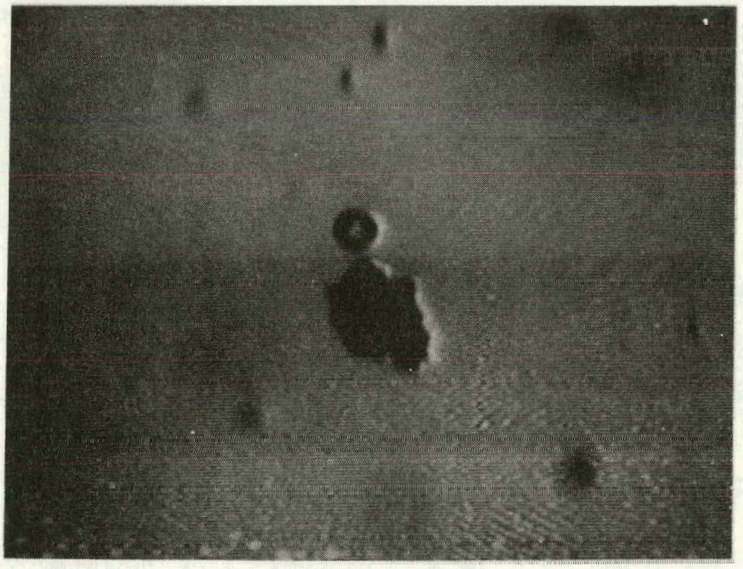

Figure 42. Photomicrograph of a microbubble floating a graphite particle.

flotation', which suggests that ultrafine particles can be floated without the formation of a contact angle. Only a weak van der Waals force is necessary for bubble-particle adhesion because small particles are not subjected to large tearing-off forces. Large particles having large tearing-off forces, on the other hand, require stronger interfacial forces that are manifested in the form of the contact angle. However, no experimental evidence is given by Derjaguin and Dukhin to support their contactless flotation concept.

Figure 42 shows a photomicrograph of a bubble-particle aggregate formed during microbubble flotation. The apparatus used for taking this photograph has been described by Yoon and Sebba (1981). Apparently, the bubble is attached to a graphite particle without forming a contact angle, suggesting that the contactless flotation may actually occur during microbubble flotation. Further investigation is necessary, however, to verify this concept. Nevertheless, the contactless flotation theory may provide a tentative explanation for the decreasing froth stability with decreasing particle size.

In conventional flotation processes, a froth that is too stable is not desirable because it hinders the downstream processes such as thickening and filtration. However, in fine particle flotation, a stable and tenacious froth may be useful in removing entrapped ash particles from the froth

layer by water spraying. It is understood that the AFT (Advanced Fuel Technology) flotation process (1983) is exploiting this concept in achieving a maximum coal recovery with a maximum ash rejection. Although the froth stability is significantly reduced when a coal sample is pulverized to ultrafine sizes, as has been discussed in the foregoing paragraphs, it appears that microbubbles produce much more stable froth than the larger bubbles used in conventional flotation. Frequently, the froth formed during microbubble flotation lasted many days without losing significant amounts of coal particles.

Further research is being carried out at present to exploit this unique property of microbubbles for improving ash rejection. One of the techniques involves the control of froth removal rate. By reducing the froth removal rate in a continuous operation, one allows a longer time for the ash particles to drain from the froth layer and fall into the pulp. The ash content profile along the depth of a froth layer, shown in Figure 32, strongly suggests the likelihood of success with this technique.

V. SUMMARY AND CONCLUSIONS

1. In the present work, microbubbles have been produced by several different techniques and used for the flotation of fine coal. The bubble size ranges from 60 to 80 microns in diameter, according to calculations based on measurements of the rates of bubbles rising through a column. The microbubbles suspended in a surfactant solution give the suspension the appearance of milk because of their small sizes and large numbers.

2. The microbubbles were generated using Methyl isobutyl carbinol (MIBC) and Dowfroth M150 (Polypropylene glycol). The latter reagent produced more stable microbubble suspensions containing a volume fraction of air up to 30%, while MIBC produced a microbubble suspension with a maximum volume fraction of 10%.

3. A streaming current apparatus similar to the one used by Dibbs et al. (1974) has been used to obtain information regarding the charges of microbubbles generated using various surfactants. The microbubbles generated with a cationic surfactant, dodecylpyridinium chloride, exhibited positive current, the current density increasing sharply near its critical micelle concentration. The microbubbles

generated both with MIBC and Dowfroth M150 exhibited negative current at neutral pH and at moderately high concentrations.

4. Flotation tests have been carried out on coal samples from seven different U.S. coal seams. Due to the nature of the microbubbles, the best results were obtained when the flotation was conducted under quiescent conditions. Typically, a flotation experiment is carried out by injecting a volume of microbubble suspension into the bottom of a cylindro-conical flotation column which contains a coal slurry. Of the two frothers tested, i.e., MIBC and Dowfroth M150, the former gives better selectivity but at the expense of recovery. Therefore, most of the flotation experiments have been carried out using Dowfroth M150 for the generation of microbubbles.

5. In general, the microbubble flotation technique gives much improved flotation recovery as compared to the conventional flotation technique using larger bubbles under turbulent conditions. This improvement can be attributed to the fast flotation rate obtained by the small bubbles; the flotation kinetics experiments carried out using different size bubbles at a constant gas flow rate show a substantial increase in flotation rate with decreasing bubble size.

6. One of the most serious problems in fine particle flotation is that of entrainment or entrapment, which causes a loss of selectivity. It appears that the flotation using larger bubbles is troubled with an entrainment problem, particularly when cleaning an ultrafine coal, while the microbubble flotation suffers from entrapment problems. Indeed, the flotation results relating the ash content of the froth products to the water recovery do not suggest that entrainment is a serious problem in microbubble flotation. Rather, particles trapped between two rising bubbles appear to be the cause of the loss of selectivity.

In order to minimize the entrapment problem, several different techniques have been employed in the present work. One such effort has been to use a two-stage flotation technique in which the first-stage froth product is repulped and floated again using minimum amounts of reagents. Significant improvements in ash rejection have been achieved by this technique but, of course, with some loss of coal recovery.

7. Another technique that has been found to be useful in minimizing the ash entrapment problem involves application of mechanical forces or shocks, such as water spraying and mechanical agitation, to the froth layer. This process may

help loosen the ash particles held to the bubbles in the froth layer. It has been found, however, that an agitation that is too strong results in a significant loss of coal recovery, requiring close control of the mechanical shock depending on the stability of the froth. The microbubble flotation technique is particularly suited for this technique because the froth layer appears to be significantly more stable than the froth formed during conventional flotation.

It has been found that the froth stability decreases with decreasing particle size, indicating that the liquid lamellae drain more quickly with decreasing particle size. This may be explained by the possibility that fine particles are weakly held to the bubble surface as compared to coarse particles. This interpretation is similar to the 'contactless flotation' concept put forth by Derjaguin and Dukhin (1981). A photomicrograph taken during the microbubble flotation of graphite shows no apparent contact angle between a bubble and a particle, which might support this view.

8. To improve the selectivity of the microbubble flotation process, several other techniques have been employed. These include i) injecting a more dilute microbubble suspension,

ii) controlling the pulp density, and iii) using dispersants to maximize liberation.

9. An analysis of the froth layer formed during microbubble flotation shows that the ash content increases significantly along its depth, suggesting that ash particles trickle to the bottom of a froth layer by drainage of the lamellae. This finding presents another method of controlling the ash entrapment problem during microbubble flotation.

10. Microbubble flotation tests have been carried out on coal samples of various sizes, i.e., -100, -200, -400 and -500 mesh. With a given coal, the ash rejection improves with decreasing particle size, although at the expense of higher reagent consumption. The improved ash rejection may be attributed to the improved liberation of mineral matter from coal. Therefore, a series of flotation tests has been conducted on coal samples attrition-ground in a stirred ball mill, which has been found to be efficient in micronizing coals. Even with such ultrafine coal samples, the microbubble flotation technique has produced high recoveries with respectable ash rejection, depending on the amounts of reagents used. In general, the amount of frother (Dowfroth M150) required for the flotation of ultrafine coal ranges

from 2-6 lb/ton. The kerosene dosage varies from one coal to another, depending on the hydrophobicity of the coal samples tested. Methods of reducing the frother requirement are currently being studied.

11. Perhaps the most encouraging finding of the present investigation is that the microbubble flotation technique is more selective than the conventional flotation process using larger bubbles. The fact that microbubbles have no turbulent wake may provide an explanation for this observation. The possibility that the effective bubble loading (S_c) increases with decreasing bubble size may also be a reason.

These advantages of the microbubble flotation technique are currently being exploited for the production of super-clean coal.

REFERENCES

Anfruns, J. P. and Kitchener, J. A., 1976. "The Absolute Rate of Capture of Single Particles by Single Bubbles," in Flotation, A. M. Gaudin Memorial Volume, vol. 2, AIME, New York, p. 625.

Anfruns, J. P. and Kitchener, 1977. "Rate of Capture of Small Particles in Flotation," Trans. IMM, 86:C9.

Aplan, Frank F., 1976. "Coal Flotation," in Flotation, A. M. Gaudin Memorial Volume, vol. 2, AIME, New York, p. 1235.

Bauer, Paul S., 1981. "Coal Cleaning Improves Boiler Performance and Reduces SO_2 Emissions," Power, September, p. S-1.

Bennett, A. J. R., Chapman, W. R. and Dell, C. C., 1958. "Froth Flotation of Coal," Proceedings, 3rd Int. Coal Preparation Congress, Brussels-Liege, E2:452-462.

Booth, R. B. and Freyberger, W. L., 1962. "Froths and Frothing Agents," in Froth Flotation, 50th Anniversary Volume, D. W. Fuerstenau (ed.), AIME, New York, pp. 258-276.

Brown, D. J., 1962. "Coal Flotation," in Froth Flotation, 50th Anniversary Volume, D. W. Fuerstenau (ed.), AIME, New York, pp. 518-538.

Brown, D. J., 1965. "A Photographic Study of Froth Flotation," Fuel Soc. J., 16:22.

Brown, R. C., 1932. "The Surface Tensions of Mixtures of Normal Propyl Alcohol and Benzene," Phil. Mag., 13:528.

Burgess, L. E., McGarry, P. E., Herman, D. E. and Koppelman, L. N., 1983. "The AFT Beneficiation System - A New Way to Clean Coal," presented at the 5th Int. Symposium on Coal Slurry Combustion and Technology, Tampa, Florida, April 25-27.

Collins, D. N. and Read, A. D., 1971. "The Treatment of Slimes," Minerals Science and Engineering, 3(2):19.

Collins, G. L. and Jameson, G. J., 1976. "Experiments on the Flotation of Fine Particles - The Influence of

Particle Size and Charge," Chem. Engng. Sci., 31:985.

Dainton, A. D., 1980. "Coal Utilization in the 80's," Mining Engineer, London, p. 129.

Derjaguin, B. V. and Dukhin, S. S., 1960. Russian J. Physical Chemistry, p. 501.

Derjaguin, B. V. and Dukhin, S. S., 1981. "Kinetic Theory of the Flotation of Fine Particles," Proceedings, 13th Mineral Processing Congress, Warsaw, Poland, J. Laskowski (ed.), Elsevier, New York, pp. 21-62.

Dibbs, H. P., Sirois, L. L. and Bredin, R., 1974. "Some Electrical Properties of Bubbles and Their Role in the Flotation of Quartz," Canadian Met. Quarterly, 13:395-404.

Falas, E. and Zick, R., 1982. "How Marietta Boosted Fines Recovery by Expanding Plant Flotation Capacity," Coal Mining and Processing, September, p. 46.

Flint, L. R. and Howarth W. J., 1971. "The Collision Efficiency of Small Particles with Spherical Air Bubbles," Chem. Engng. Sci., 26:1155.

Fuerstenau, D. W., 1980. "Fine Particle Flotation," in Fine Particles Processing, vol. 1, AIME, New York, pp. 669-705.

Gaudin, A. M., 1957. Flotation, 2nd edition, McGraw-Hill, New York.

Halsey, G. S., Yoon, R. H. and Sebba, F., 1982. "Cleaning of Fine Coal by Flotation Using Colloidal Gas Aphrons," Proceedings of the Technical Program, International Powder and Bulk Solids Handling and Processing, Rosemont, Illinois, May, pp. 67-75.

Hines, Pierre R., 1962. "Before Flotation," in Froth Flotation, 50th Anniversary Volume, D. W. Fuerstenau (ed.), AIME, New York, p. 9.

Jameson, G. J., 1983. Personal Communication, The University of Newcastle, New South Wales, Australia, July.

Jameson, G. J., Nam, S. and Young, M. M., 1977. "Physical Factors Affecting Recovery Rates in Flotation," Minerals Sci. Engng., 9(3):103.

Jowett, A., 1980. "Formation and Disruption of Particle-Bubble Aggregates in Flotation," in Fine Particles Processing, vol. 1, P. Somasundaran (ed.), AIME, New York, pp. 720-754.

Kalra, T. R. and Uhlherr, P. H. T., 1971. 4th Aust. Conf. Hydraul. Fluid Mech., Melbourne, Australia.

Kiefer, J. E. and Wilson, D., 1980. "Electrical Aspects of Adsorbing Colloid Flotation. XI. Surfactant Adsorption Isotherms, Particle Displacement and Differential Capacitance," Separation Science and Technology, 15(1): 57-74.

Klassen, V. I. and Mokrousov, V. A., 1963. An Introduction to the Theory of Flotation, translated by J. Leja and G. W. Poling, Butterworths, London, p. 111.

Konar, B. B. and Sarkar, G. G., 1982. "Developments in Coal Preparation - New Vistas," Journal of Mines, Metals and Fuels, March, p. 120.

Levich, V. G., 1962. Physicochemical Hydrodynamics, Prentice-Hall, New Jersey, p. 221.

Luttrell, G. H. and Yoon, R. H., 1983. "Automation of a Laboratory Flotation Machine for Improved Performance," Int. J. Min. Proc., 10:165-172.

Lynch, A. J., Johnson, N. W., McKee, D. J. and Thorne, G. C., 1974. "The Behavior of Minerals in Sulfide Flotation Processes with Reference to Simulation and Control," J. S. Afr. Inst. Min. Metall., 74:349.

McCabe and Smith, 1976. Unit Operations of Chemical Engineering, McGraw-Hill Chemical Engineering Series, 3rd edition, New York, p. 157.

Morris, T. M., 1952. Trans. AIME, 193:794.

Packham, R. F. and Richards, W. N., 1975. "Water Clarification by Flotation - 3," Technical Report 2, Water Research Center, Medmenham Lab, Marlow, Bucks, England.

Reay, D. and Ratcliff, G. A., 1973. "Experimental Testing of the Hydrodynamic Collision Model of Fine Particle Flotation," Can. J. Chem. Engng., 53:178-185.

Reay, D. and Ratcliff, G. A., 1975. "A Removal of Fine Particles from Water by Dispersed Air Flotation: Effects of Bubble Size and Particle Size on Collection Efficiency," Can. J. Chem. Engng., 53:481-486.

Roe, L. A., 1980. "Flotation of Liquids and Fine Particles from Liquids," in Fine Particles Processing, vol. 1, P. Somasundaran (ed.), AIME, New York, pp. 871-885.

Sebba, F., 1971. "Microfoams - An Unexploited Colloid System," J. Colloid and Interface Sci., 35:643-646.

Sebba, F. and Yoon, R. H., 1982. "The Use of Micron-Sized Bubbles in Mineral Processing," Interfacial Phenomena in Mineral Processing (Proceedings of the Engineering Foundation Conference, Rindge, New Hampshire, August, 1981), B. Yarar and D. Spottiswood (eds.), United Engineering Trustees, Inc., New York, pp. 271-285.

Somasundaran, P., 1979. "Processing Mineral Fines," Engng. and Mining Journal, December, p. 64-68.

Sutherland, K. L., 1948. "Kinetics of the Flotation," J. Phys. Chem., 52:394-425.

Tomlinson, H. S. and Fleming, M. G., 1965. "Flotation Rate Studies," Proceedings, 6th International Mineral Processing Congress, Cannes, A. Roberts (ed.), Pergamon, Oxford, p. 563.

Trahar, W. J., 1981. "A Rational Interpretation of the Role of Particle Size in Flotation," Int. J. Min. Proc., 8:289.

Wark, I. W., 1933. "Physical Chemistry of Flotation. 1. The Significance of Contact Angle in Flotation," J. Phys. Chem., 37:623-644.

Wark, I. W., 1938. Principles of Flotation, Australian Inst. of Mining and Met., Melbourne, p. 7.

Whelan and Mainhood, 1955. "Flotation Frothers for Low-Rank Coals," J. Appl. Chem., 5:133.

Yoon, R. H., 1982. "Flotation of Fine Coal Using Microbubbles and Inorganic Salts," Mining Congress Journal, 68(12):76-80.

Yoon, R. H. and Miller, K. J., 1982. "A Preliminary Investigation on the Application of Microgas Dispersion for

Fine Coal Flotation," Proceedings of the Technical Program, International Powder and Bulk Solids Handling and Processing, Rosemont, Illinois, May, pp. 357-370.

Yoon, R. H. and Sebba, F., 1981. "Microgas Dispersion for Fine Coal Cleaning," Technical Progress Report for the Period September 1, 1980 - February 28, 1981; Report No. DOE/PC/30234-T1, 22 pp.

Zimmerman, R. E., 1979. "Flotation in Practice," in Coal Preparation, J. W. Leonard (ed.), AIME, New York, pp. 10-82.

APPENDIX I.

Calibration of Electrophoresis Apparatus

Determination of the eyepiece graticule:

A stage micrometer was used to determine the distance measured by the eyepiece graticule. The distance was determined to be 70 microns.

Determination of the stationary levels:

The positions of the stationary levels were found using Komagata's equation*:

$$\frac{s}{D} = 0.500 - 0.0833 + \frac{32}{\pi s}\left(\frac{d}{h}\right)^{\frac{1}{2}}$$

where s is the distance from the cell wall, d is the cell width and h is the cell height. Substituting the appropriate values for d and h, s was calculated. Once the cell holder had been secured in the bath and the cell walls located, the eyepiece was focused a distance s from the cell walls and measurements were made.

Determination of the interelectrode distance:

The interelectrode distance, l, was determined by calculating the cross-sectional area of the cell, A, and measuring the resistance, R, of the cell using a solution of

known specific conductance, K. Using the relation:

$$l = RKA,$$

the interelectrode distance was calculated.

---

*Operating instructions and manual for the Particle Micro-Electrophoresis Apparatus Mark II, Rank Brothers, High Street, Bottisham, Cambridge C85 90A, England.

APPENDIX II.

Tables of Experimental Results Presented in Figures

Figure No. 10

Stability of Microbubble Suspensions Produced with Dowfroth M150 and MIBC (Frother Concentration 250 mg/l)

Volume of Clear Solution (ml)	Time (sec) DF M150	MIBC
10	38	5
20	98	30
30	130	50
40	155	65
50	190	80
60	213	95
70	245	105
80	-	125
90	-	140
100	-	-
	Final Volume (ml)	
	73	90

Figure No. 11

Surface Tension of Dowfroth M150 and MIBC Solutions as a Function of Concentration

Frother Concentration (mg/l)	Surface Tension (dynes/cm)	
	DF M150	MIBC
5.0	67.5	71.8
14.0	66.1	71.4
60.0	62.0	70.0
500.0	57.2	65.0

Figure No. 12

Electrophoretic Mobilities of Coal and Quartz Particles as a Function of Frother Concentration at pH 7

Frother Concentration (ml/l)		Mobility (cm^2/volt · sec x 10^{-4})	
Quartz	Coal	Quartz	Coal
Dowfroth M150			
0.00	0.05	-2.80	-1.58
0.50	1.00	-3.41	-2.21
2.00	5.00	-4.23	-3.62
20.00	20.00	-5.81	-4.99
MIBC			
0.04	0.04	-2.64	-1.78
1.00	1.00	-2.36	-1.49
5.00	5.00	-2.35	-1.48
20.00	20.00	-2.06	-1.40

Figure No. 13

Streaming Currents of Microbubbles as a Function of Frother (Dowfroth M150 and MIBC) Concentration

Frother Concentration (ml/l)		Current (amps x 10^{-9})	
DF M150	MIBC	DF M150	MIBC
0.06	0.067	-0.20	1.07
0.10	0.30	-0.25	-0.58
0.20	1.00	-1.50	-2.16
0.50	5.00	-1.90	-0.54
1.00	10.00	-1.81	-0.22
3.00		-2.70	
5.00		-3.90	

Figure No. 14

Streaming Currents of Microbubbles Produced with Dowfroth M150 as a Function of pH

pH	Current (amps x 10^{-9})
3.04	4.40
4.20	2.86
5.01	-0.74
6.85	-1.96
8.20	-2.60

Figure No. 15

Contact Angles of Sessile Drops of Frother Solutions on Pittsburgh No. 8 Seam Coal as a Function of Concentration

Surfactant Concentration (mg/l)	Contact Angle (degrees)	
	DF MI50	MIBC
0	70	70
0.2	70	70
0.9	70	70
1.5	70	80
2.3	75	85
3.1	80	90
6.2	80	90

Figure No. 16

Viscosity of Dowfroth M150 and MIBC Solutions as a Function of Concentration

Surfactant Concentration (mg/l)		Viscosity (centipoise)	
DF M150	MIBC	DF M150	MIBC
10	10	1.40	1.38
50	50	1.40	1.30
160	160	1.38	1.22
---	300	--	1.22
500	---	1.40	--
600	---	1.42	--
5000	---	1.92	--
---	9000	--	1.70

Figure No. 17 Test No. DT-PS-1 1 lb/ton MIBC

	Sample Weight (g)	Yield (% wt)	Ash (% wt)	Coal (% wt)	Recovery (% wt) Ash	Recovery (% wt) Coal
1st stage concentrate	2.3	9.5	15.5	84.5	3.5	13.8
1st stage refuse	22.0	90.5	44.7	55.3	96.5	86.2
Feed	24.3	100.0	41.9	58.1	100.0	100.0

Figure No. 17 Test No. DT-PS-2 2 lb/ton MIBC

	Sample Weight (g)	Yield (% wt)	Ash (% wt)	Coal (% wt)	Recovery (% wt) Ash	Recovery (% wt) Coal
1st stage concentrate	3.2	13.0	10.4	89.6	3.3	20.0
1st stage refuse	21.4	87.0	46.4	53.6	96.8	80.0
Feed	24.6	100.0	41.7	58.3	100.0	100.0

Figure No. 17 Test No. DT-PS-3 3 lb/ton MIBC

	Sample Weight (g)	Yield (% wt)	Ash (% wt)	Coal (% wt)	Recovery (% wt) Ash	Recovery (% wt) Coal
1st stage concentrate	6.6	26.8	12.5	87.5	8.1	40.1
1st stage refuse	18.0	73.2	52.1	47.9	91.9	59.9
Feed	24.6	100.0	41.5	58.5	100.0	100.0

Figure No. 17 Test No. DT-PS-4 4 lb/ton MIBC

	Sample Weight (g)	Yield (% wt)	Ash (% wt)	Coal (% wt)	Recovery (% wt) Ash	Coal
1st stage concentrate	5.9	24.1	10.2	89.8	6.3	35.5
1st stage refuse	18.6	75.9	48.2	51.8	93.7	64.5
Feed	24.5	100.0	39.0	61.0	100.0	100.0

Figure No. 17 Test No. DT-PS-5 5 lb/ton MIBC

	Sample Weight (g)	Yield (% wt)	Ash (% wt)	Coal (% wt)	Recovery (% wt) Ash	Coal
1st stage concentrate	5.2	21.3	12.0	88.0	6.4	31.2
1st stage refuse	19.2	78.7	47.4	52.6	93.6	68.8
Feed	24.4	100.0	39.8	60.2	100.0	100.0

Figure No. 17 Test No. DT-PS-6 6 lb/ton MIBC

	Sample Weight (g)	Yield (% wt)	Ash (% wt)	Coal (% wt)	Recovery (% wt) Ash	Coal
1st stage concentrate	6.8	27.5	11.4	88.6	8.0	40.1
1st stage refuse	17.9	72.5	49.6	50.4	92.0	59.9
Feed	24.7	100.0	39.1	60.9	100.0	100.0

Figure No. 17 Test No. DT-PS-7 6 lb/ton DF M150

	Sample Weight (g)	Yield (% wt)	Ash (% wt)	Coal (% wt)	Recovery (% wt) Ash	Recovery (% wt) Coal
1st stage concentrate	17.9	80.3	19.9	80.2	47.2	97.1
1st stage refuse	4.4	19.7	90.3	9.7	52.8	2.9
Feed	22.3	100.0	33.7	66.3	100.0	100.0

Figure No. 17 Test No. DT-PS-8 5 lb/ton DF M150

	Sample Weight (g)	Yield (% wt)	Ash (% wt)	Coal (% wt)	Recovery (% wt) Ash	Recovery (% wt) Coal
1st stage concentrate	18.6	76.9	19.3	80.7	41.9	96.0
1st stage refuse	5.6	23.1	88.7	11.3	58.1	4.0
Feed	24.2	100.0	35.3	64.7	100.0	100.0

Figure No. 17 Test No. DT-PS-9 4 lb/ton DF M150

	Sample Weight (g)	Yield (% wt)	Ash (% wt)	Coal (% wt)	Recovery (% wt) Ash	Recovery (% wt) Coal
1st stage concentrate	18.9	79.1	20.2	79.8	46.1	96.6
1st stage refuse	5.0	20.9	89.3	10.7	53.9	3.4
Feed	23.9	100.0	34.7	65.3	100.0	100.0

Figure No. 17 Test No. DT-PS-10 3 lb/ton DF M150

	Sample Weight (g)	Yield (% wt)	Ash (% wt)	Coal (% wt)	Recovery (% wt) Ash	Recovery (% wt) Coal
1st stage concentrate	18.2	77.8	19.3	80.7	42.7	96.8
1st stage refuse	5.2	22.2	90.7	9.3	57.3	3.2
Feed	23.4	100.0	35.2	64.8	100.0	100.0

Figure No. 17 Test No. DT-PS-11 2 lb/ton DF M150

	Sample Weight (g)	Yield (% wt)	Ash (% wt)	Coal (% wt)	Recovery (% wt) Ash	Recovery (% wt) Coal
1st stage concentrate	17.5	75.8	16.3	83.7	36.3	96.1
1st stage refuse	5.6	24.2	89.5	10.5	63.7	3.9
Feed	23.1	100.0	34.1	65.9	100.0	100.0

Figure No. 17 Test No. DT-PS-12 1 lb/ton DF M150

	Sample Weight (g)	Yield (% wt)	Ash (% wt)	Coal (% wt)	Recovery (% wt) Ash	Recovery (% wt) Coal
1st stage concentrate	14.8	62.7	14.4	85.6	25.1	83.9
1st stage refuse	8.8	37.3	72.3	27.7	74.9	16.1
Feed	23.6	100.0	36.0	64.0	100.0	100.0

Figure No. 18 Test No. DT-PS-7 6 lb/ton DF M150

	Sample Weight (g)	Yield (% wt)	Ash (% wt)	Coal (% wt)	Recovery (% wt) Ash	Coal
2nd stage concentrate	15.5	69.5	12.6	87.4	26.0	91.7
2nd stage refuse	2.4	10.8	66.5	33.5	21.2	5.5
1st stage concentrate	17.9	80.3	19.9	80.2	47.2	97.1
1st stage refuse	4.4	19.7	90.3	9.7	52.8	2.9
Feed	22.3	100.0	33.7	66.3	100.0	100.0

Figure No. 18 Test No. DT-PS-8 5 lb/ton DF M150

	Sample Weight (g)	Yield (% wt)	Ash (% wt)	Coal (% wt)	Recovery (% wt) Ash	Coal
2nd stage concentrate	15.7	64.9	10.7	89.3	19.6	89.6
2nd stage refuse	2.9	12.0	65.7	34.3	22.3	6.4
1st stage concentrate	18.6	76.9	19.3	80.7	41.9	96.0
1st stage refuse	5.6	23.1	88.7	11.3	58.1	4.0
Feed	24.2	100.0	35.3	64.7	100.0	100.0

Figure No. 18 Test No. DT-PS-9 4 lb/ton DF M150

	Sample Weight (g)	Yield (% wt)	Ash (% wt)	Coal (% wt)	Recovery (% wt) Ash	Coal
2nd stage concentrate	15.4	64.4	11.8	88.2	22.0	87.0
2nd stage refuse	3.5	14.6	57.3	42.7	24.2	9.6
1st stage concentrate	18.9	79.1	20.2	79.8	46.1	96.6
1st stage refuse	5.0	20.9	89.3	10.7	53.9	3.4
Feed	23.9	100.0	34.7	65.3	100.0	100.0

Figure No. 18 Test No. DT-PS-10 3 lb/ton DF M150

	Sample Weight (g)	Yield (% wt)	Ash (% wt)	Coal (% wt)	Recovery (% wt) Ash	Coal
2nd stage concentrate	14.2	60.7	10.8	89.2	18.7	83.5
2nd stage refuse	4.0	17.1	49.4	50.6	24.0	13.3
1st stage concentrate	18.2	77.8	19.3	80.7	42.7	96.8
1st stage refuse	5.2	22.2	90.7	9.3	57.3	3.2
Feed	23.4	100.0	35.2	64.8	100.0	100.0

Figure No. 18 Test No. DT-PS-11 2 lb/ton DF M150

	Sample Weight (g)	Yield (% wt)	Ash (% wt)	Coal (% wt)	Recovery (% wt) Ash	Recovery (% wt) Coal
2nd stage concentrate	14.1	61.0	9.9	90.1	17.7	83.4
2nd stage refuse	3.4	14.7	43.1	56.9	18.6	12.7
1st stage concentrate	17.5	75.8	16.3	83.7	36.3	96.1
1st stage refuse	5.6	24.2	89.6	10.5	63.7	3.9
Feed	23.1	100.0	34.1	65.9	100.0	100.0

Figure No. 18 Test No. DT-PS-12 1 lb/ton DF M150

	Sample Weight (g)	Yield (% wt)	Ash (% wt)	Coal (% wt)	Recovery (% wt) Ash	Recovery (% wt) Coal
2nd stage concentrate	12.4	52.5	9.0	91.0	13.2	74.7
2nd stage refuse	2.4	10.2	42.3	57.7	12.0	9.2
1st stage concentrate	14.8	62.7	14.4	85.6	25.1	83.9
1st stage refuse	8.8	37.3	72.3	27.7	74.9	16.1
Feed	23.6	100.0	36.0	64.0	100.0	100.0

Figure No. 19 Test No. DT-PS-141 3.6 lb/ton DF M150

	Sample Weight (g)	Yield (% wt)	Ash (% wt)	Coal (% wt)	Recovery (% wt) Ash	Recovery (% wt) Coal
2nd stage concentrate	16.1	87.7	2.1	97.9	45.2	89.5
2nd stage refuse	1.8	9.9	9.0	91.0	22.2	9.4
1st stage concentrate	18.0	97.6	2.8	97.2	67.4	98.9
1st stage refuse	0.4	2.4	54.8	45.2	32.6	1.1
Feed	18.4	100.0	4.0	96.0	100.0	100.0

Figure No. 19 Test No. DT-PS-142 4.5 lb/ton DF M150

	Sample Weight (g)	Yield (% wt)	Ash (% wt)	Coal (% wt)	Recovery (% wt) Ash	Recovery (% wt) Coal
2nd stage concentrate	14.9	95.9	1.8	98.2	50.7	97.5
2nd stage refuse	0.4	2.3	24.7	75.3	16.9	1.8
1st stage concentrate	15.3	98.3	2.3	97.7	67.6	99.3
1st stage refuse	0.3	1.7	63.2	36.8	32.4	0.7
Feed	15.6	100.0	3.4	96.6	100.0	100.0

Figure No. 19 Test No. DT-PS-143 6.8 lb/ton DF M150

	Sample Weight (g)	Yield (% wt)	Ash (% wt)	Coal (% wt)	Recovery (% wt) Ash	Recovery (% wt) Coal
2nd stage concentrate	15.6	87.9	1.9	98.1	45.9	89.5
2nd stage refuse	1.7	9.8	8.4	91.6	22.6	9.3
1st stage concentrate	17.3	97.7	2.5	97.5	68.5	98.8
1st stage refuse	0.4	2.3	49.4	50.6	31.5	1.2
Feed	17.8	100.0	3.6	96.4	100.0	100.0

Figure No. 19 Test No. DT-PS-144 8.9 lb/ton DF M150

	Sample Weight (g)	Yield (% wt)	Ash (% wt)	Coal (% wt)	Recovery (% wt) Ash	Recovery (% wt) Coal
2nd stage concentrate	13.8	79.3	1.9	98.1	49.0	80.2
2nd stage refuse	3.4	19.5	5.3	94.7	33.6	19.1
1st stage concentrate	17.2	98.8	2.6	97.4	82.6	99.3
1st stage refuse	0.2	1.2	44.0	56.0	17.4	0.7
Feed	17.4	100.0	3.1	96.9	100.0	100.0

Figure No. 20 Test No. 164 0.5 lb/ton DF M150

	Sample Weight (g)	Yield (% wt)	Ash (% wt)	Coal (% wt)	Recovery (% wt) Ash	Recovery (% wt) Coal
2nd stage concentrate	2.6	13.5	2.2	97.8	5.7	14.0
2nd stage refuse	0.6	3.4	10.8	89.2	7.0	3.2
1st stage concentrate	3.2	16.9	4.0	96.1	12.7	17.2
1st stage refuse	15.7	83.1	5.5	94.5	87.3	82.8
Feed	18.8	100.0	5.3	94.7	100.0	100.0

Figure No. 20 Test No. DT-PS-165 0.9 lb/ton DF M150

	Sample Weight (g)	Yield (% wt)	Ash (% wt)	Coal (% wt)	Recovery (% wt) Ash	Recovery (% wt) Coal
2nd stage concentrate	7.3	39.8	2.4	97.6	18.4	41.0
2nd stage refuse	1.5	8.0	10.1	90.0	15.7	7.6
1st stage concentrate	8.8	47.8	3.7	96.4	34.1	48.6
1st stage refuse	9.6	52.2	6.5	93.5	34.1	48.6
Feed	18.4	100.0	5.1	94.9	100.0	100.0

Figure No. 20 Test No. DT-PS-166 1.9 lb/ton DF M150

	Sample Weight (g)	Yield (% wt)	Ash (% wt)	Coal (% wt)	Recovery (% wt) Ash	Recovery (% wt) Coal
2nd stage concentrate	6.6	32.0	2.3	97.7	14.6	32.9
2nd stage refuse	5.5	27.1	5.1	94.9	27.2	27.1
1st stage concentrate	12.1	59.1	3.6	96.4	41.8	60.0
1st stage refuse	8.4	40.9	7.2	92.8	58.2	40.0
Feed	20.5	100.0	5.0	95.0	100.0	100.0

Figure No. 20 Test No. DT-PS-167 3.1 lb/ton DF M150

	Sample Weight (g)	Yield (% wt)	Ash (% wt)	Coal (% wt)	Recovery (% wt) Ash	Recovery (% wt) Coal
2nd stage concentrate	9.9	52.3	2.7	97.3	28.2	53.5
2nd stage refuse	4.3	22.5	6.3	93.8	28.1	22.2
1st stage concentrate	14.2	74.8	3.8	96.2	56.3	75.8
1st stage refuse	4.8	25.2	8.7	91.3	43.7	24.2
Feed	19.0	100.0	5.0	95.0	100.0	100.0

Figure No. 20 Test No. DT-PS-168 5.9 lb/ton DF M150

	Sample Weight (g)	Yield (% wt)	Ash (% wt)	Coal (% wt)	Recovery (% wt) Ash	Recovery (% wt) Coal
2nd stage concentrate	11.6	56.8	2.7	97.3	32.5	58.0
2nd stage refuse	7.7	37.6	5.3	94.7	41.8	37.3
1st stage concentrate	19.3	94.4	3.8	96.2	74.3	95.4
1st stage refuse	1.2	5.6	21.9	78.2	25.7	4.6
Feed	20.5	100.0	4.8	95.2	100.0	100.0

Figure No. 20 Test No. DT-PS-169 11.5 lb/ton DF M150

	Sample Weight (g)	Yield (% wt)	Ash (% wt)	Coal (% wt)	Recovery (% wt) Ash	Recovery (% wt) Coal
2nd stage concentrate	7.4	42.9	2.5	97.5	23.1	43.9
2nd stage refuse	9.0	51.9	4.0	96.0	44.5	52.3
1st stage concentrate	16.4	94.9	3.3	96.7	67.6	96.2
1st stage refuse	0.9	5.1	29.5	70.5	32.4	3.8
Feed	17.3	100.0	4.7	95.3	100.0	100.0

Figure No. 21 Test No. DT-PS-37 1 lb/ton DF M150

	Sample Weight (g)	Yield (% wt)	Ash (% wt)	Coal (% wt)	Recovery (% wt) Ash	Recovery (% wt) Coal
2nd stage concentrate	12.2	49.3	13.1	86.9	18.3	66.0
2nd stage refuse	6.5	26.2	36.3	63.7	27.1	25.7
1st stage concentrate	18.6	75.4	21.1	78.9	45.4	91.7
1st stage refuse	6.1	24.6	78.1	21.9	54.6	8.3
Feed	24.7	100.0	35.1	64.9	100.0	100.0

Figure No. 21 Test No. DT-PS-38 2 lb/ton DF M150

	Sample Weight (g)	Yield (% wt)	Ash (% wt)	Coal (% wt)	Recovery (% wt) Ash	Recovery (% wt) Coal
2nd stage concentrate	15.6	63.2	13.7	86.3	24.9	83.4
2nd stage refuse	3.1	12.6	59.5	40.5	21.5	7.8
1st stage concentrate	18.7	75.7	21.3	78.7	46.5	91.2
1st stage refuse	6.0	24.3	76.4	23.6	53.6	8.7
Feed	24.7	100.0	34.7	65.3	100.0	100.0

Figure No. 21 Test No. DT-PS-39 3 lb/ton DF M150

	Sample Weight (g)	Yield (% wt)	Ash (% wt)	Coal (% wt)	Recovery (% wt) Ash	Recovery (% wt) Coal
2nd stage concentrate	15.9	65.3	15.3	84.7	28.8	84.5
2nd stage refuse	2.1	8.7	67.6	32.4	16.9	4.3
1st stage concentrate	18.0	74.0	21.5	78.5	45.7	89.1
1st stage refuse	6.3	26.0	72.7	27.3	54.3	10.9
Feed	24.4	100.0	34.8	65.2	100.0	100.0

Figure No. 21 Test No. DT-PS-40 4 lb/ton DF M150

	Sample Weight (g)	Yield (% wt)	Ash (% wt)	Coal (% wt)	Recovery (% wt) Ash	Recovery (% wt) Coal
2nd stage concentrate	15.7	63.6	14.5	86.5	26.4	83.5
2nd stage refuse	2.3	9.3	62.2	37.8	16.6	5.4
1st stage concentrate	18.0	72.9	20.6	79.4	43.1	88.9
1st stage refuse	6.7	27.1	73.2	26.8	56.9	11.1
Feed	24.7	100.0	34.9	65.2	100.0	100.0

Figure No. 21 Test No. DT-PS-41 5 lb/ton DF M150

	Sample Weight (g)	Yield (% wt)	Ash (% wt)	Coal (% wt)	Recovery (% wt) Ash	Coal
2nd stage concentrate	14.9	60.5	13.1	86.9	22.9	80.5
2nd stage refuse	1.8	7.4	64.2	35.8	13.7	4.1
1st stage concentrate	16.7	67.9	18.7	81.3	36.7	84.5
1st stage refuse	7.9	32.1	68.6	31.5	63.4	15.5
Feed						

Figure No. 22 Test No. DT-PS-31 1 lb/ton DF M150

	Sample Weight (g)	Yield (% wt)	Ash (% wt)	Coal (% wt)	Recovery (% wt) Ash	Coal
2nd stage concentrate	15.2	61.6	11.9	88.1	21.1	83.2
2nd stage refuse	2.3	9.1	61.2	38.8	16.1	5.4
1st stage concentrate	17.5	70.7	18.3	81.7	37.1	88.6
1st stage refuse	7.3	29.3	74.6	25.4	62.9	11.4
Feed	24.8	100.0	34.8	65.2	100.0	100.0

Figure No. 22 Test No. DT-PS-32 2 lb/ton DF M150

	Sample Weight (g)	Yield (% wt)	Ash (% wt)	Coal (% wt)	Recovery (% wt) Ash	Recovery (% wt) Coal
2nd stage concentrate	15.1	61.0	13.0	87.0	22.8	81.3
2nd stage refuse	1.6	6.3	74.6	25.4	13.4	2.4
1st stage concentrate	16.7	67.3	18.7	81.3	36.3	83.7
1st stage refuse	8.1	32.7	67.6	32.4	63.7	16.3
Feed	24.8	100.0	34.7	65.3	100.0	100.0

Figure No. 22 Test No. DT-PS-33 3 lb/ton DF M150

	Sample Weight (g)	Yield (% wt)	Ash (% wt)	Coal (% wt)	Recovery (% wt) Ash	Recovery (% wt) Coal
2nd stage concentrate	15.7	62.8	13.8	86.2	25.0	82.8
2nd stage refuse	1.4	5.5	77.8	22.2	12.5	1.9
1st stage concentrate	17.0	68.3	19.0	81.1	37.5	84.6
1st stage refuse	7.9	31.7	68.2	31.8	62.5	15.4
Feed	24.9	100.0	34.6	65.4	100.0	100.0

Figure No. 22 Test No. DT-PS-34 4 lb/ton DF M150

	Sample Weight (g)	Yield (% wt)	Ash (% wt)	Coal (% wt)	Recovery (% wt) Ash	Recovery (% wt) Coal
2nd stage concentrate	16.2	66.1	14.9	85.1	28.4	86.2
2nd stage refuse	1.4	5.7	75.9	24.1	12.38	2.1
1st stage concentrate	17.6	71.8	19.7	80.2	40.8	88.3
1st stage refuse	6.9	28.2	72.9	27.1	59.2	11.7
Feed	24.5	100.0	34.8	65.2	100.0	100.0

Figure No. 22 Test No. DT-PS-35 5 lb/ton DF M150

	Sample Weight (g)	Yield (% wt)	Ash (% wt)	Coal (% wt)	Recovery (% wt) Ash	Recovery (% wt) Coal
2nd stage concentrate	16.6	67.5	15.2	84.8	30.1	86.9
2nd stage refuse	1.2	4.8	79.5	20.5	11.3	1.5
1st stage concentrate	17.8	72.3	19.5	80.5	41.4	88.4
1st stage refuse	6.8	27.7	72.3	27.7	58.6	11.6
Feed	24.6	100.0	34.1	65.9	100.0	100.0

Figure No. 23 Test No. DT-PS-170 0.5 lb/ton DF M150

	Sample Weight (g)	Yield (% wt)	Ash (% wt)	Coal (% wt)	Recovery (% wt) Ash	Coal
2nd stage concentrate	5.0	30.7	2.3	97.7	13.9	31.6
2nd stage refuse	10.1	62.9	3.5	96.5	42.8	64.0
1st stage concentrate	15.1	93.7	3.1	96.9	56.7	95.7
1st stage refuse	1.0	6.3	35.2	64.8	43.3	4.3
Feed	16.1	100.0	5.2	94.9	100.0	100.0

Figure No. 23 Test No. DT-PS-171 1.0 lb/ton DF M150

	Sample Weight (g)	Yield (% wt)	Ash (% wt)	Coal (% wt)	Recovery (% wt) Ash	Coal
2nd stage concentrate	10.3	52.3	2.5	97.5	26.9	53.6
2nd stage refuse	8.2	41.6	4.3	95.7	36.5	41.9
1st stage concentrate	18.5	93.9	3.3	96.7	63.4	95.4
1st stage refuse	1.2	6.1	29.4	70.6	36.6	4.6
Feed	19.7	100.0	4.9	95.1	100.0	100.0

Figure No. 23 Test No. DT-PS-172 1.2 lb/ton DF M150

	Sample Weight (g)	Yield (% wt)	Ash (% wt)	Coal (% wt)	Recovery (% wt) Ash	Coal
2nd stage concentrate	13.3	60.5	2.8	97.2	34.6	61.8
2nd stage refuse	6.3	28.8	5.2	94.8	30.7	28.7
1st stage concentrate	19.6	89.3	3.6	96.4	65.3	90.5
1st stage refuse	2.4	10.7	15.8	84.2	34.7	9.5
Feed	22.0	100.0	4.9	95.1	100.0	100.0

Figure No. 23 Test No. DT-PS-173 2.8 lb/ton DF M150

	Sample Weight (g)	Yield (% wt)	Ash (% wt)	Coal (% wt)	Recovery (% wt) Ash	Coal
2nd stage concentrate	16.6	82.2	2.3	97.7	39.6	84.3
2nd stage refuse	2.6	12.7	9.5	90.5	24.8	12.0
1st stage concentrate	19.2	94.8	3.3	96.7	64.5	96.4
1st stage refuse	1.1	5.2	33.1	66.9	35.6	3.7
Feed	20.2	100.0	4.8	95.2	100.0	100.0

Figure No. 23 Test No. DT-PS-174 6.9 lb/ton DF M150

	Sample Weight (g)	Yield (% wt)	Ash (% wt)	Coal (% wt)	Recovery (% wt) Ash	Recovery (% wt) Coal
2nd stage concentrate	16.7	90.3	2.2	97.8	42.0	92.7
2nd stage refuse	0.9	4.8	18.5	81.5	18.5	4.1
1st stage concentrate	17.6	95.1	3.1	97.0	60.5	96.8
1st stage refuse	0.9	4.9	38.6	61.4	39.5	3.2
Feed	18.5	100.0	4.8	95.2	100.0	100.0

Figure No. 23 Test No. DT-PS-175 8.9 lb/ton DF M150

	Sample Weight (g)	Yield (% wt)	Ash (% wt)	Coal (% wt)	Recovery (% wt) Ash	Recovery (% wt) Coal
2nd stage concentrate	18.5	91.5	2.4	97.7	43.7	94.0
2nd stage refuse	0.6	3.1	33.6	66.4	20.9	2.1
1st stage concentrate	19.1	94.6	3.4	96.6	64.6	96.1
1st stage refuse	1.1	5.4	32.0	68.0	35.4	3.9
Feed	20.2	100.0	4.9	95.1	100.0	100.0

Figure No. 24 Test No. DT-PS-13 0 lb/ton Kerosene

	Sample Weight (g)	Yield (% wt)	Ash (% wt)	Coal (% wt)	Recovery (% wt) Ash	Recovery (% wt) Coal
2nd stage concentrate	8.6	39.5	10.5	89.5	12.3	53.3
2nd stage refuse	5.0	22.9	35.8	64.2	24.4	22.2
1st stage concentrate	13.6	62.4	19.8	80.2	36.6	75.5
1st stage refuse	8.2	37.6	56.8	43.2	63.4	24.5
Feed	21.8	100.0	33.7	66.3	100.0	100.0

Figure No. 24 Test No. DT-PS-15 2 lb/ton Kerosene

	Sample Weight (g)	Yield (% wt)	Ash (% wt)	Coal (% wt)	Recovery (% wt) Ash	Recovery (% wt) Coal
2nd stage concentrate	10.6	52.0	7.7	92.3	13.9	67.3
2nd stage refuse	5.0	24.5	32.3	67.7	27.5	23.3
1st stage concentrate	15.6	76.5	15.6	84.4	41.5	90.6
1st stage refuse	4.8	23.5	71.6	28.4	58.5	9.4
Feed	20.4	100.0	28.8	71.2	100.0	100.0

Figure No. 24 Test No. DT-PS 16 3 lb/ton Kerosene

	Sample Weight (g)	Yield (% wt)	Ash (% wt)	Coal (% wt)	Recovery (% wt) Ash	Coal
2nd stage concentrate	14.6	76.0	10.4	89.6	31.0	91.4
2nd stage refuse	1.8	9.4	58.9	41.2	21.7	5.2
1st stage concentrate	16.4	85.4	15.7	84.3	52.7	96.6
1st stage refuse	2.8	14.6	82.7	17.3	47.3	3.4
Feed	19.2	100.0	25.5	74.5	100.0	100.0

Figure No. 24 Test No. DT-PS-17 4 lb/ton Kerosene

	Sample Weight (g)	Yield (% wt)	Ash (% wt)	Coal (% wt)	Recovery (% wt) Ash	Coal
2nd stage concentrate	15.2	78.4	12.3	87.7	38.7	91.6
2nd stage refuse	2.1	10.8	60.5	39.5	26.2	5.7
1st stage concentrate	17.3	89.2	18.2	81.8	64.9	97.3
1st stage refuse	2.1	10.8	81.1	18.9	35.1	2.7
Feed	19.4	100.0	25.0	75.0	100.0	100.0

Figure No. 24 Test No. DT-PS-18 5 lb/ton Kerosene

	Sample Weight (g)	Yield (% wt)	Ash (% wt)	Coal (% wt)	Recovery (% wt) Ash	Coal
2nd stage concentrate	15.3	68.9	12.9	87.1	27.6	88.6
2nd stage refuse	2.3	10.4	58.0	42.0	18.7	6.4
1st stage concentrate	17.6	79.3	18.8	81.2	46.2	95.0
1st stage refuse	4.6	20.7	83.5	16.5	53.8	5.0
Feed	22.2	100.0	32.2	67.8	100.0	100.0

Figure No. 25 Test No. DT-PS-158 0.3 lb/ton Kerosene

	Sample Weight (g)	Yield (% wt)	Ash (% wt)	Coal (% wt)	Recovery (% wt) Ash	Coal
2nd stage concentrate	16.5	89.0	2.6	97.4	49.9	90.9
2nd stage refuse	1.3	6.8	15.7	84.3	23.1	6.0
1st stage concentrate	17.8	95.8	3.5	96.5	73.0	96.9
1st stage refuse	0.8	4.2	29.6	70.4	27.0	3.1
Feed	18.6	100.0	4.6	95.4	100.0	100.0

Figure No. 25 Test No. DT-PS-159 1.1 lb/ton Kerosene

	Sample Weight (g)	Yield (% wt)	Ash (% wt)	Coal (% wt)	Recovery (% wt) Ash	Coal
2nd stage concentrate	16.0	91.4	2.4	97.7	49.3	93.3
2nd stage refuse	0.6	3.5	19.6	80.4	15.7	2.9
1st stage concentrate	16.6	94.9	3.0	97.0	65.0	96.3
1st stage refuse	0.9	5.1	29.9	70.1	35.0	3.7
Feed	17.5	100.0	4.4	95.7	100.0	100.0

Figure No. 25 Test No. DT-PS-160 3.2 lb/ton Kerosene

	Sample Weight (g)	Yield (% wt)	Ash (% wt)	Coal (% wt)	Recovery (% wt) Ash	Coal
2nd stage concentrate	16.6	87.8	2.3	97.7	47.1	89.7
2nd stage refuse	1.3	6.7	12.8	87.2	19.9	6.1
1st stage concentrate	17.9	94.5	3.1	96.9	67.0	95.8
1st stage refuse	1.0	5.5	26.3	73.7	33.1	4.2
Feed	18.9	100.0	4.4	95.7	100.0	100.0

Figure No. 25 Test No. DT-PS-161 11.6 lb/ton Kerosene

	Sample Weight (g)	Yield (% wt)	Ash (% wt)	Coal (% wt)	Recovery (% wt) Ash	Coal
2nd stage concentrate	15.7	90.8	2.2	97.8	49.3	92.5
2nd stage refuse	0.9	5.1	12.7	87.3	16.0	4.6
1st stage concentrate	16.5	95.9	2.8	97.2	65.3	97.2
1st stage refuse	0.7	4.1	34.1	65.9	34.7	2.8
Feed	17.2	100.0	4.1	96.0	100.0	100.0

Figure No. 25 Test No. DT-PS-162 37.1 lb/ton Kerosene

	Sample Weight (g)	Yield (% wt)	Ash (% wt)	Coal (% wt)	Recovery (% wt) Ash	Coal
2nd stage concentrate	15.7	96.8	2.1	97.9	82.4	97.2
2nd stage refuse	0.3	1.6	27.3	72.7	17.6	1.2
1st stage concentrate	15.9	98.4	2.5	97.5	100.0	98.4
1st stage refuse	0.3	1.6	*	*	*	1.6
Feed	16.2	100.0	2.5	97.5	100.0	100.0

* Sample was too small to be analyzed for ash

Figure No. 25 Test No. DT-PS-163 109.1 lb/ton Kerosene

	Sample Weight (g)	Yield (% wt)	Ash (% wt)	Coal (% wt)	Recovery (% wt) Ash	Recovery (% wt) Coal
2nd stage concentrate	18.0	98.2	2.1	97.9	*	98.1
2nd stage refuse	0.2	1.0	*	*	*	*
1st stage concentrate	18.2	99.1	2.1	97.9	*	99.1
1st stage refuse	0.2	0,9	*	*	*	*
Feed	18.3	100.0	2.1	97.9	100.0	100.0

* Sample too small to be analyzed for ash

Figure No. _____ Test No. _____

	Sample Weight (g)	Yield (% wt)	Ash (% wt)	Coal (% wt)	Recovery (% wt) Ash	Recovery (% wt) Coal
2nd stage concentrate						
2nd stage refuse						
1st stage concentrate						
1st stage refuse						
Feed						

Figure No. 26 Test No. DT-PS-248 Microbubble Volume 95 ml

	Sample Weight (g)	Yield (% wt)	Ash (% wt)	Coal (% wt)	Recovery (% wt) Ash	Recovery (% wt) Coal
1st stage concentrate	5.0	23.5	5.4	94.7	14.4	24.3
1st stage refuse	16.3	76.5	9.8	90.2	85.6	75.7
Feed	21.3	100.0	8.7	91.3	100.0	100.0

Figure No. 26 Test No. DT-PS-249 Microbubble Volume 200 ml

	Sample Weight (g)	Yield (% wt)	Ash (% wt)	Coal (% wt)	Recovery (% wt) Ash	Recovery (% wt) Coal
1st stage concentrate	12.2	63.5	5.4	94.6	39.9	65.7
1st stage refuse	7.0	36.5	14.1	85.9	60.2	34.3
Feed	19.2	100.0	8.6	91.4	100.0	100.0

Figure No. 26 Test No. DT-PS-250 Microbubble Volume 360 ml

	Sample Weight (g)	Yield (% wt)	Ash (% wt)	Coal (% wt)	Recovery (% wt) Ash	Recovery (% wt) Coal
1st stage concentrate	15.8	83.8	5.6	94.4	55.9	86.3
1st stage refuse	3.1	16.2	22.8	77.2	44.2	13.7
Feed	18.8	100.0	8.4	91.6	100.0	100.0

Figure No. 26 Test No. DT-PS-251 Microbubble Volume 500 ml

	Sample Weight (g)	Yield (% wt)	Ash (% wt)	Coal (% wt)	Recovery (% wt) Ash	Recovery (% wt) Coal
1st stage concentrate	18.8	89.6	5.9	94.1	63.2	92.1
1st stage refuse	2.2	10.4	29.7	70.3	36.8	8.0
Feed	20.9	100.0	8.4	91.6	100.0	100.0

Figure No. 27 Test No. DT-PS-234 pH 4

	Sample Weight (g)	Yield (% wt)	Ash (% wt)	Coal (% wt)	Recovery (% wt) Ash	Recovery (% wt) Coal
1st stage concentrate	3.3	16.5	6.2	93.8	13.5	16.7
1st stage refuse	16.8	83.5	7.8	92.2	86.5	83.3
Feed	20.2	100.0	7.5	92.5	100.0	100.0

Figure No. 27 Test No. DT-PS-235 pH 6

	Sample Weight (g)	Yield (% wt)	Ash (% wt)	Coal (% wt)	Recovery (% wt) Ash	Recovery (% wt) Coal
1st stage concentrate	9.8	46.1	5.2	94.8	31.3	47.3
1st stage refuse	11.5	53.9	9.7	90.3	68.7	52.7
Feed	21.3	100.0	7.6	92.4	100.0	100.0

Figure No. 27 Test No. DT-PS-236 pH 7

	Sample Weight (g)	Yield (% wt)	Ash (% wt)	Coal (% wt)	Recovery (% wt) Ash	Recovery (% wt) Coal
1st stage concentrate	16.2	77.3	5.4	94.6	56.7	78.9
1st stage refuse	4.8	22.7	14.1	85.9	43.3	21.2
Feed	20.9	100.0	7.4	92.6	100.0	100.0

Figure No. 27 Test No. DT-PS-237 pH 8

	Sample Weight (g)	Yield (% wt)	Ash (% wt)	Coal (% wt)	Recovery (% wt) Ash	Recovery (% wt) Coal
1st stage concentrate	15.7	77.5	4.8	95.2	50.2	79.7
1st stage refuse	4.5	22.5	16.3	83.7	49.8	20.3
Feed	20.2	100.0	7.4	92.6	100.0	100.0

Figure No. 27 Test No. DT-PS-238 pH 10

	Sample Weight (g)	Yield (% wt)	Ash (% wt)	Coal (% wt)	Recovery (% wt) Ash	Recovery (% wt) Coal
1st stage concentrate	13.6	68.7	5.7	94.3	51.2	70.2
1st stage refuse	6.2	31.3	11.9	88.1	48.8	29.8
Feed	19.8	100.0	7.6	92.4	100.0	100.0

Figure No. 28 Test No. DT-PS-239 Pulp Density - 7.6

	Sample Weight (g)	Yield (% wt)	Ash (% wt)	Coal (% wt)	Recovery (% wt) Ash	Recovery (% wt) Coal
1st stage concentrate	19.0	90.4	5.7	94.3	66.9	92.3
1st stage refuse	2.0	9.7	26.2	73.8	33.1	7.7
Feed	21.0	100.0	7.7	92.4	100.0	100.0

Figure No. 28 Test No. DT-PS-240 Pulp Density - 5.4

	Sample Weight (g)	Yield (% wt)	Ash (% wt)	Coal (% wt)	Recovery (% wt) Ash	Recovery (% wt) Coal
1st stage concentrate	19.9	92.9	5.7	94.3	71.4	94.6
1st stage refuse	1.5	7.2	29.5	70.6	28.6	5.4
Feed	21.4	100.0	7.4	92.6	100.0	100.0

Figure No. 28 Test No. DT-PS-241 Pulp Density - 3.7

	Sample Weight (g)	Yield (% wt)	Ash (% wt)	Coal (% wt)	Recovery (% wt) Ash	Recovery (% wt) Coal
1st stage concentrate	19.3	88.1	5.7	94.3	65.1	90.0
1st stage refuse	2.6	11.9	22.6	77.4	34.9	10.0
Feed	22.0	100.0	7.7	92.3	100.0	100.0

Figure No. 28 Test No. DT-PS-242 Pulp Density - 2.4

	Sample Weight (g)	Yield (% wt)	Ash (% wt)	Coal (% wt)	Recovery (% wt) Ash	Recovery (% wt) Coal
1st stage concentrate	15.9	82.1	5.4	94.6	57.0	84.3
1st stage refuse	3.5	17.9	18.7	81.3	43.1	15.8
Feed	19.3	100.0	7.7	92.3	100.0	100.0

Figure No. 28 Test No. DT-PS-243 Pulp Density - 2.0

	Sample Weight (g)	Yield (% wt)	Ash (% wt)	Coal (% wt)	Recovery (% wt) Ash	Recovery (% wt) Coal
1st stage concentrate	14.1	61.5	5.0	95.0	40.7	63.2
1st stage refuse	8.8	38.5	11.7	88.3	59.3	36.8
Feed	22.9	100.0	7.6	92.4	100.0	100.0

Figure No. 29 Test No. DT-PS-216 1.2 lb/ton DF M150

	Sample Weight (g)	Yield (% wt)	Ash (% wt)	Coal (% wt)	Recovery (% wt) Ash	Recovery (% wt) Coal
1st stage concentrate	8.1	43.9	5.5	94.5	30.4	45.1
1st stage refuse	10.4	56.1	9.9	90.1	69.6	54.9
Feed	18.5	100.0	8.0	92.1	100.0	100.0

Figure No. 29 Test No. DT-PS-217 2.5 lb/ton DF M150

	Sample Weight (g)	Yield (% wt)	Ash (% wt)	Coal (% wt)	Recovery (% wt) Ash	Recovery (% wt) Coal
1st stage concentrate	11.5	65.4	4.8	95.2	39.9	67.6
1st stage refuse	6.1	34.6	13.8	86.2	60.2	32.4
Feed	17.7	100.0	7.9	92.1	100.0	100.0

Figure No. 29 Test No. DT-PS-211 3.9 lb/ton DF M150

	Sample Weight (g)	Yield (% wt)	Ash (% wt)	Coal (% wt)	Recovery (% wt) Ash	Recovery (% wt) Coal
1st stage concentrate	15.5	85.4	5.1	94.9	56.8	87.7
1st stage refuse	2.7	14.6	22.7	77.3	43.2	12.3
Feed	18.1	100.0	7.7	92.3	100.0	100.0

Figure No. 29 Test No. DT-PS-212 8.5 lb/ton DF M150

	Sample Weight (g)	Yield (% wt)	Ash (% wt)	Coal (% wt)	Recovery (% wt) Ash	Recovery (% wt) Coal
1st stage concentrate	17.8	94.8	4.2	95.9	57.2	97.6
1st stage refuse	1.0	5.2	56.3	43.7	42.8	2.5
Feed	18.8	100.0	6.9	93.1	100.0	100.0

Figure No. 29 Test No. DT-PS-213 26.0 lb/ton DF M150

	Sample Weight (g)	Yield (% wt)	Ash (% wt)	Coal (% wt)	Recovery (% wt) Ash	Recovery (% wt) Coal
1st stage concentrate	16.6	96.1	4.5	95.5	66.9	98.1
1st stage refuse	0.7	3.9	54.4	45.6	33.1	1.9
Feed	17.3	100.0	6.5	93.6	100.0	100.0

Figure No. 29 Test No. DT-PS-214 53.1 lb/ton DF M150

	Sample Weight (g)	Yield (% wt)	Ash (% wt)	Coal (% wt)	Recovery (% wt) Ash	Recovery (% wt) Coal
1st stage concentrate	18.6	91.7	4.9	95.1	66.0	93.6
1st stage refuse	1.7	8.3	28.0	72.0	34.0	6.4
Feed	20.3	100.0	6.9	93.2	100.0	100.0

Figure No. 29 Test No. DT-PS-218 1.2 lb/ton DF M150

	Sample Weight (g)	Yield (% wt)	Ash (% wt)	Coal (% wt)	Recovery (% wt) Ash	Recovery (% wt) Coal
1st stage concentrate	10.1	56.7	4.6	95.4	35.7	58.3
1st stage refuse	7.8	43.3	10.8	89.2	64.3	41.7
Feed	17.9	100.0	7.3	92.7	100.0	100.0

Figure No. 30 Test No. DT-PS-219 2.5 lb/ton DF M150

	Sample Weight (g)	Yield (% wt)	Ash (% wt)	Coal (% wt)	Recovery (% wt) Ash	Recovery (% wt) Coal
1st stage concentrate	9.6	66.0	3.6	96.5	33.0	68.6
1st stage refuse	4.9	34.0	14.0	86.0	67.0	31.5
Feed	14.5	100.0	7.1	92.9	100.0	100.0

Figure No. 30 Test No. DT-PS-220 3.4 lb/ton DF M150

	Sample Weight (g)	Yield (% wt)	Ash (% wt)	Coal (% wt)	Recovery (% wt) Ash	Recovery (% wt) Coal
1st stage concentrate	14.6	79.5	4.2	95.8	46.9	82.0
1st stage refuse	3.8	20.5	18.4	81.6	53.1	18.0
Feed	18.4	100.0	7.1	92.9	100.0	100.0

Figure No. 30 Test No. DT-PS-221 10.7 lb/ton DF M150

	Sample Weight (g)	Yield (% wt)	Ash (% wt)	Coal (% wt)	Recovery (% wt) Ash	Recovery (% wt) Coal
1st stage concentrate	14.5	93.9	3.4	96.6	48.8	97.0
1st stage refuse	1.0	6.2	55.0	45.1	51.2	3.0
Feed	15.4	100.0	6.6	93.4	100.0	100.0

Figure No. 30 Test No. DT-PS-222 22.9 lb/ton DF M150

	Sample Weight (g)	Yield (% wt)	Ash (% wt)	Coal (% wt)	Recovery (% wt) Ash	Recovery (% wt) Coal
1st stage concentrate	16.0	90.3	4.2	95.9	54.8	92.9
1st stage refuse	1.7	9.7	31.8	68.2	45.2	7.1
Feed	17.7	100.0	6.8	93.2	100.0	100.0

Figure No. 30 Test No. DT-PS-223 81.5 lb/ton DF M150

	Sample Weight (g)	Yield (% wt)	Ash (% wt)	Coal (% wt)	Recovery (% wt) Ash	Recovery (% wt) Coal
1st stage concentrate	14.1	94.8	4.4	95.6	59.4	97.5
1st stage refuse	0.8	5.2	54.6	45.5	40.6	2.5
Feed	14.8	100.0	7.0	93.0	100.0	100.0

Figure No. _____ Test No. _____

	Sample Weight (g)	Yield (% wt)	Ash (% wt)	Coal (% wt)	Recovery (% wt) Ash	Recovery (% wt) Coal
1st stage concentrate						
1st stage refuse						
Feed						

Figure No. 31 Test No. DT-61 0.0 lb/ton Sodium Silicate

	Sample Weight (g)	Yield (% wt)	Ash (% wt)	Coal (% wt)	Recovery (% wt) Ash	Recovery (% wt) Coal
2nd stage concentrate	9.0	36.7	11.8	88.2	12.5	49.6
2nd stage refuse	9.0	36.8	31.6	68.4	33.5	38.6
1st stage concentrate	18.0	73.6	21.7	78.3	46.0	88.2
1st stage refuse	6.5	26.5	70.9	29.1	54.0	11.8
Feed	24.5	100.0	34.7	65.3	100.0	100.0

Figure No. 31 Test No. DT-62 16 lb/ton Sodium Silicate

	Sample Weight (g)	Yield (% wt)	Ash (% wt)	Coal (% wt)	Recovery (% wt) Ash	Recovery (% wt) Coal
2nd stage concentrate	10.2	40.0	9.7	90.3	11.0	55.7
2nd stage refuse	6.1	23.8	33.4	66.6	22.6	24.5
1st stage concentrate	16.3	63.8	18.6	81.5	33.6	80.2
1st stage refuse	9.3	36.2	64.6	35.4	66.4	19.8
Feed	25.6	100.0	35.2	64.8	100.0	100.0

Figure No. 31 Test No. DT-63 32 lb/ton Sodium Silicate

	Sample Weight (g)	Yield (% wt)	Ash (% wt)	Coal (% wt)	Recovery (% wt) Ash	Coal
2nd stage concentrate	9.7	39.6	9.8	90.2	11.3	54.5
2nd stage refuse	5.2	21.3	30.3	69.8	18.6	22.6
1st stage concentrate	14.9	60.8	17.0	83.0	29.9	77.1
1st stage refuse	9.6	39.2	61.8	38.3	70.1	22.9
Feed	24.5	100.0	34.5	65.5	100.0	100.0

Figure No. 31 Test No. DT-64 64 lb/ton Sodium Silicate

	Sample Weight (g)	Yield (% wt)	Ash (% wt)	Coal (% wt)	Recovery (% wt) Ash	Coal
2nd stage concentrate	9.6	39.1	10.0	90.0	11.4	53.6
2nd stage refuse	5.6	22.7	31.0	69.0	20.4	23.9
1st stage concentrate	15.1	61.8	17.7	82.3	31.8	77.5
1st stage refuse	9.4	38.2	61.4	38.6	68.2	22.5
Feed	24.5	100.0	34.4	65.6	100.0	100.0

Figure No. 31 Test No. DT-65 96 lb/ton Sodium Silicate

	Sample Weight (g)	Yield (% wt)	Ash (% wt)	Coal (% wt)	Recovery (% wt) Ash	Recovery (% wt) Coal
2nd stage concentrate	9.8	40.1	10.1	90.0	11.7	54.9
2nd stage refuse	5.0	20.4	32.8	67.2	19.5	20.9
1st stage concentrate	14.8	60.5	17.8	82.3	31.2	75.8
1st stage refuse	9.7	39.5	59.8	40.2	68.8	24.2
Feed	24.5	100.0	34.4	65.6	100.0	100.0

Figure No. 31 Test No. DT-66 160 lb/ton Sodium Silicate

	Sample Weight (g)	Yield (% wt)	Ash (% wt)	Coal (% wt)	Recovery (% wt) Ash	Recovery (% wt) Coal
2nd stage concentrate	8.6	35.2	9.4	90.6	9.5	48.9
2nd stage refuse	5.0	20.7	32.7	67.3	19.4	21.3
1st stage concentrate	13.6	55.8	18.0	82.0	28.8	70.2
1st stage refuse	10.8	44.2	56.1	43.9	71.2	29.8
Feed	24.4	100.0	34.8	65.2	100.0	100.0

Figure No. 32

Ash Profile Along the Depth of the Froth Formed During the Microbubble Flotation Tests Conducted on the Pittsburgh No. 8 Seam Coal

Distance from Top of Froth (cm)	% Ash
1.5	4.1
3.0	4.0
4.5	4.1
5.0	5.1

Figure No. 33 Test No. DT-PS-261 0 min. Grinding Time

	Sample Weight (g)	Yield (% wt)	Ash (% wt)	Coal (% wt)	Recovery (% wt) Ash	Coal
2nd stage concentrate	12.9	94.0	4.8	95.2	89.8	94.2
2nd stage refuse	0.5	3.6	7.4	92.6	5.3	3.5
1st stage concentrate	13.3	97.6	4.9	95.1	95.1	97.7
1st stage refuse	0.3	2.4	10.1	89.9	4.9	2.3
Feed	13.7	100.0	5.0	95.0	100.0	100.0

Figure No. 33 Test No. DT-PS-262 5 min. Grinding Time

	Sample Weight (g)	Yield (% wt)	Ash (% wt)	Coal (% wt)	Recovery (% wt) Ash	Coal
2nd stage concentrate	12.63	92.8	4.1	95.9	67.2	94.4
2nd stage refuse	0.1	1.0	19.0	81.0	3.2	0.8
1st stage concentrate	12.8	93.8	4.3	95.7	70.3	95.2
1st stage refuse	0.9	6.3	27.1	72.9	29.7	4.8
Feed	13.6	100.0	5.7	94.3	100.0	100.0

Figure No. 33 Test No. DT-PS-263 15 min. Grinding Time

	Sample Weight (g)	Yield (% wt)	Ash (% wt)	Coal (% wt)	Recovery (% wt) Ash	Recovery (% wt) Coal
2nd stage concentrate	9.7	66.2	2.8	97.2	31.0	68.4
2nd stage refuse	1.2	8.0	11.3	88.7	15.2	7.5
1st stage concentrate	10.9	74.2	3.7	96.3	46.2	76.0
1st stage refuse	3.8	25.8	12.4	87.6	53.8	24.0
Feed	14.7	100.0	6.0	94.0	100.0	100.0

Figure No. 33 Test No. DT-PS-264 25 min. Grinding Time

	Sample Weight (g)	Yield (% wt)	Ash (% wt)	Coal (% wt)	Recovery (% wt) Ash	Recovery (% wt) Coal
2nd stage concentrate	9.4	61.5	3.0	97.0	25.9	64.2
2nd stage refuse	0.9	5.5	15.3	84.7	11.8	5.1
1st stage concentrate	10.3	67.0	4.1	95.9	37.7	69.3
1st stage refuse	5.1	33.0	13.6	86.4	62.3	30.7
Feed	15.4	100.0	7.2	92.8	100.0	100.0

Figure No. 34 Test No. DT-C-25 0 min. Grinding Time

	Sample Weight (g)	Yield (% wt)	Ash (% wt)	Coal (% wt)	Recovery (% wt) Ash	Recovery (% wt) Coal
2nd stage concentrate	81.5	83.7	5.4	94.6	78.1	84.1
2nd stage refuse	5.3	5.5	6.9	93.1	6.5	5.4
1st stage concentrate	86.8	89.2	5.5	94.5	84.6	89.4
1st stage refuse	10.6	10.8	8.3	91.7	15.4	10.6
Feed	97.3	100.0	5.8	94.2	100.0	100.0

Figure No. 34 Test No. DT-C-26 5 min. Grinding Time

	Sample Weight (g)	Yield (% wt)	Ash (% wt)	Coal (% wt)	Recovery (% wt) Ash	Recovery (% wt) Coal
2nd stage concentrate	45.8	42.5	2.8	97.2	18.7	44.1
2nd stage refuse	19.1	17.7	5.5	94.5	15.5	17.9
1st stage concentrate	64.9	60.2	3.6	96.4	34.2	61.9
1st stage refuse	42.9	39.8	10.4	89.6	65.8	38.1
Feed	107.8	100.0	6.3	93.7	100.0	100.0

Figure No. 34 Test No. DT-C-27 15 min. Grinding Time

	Sample Weight (g)	Yield (% wt)	Ash (% wt)	Coal (% wt)	Recovery (% wt) Ash	Recovery (% wt) Coal
2nd stage concentrate	26.4	25.0	2.2	97.8	8.6	26.1
2nd stage refuse	20.8	19.7	5.3	94.8	15.8	20.0
1st stage concentrate	47.2	44.7	3.6	96.4	24.4	46.1
1st stage refuse	58.5	55.3	8.9	91.1	75.6	53.9
Feed	105.6	100.0	6.5	93.5	100.0	100.0

Figure No. 34 Test No. DT-C-28 25 min. Grinding Time

	Sample Weight (g)	Yield (% wt)	Ash (% wt)	Coal (% wt)	Recovery (% wt) Ash	Recovery (% wt) Coal
2nd stage concentrate	16.0	15.6	2.0	98.0	4.2	16.6
2nd stage refuse	11.4	11.1	6.3	93.7	9.1	11.3
1st stage concentrate	27.4	26.7	3.8	96.2	13.3	27.8
1st stage refuse	75.2	73.3	9.0	91.0	86.7	72.2
Feed	102.6	100.0	7.6	92.4	100.0	100.0

Figure No. 35

Results of Flotation Kinetics Experiments Conducted on the Eagle Seam Coal (-100 Mesh) as a Function of Bubble Size

	Microbubble		4-8 μm		145-175 μm	
Time (min.)	Recovery (%)	Ash (%)	Recovery (%)	Ash (%)	Recovery (%)	Ash (%)
0.25	12.5	20.9	8.8	12.0	--	--
0.50	65.7	18.9	20.4	18.5	9.3	18.3
0.75	75.5	24.7	--	--	--	--
1.0	84.4	22.1	33.2	12.5	14.0	16.9
1.5	89.2	28.4	42.3	10.2	16.9	16.6
2.0	91.0	36.5	51.0	12.0	20.3	16.6
3.0	91.9	36.5	64.0	18.3	26.9	20.2
4.0	92.4	36.5	70.5	20.6	34.6	23.5
5.0	--	--	77.0	24.5	42.1	26.1
6.0	92.6	36.5	82.4	29.5	49.0	27.9
Tail	100.0	77.9	100.0	66.0	100.0	43.3

★U.S. GOVERNMENT PRINTING OFFICE:1984 -746 -081/ 2654 REGION NO. 4